AN ABSTRACT OF THE THESIS OF

Matthew S. Boyd for the degree of Master of Science in Civil Engineering and Bioresource Engineering presented on October 10, 1996. Title: Heat Source: Stream, River and Open Channel Temperature Prediction.

Abstract approved: Redacted for privacy
Richard Cuenca

Abstract approved: Redacted for privacy
Ronald Miner

Reach defined analysis concentrated on the water temperature change that occurred in a stream/river segment over the course of one full diurnal cycle. Digital thermistors, data loggers and computer model development were utilized in reach analysis to link parameters of the stream system to a specific temperature change. The methodology employed was relatively simple and fast, and many successive stream segments were analyzed simultaneously. Reach analysis of stream temperature change identified the existing components of the stream system that caused increased water temperature and predicted the effectiveness of managed improvements to the stream system.

Stream and river temperature regulation has focused on system and basin wide management. Often, the source of increased water temperature originates in only a part of the stream system. Reach defined analysis identified the portions of the stream system in which most water temperature change occurred, offered an explanation for the

temperature response and provided specific information about the alternate strategies that may ameliorate undesired water temperatures.

The development of the computer model Heat Source included physically based mathematical descriptions of stream energy and hydrologic processes. An implicit finite difference numerical method was implemented for simultaneous solution. The methodology presented in Heat Source is portable and applicable to all streams, rivers and open channels.

Heat Source: Stream, River and Open Channel Temperature Prediction

by

Matthew S. Boyd

A THESIS

submitted to

Oregon State University

in partial fulfillment of
the requirements for the
degree of

Masters of Science

Completed October 10, 1996
Commencement June, 1997

Masters of Science thesis of Matthew S. Boyd presented on October 10, 1996

APPROVED:

Redacted for privacy

Co-Major Professor, representing Bioresource Engineering

Redacted for privacy

Co-Major Professor, representing Civil Engineering

Redacted for privacy

Head of Department of Bioresource Engineering

Redacted for privacy

Head of Department of Civil Construction and Environmental Engineering

Redacted for privacy

Dean of Graduate School

I understand that my thesis will become part of the permanent collection of Oregon State University libraries. My signature below authorizes release of my thesis to any reader upon request.

Redacted for privacy

Matthew S. Boyd, Author

Acknowledgment

I am truly grateful for the support that my family has given me throughout my Oregon State graduate studies. My parents have instilled in me the importance of education and social service and I hope to live up to their example and tradition. My wife, Christine, has made adjustments in her professional life that enabled me to pursue my graduate studies, and I am thankful. Her support and patience were more than I could have expected or anticipated.

Dr. Miner encouraged me to become involved in this research project and provided direction and guidance. Dr. Moore was just as helpful. I really consider myself lucky to work for such personable and knowledgeable professors. I appreciate the relationship that I have developed with Dr. Moore and Dr. Miner and will look forward to working with them in the future.

Dr. Bolte deserves thanks for his time and patience. He introduced me to numerical methods and stimulated my interest in computer modeling. The graphing routines that were written into the Heat Source code were developed by Dr. Cuenca. His experience with computer modeling was helpful and I often found myself at his door when I had a programming problem.

Well, after three years of study and work I find myself at the end of my Master's research effort. I could not have asked for a more interesting and challenging project. The support that I received from the beginning to the end was incredible. My terrific academic experience would not have been possible without the professors and friends that I was lucky enough to encounter at Oregon State University.

TABLE OF CONTENTS

TABLE OF CONTENTS (continued)

LIST OF FIGURES

LIST OF FIGURES (continued)

LIST OF FIGURES (continued)

LIST OF TABLES

TABLE OF EQUATIONS

TABLE OF EQUATIONS (continued)

TABLE OF EQUATIONS (continued)

TABLE OF EQUATIONS (continued)

HEAT SOURCE: STREAM, RIVER AND OPEN CHANNEL TEMPERATURE PREDICTION

1. INTRODUCTION

1.1 Problem Definition

The temperatures of streams and rivers in the Pacific Northwest, spawned by water quality concerns, have gained considerable attention over the past quarter century. Degraded habitat in streams and rivers due to increased water temperature remains a significant barrier to many of the ongoing stream restoration and enhancement projects. The bulk of past stream and river temperature research has implicated several profitable and culturally ingrained land use activities, such as: livestock grazing, forest practices and urbanization. Regulators are faced with difficult decisions that may affect the way of life for many that choose to live and work near streams and rivers in the Pacific Northwest.

In an attempt to monitor the temperatures of streams and rivers, several academic institutions and government agencies have been collecting stream temperature data. Digital Hobo® thermistors, which have excellent temperature resolution and are capable of taking 1800 measurements, are most commonly used. The increased desire to monitor water temperatures, coupled with advantages of the digital Hobo® measurement devices, has resulted in a wealth of temperature data. With the ease of massive data collection, however, problems have emerged.

There is no current standard for collecting stream temperature data. Temperature data collected in various fashions may produce varied temperature magnitudes. Further,

no standard exists for the analysis of stream temperature data. Developing a standard method for data collection and analysis would be helpful when comparing temperature response for different stream reaches and systems. Without the proper measurement of several site and time specific stream parameters, stream temperature data is of little use. Unfortunately, the majority of stream temperature data is taken with little description of the stream and the surrounding environment.

The current understanding of energy processes that are inherent to all streams and rivers facilitate accurate model development and stream temperature simulation. Numerous models have been presented and used in the last twenty years. While each model is unique, many share common methods and procedures. It would be worthwhile to review past modeling efforts and utilize the most accurate and robust methodology for the development of a new stream temperature model that is capable of temperature data analysis. Such a model would promote standardized data collection and uniform data analysis.

1.2 Statement of Purpose

Stream system thermodynamics are the result of heat energy exchange between the atmosphere, stream and terrestrial environment. Mathematical descriptions of these energy processes provide insight as to the magnitude of impact, either by cooling or heating, for which each thermal process is responsible. Accurate quantitative accounting of the thermal energy entering, leaving and stored in the stream system, implies understanding of the complexities represented by individual stream system heat energy

components. Distinguishing heat energy components within the stream system requires organized physically based algorithms and modeling processes.

This research effort describes, by use of a developed mathematical model, *Heat Source*, the physical and thermodynamic processes inherent to all stream, river and open channel systems. Fundamental to this methodology is the assumption that accurate mathematical descriptions of advection, dispersion and heat energy balance relationships are primarily responsible for comprising the temperature of a stream system at any particular location and time along a specified stream reach. Further, stream temperature change occurring in a defined reach provides a direct description of the individual physical and thermal processes occurring in a specific stream system and the surrounding environment.

Several stream reaches were defined and temperature measurements were collected at the upstream and downstream boundary of the reach for one full diurnal cycle. The difference in temperature between the upstream and downstream boundary is a direct result of the thermal and hydraulic processes inherent to the stream system. Model simulation predicted the change in temperature between the upstream and downstream boundary, the temperature profile at the downstream boundary and the heat energy balance that induces temperature change. Actual stream temperature data was used for validation purposes. Upon validation, a sensitivity analysis served to highlight the various components of the stream system which protect a stream from increased water temperatures.

Although *Heat Source* was developed for the use of this research project, the model has evolved into a valuable tool when analyzing stream temperature data. It works

particularly well with the Hobo® thermistor units, with which most stream temperature data is collected. When analyzing stream temperature data, *Heat Source* provides a record of the energy flux components, as well as, the predicted temperature increase. The use of *Heat Source* promotes standardized data collection and analysis so that the results of every stream temperature simulation may then be used for comparison with results from different stream and river reaches and systems.

The temperatures of streams and rivers remain an important water quality concern. Future stream temperature modeling must refine and enhance the mathematical descriptions of the individual energy components that affect stream temperature. The complexity of the heat energy balance, coupled with the hydraulic characteristics of all flowing bodies of water, create a difficult modeling scenario. Unsteady flow conditions inherent to all streams and rivers require that flow data input is frequent and/or model simulation is limited to a small duration in which the flow is considered steady.

2. LITERATURE REVIEW

2.1 Stream/River Temperature Models

Prior stream/river temperature modeling efforts have utilized an energy balance approach coupled with equations governing the conservation of mass (Brown 1972, Wunderlich 1972, Jobson and Keefer 1979, Beschta 1984, Sinokrot and Stefan 1992). *Heat Source*, the stream/river temperature prediction model developed in this paper, draws from several methodologies presented and tested over the last thirty years. The most notable and cited energy balance and mass transport methodologies are worthy of brief discussion.

2.1.1 Brown's Equation

Brown's stream temperature studies established a link between stream side vegetation and the stream energy processes that contribute to stream temperature magnitude. Brown concluded that water temperature can be identified as a part of the riparian system that is affected by the activities of humans which alter the shading levels experienced by streams (Brown et. al. 1971). Brown's contribution focused research on the individual heat energy components that lead to stream temperature change.

Perhaps Brown's greatest contribution to stream temperature dynamics is represented in what has become known as *Brown's Equation* which predicts a change in stream temperature as a function of the heat energy flux (Φ), surface area (A), and stream flow (Q) (Brown 1970):

Equation 2.1. Brown's Equation,

$$\Delta T = \frac{(\Phi)(A)}{(Q)}.$$

While stream surface area (A) and flow (Q) are easily quantified, the heat energy flux (Φ) cannot be simply measured nor derived. *Brown's Equation* is an oversimplification of the physical processes that contribute to stream temperature, but it proves useful in conceptualizing water body temperature dynamics and serves as a starting point when discussing stream temperature.

2.1.2 Tennessee Valley Authority

Wunderlich (1972) developed a mathematical model for the Tennessee Valley Authority that predicted temperatures in rivers and reservoirs. This research effort provided the most comprehensive and complete description of algorithms used to estimate the energy flux components: solar radiation, terrestrial radiation, evaporation and sensible heat. Multiple methods are developed, presented and compared for accuracy and applicability.

A significant contribution of the Tennessee Valley Authority's developed energy balance stems from the discussion of the difficulties in estimating the evaporative heat energy flux. Three methods are presented and discussed for calculating the evaporation phenomena: the *water budget method,* the *energy budget method* and the *empirical method.*

The *water budget method* is dependent on the conservation of mass and is only applicable if all incoming and outgoing quantities, including rainfall and seepage, can be

evaluated accurately. As a general rule, this method fails if the change in mass over a defined reach is greater than the evaporative transfer of mass. The application of this method relies heavily on accurate measurement of the change in storage over a defined reach. Unless in-stream measurement devices (i.e. weirs or flumes) are used to measure flow rates, the *mass balance* approach is not suitable, thus prohibiting it from general application (Wunderlich 1972).

The *energy budget method* relies on the conservation of heat energy which must be accurately measured by thermal surveys of the water body. Harbeck and Meyers (1970) employed the *energy budget method* to determine specific mass transfer coefficients for defined stream/river reaches. Unfortunately, for general application, this method is not easily applied, and therefore, is not practical.

Empirical methods correlate evaporation values obtained from evaporation pans to those observed at or estimated for specific water bodies using *water and energy balance methods*. The aerodynamic exposure and heat distribution that exists in a natural water body is quite different from that experienced by an evaporation pan. To complicate matters further, most empirical relationships are developed for lakes and reservoirs and not for open channel systems. At best, long-term averaged values may be expected from the developed empirical evaporation relationships (Kohler et. al. 1955). Wunderlich (1972) acknowledges the difficulty in evaporation flux estimation by providing numerous methods that are developed for specific North American climate types and regions.

2.1.3 Jobson and Keefer

Jobson and Keefer (1979) developed the methodology to predict heat and mass transfer for highly transient flow in the Chattahoochee River near Atlanta, Georgia. Linear implicit finite-difference methods were utilized to simulate the effect of hydropulsation from Buford Dam on river temperature. The reach length of study was 27.9 km between Buford and Norcross, Georgia. The greatest simulated change in river temperature magnitude occurring over the defined reach was 5.8° C (10.4° F) during a daily minimum flow of 15.4 m^3/s (543.9 ft^3/s). The modeling scenario was complicated due to the pulsation of 215 m^3/s (7592.7 ft^3/s) which occurs twice daily during week days. Temperature prediction was considered fairly accurate for the defined reach where the root-mean-square of predicted temperature change was 0.32° C (0.58° F) in October and 0.20° C (0.36° F) in March, 1975 (Jobson and Keefer 1979).

Investigations made by Jobson and Keefer (1979) correlated the effects of river flow volume and increased river temperatures. During low flow periods the mid-day change in river temperature was roughly 1° C (1.8° F) over a distance of 0.48 km (1575 ft). The observed river temperatures were primarily dependent on flow scheduling from dam operations. Timing the dam releases helped to buffer river temperature change. High flows coincided with the larger mid-day solar flux magnitudes, and conversely, low flow periods occurred during weak solar flux portions of the day (i.e. early morning and late afternoon periods). Jobson and Keefer (1979) demonstrated that in-stream temperatures are directly dependent on the flow volume.

2.1.4 TEMP86

Beschta's early 1980's research, drawing from quantitative descriptions of the heat energy flux components, estimated the heat energy processes inherent to small forested streams. TEMP84, later updated to TEMP86, developed by Beschta, is a computer simulation of the heat energy processes that actively affect stream temperature. Through accurate estimation of site dependent heat energy processes, Beschta successfully employed TEMP86 as a means to simulate the temperature responses in small mountain streams that result from shade removal (Beschta and Weatherred 1984).

The methodology utilized by TEMP86 contributed greatly to the understanding of solar routing simulation. Jobson and Keefer (1979) had expressed concern over the errors produced by either ignoring or underestimating the effect of attenuation and scattering of solar energy induced by the topographic and vegetation barriers. Further, TEMP86 includes the effects of stream side vegetation in long-wave energy estimation, accounting for long-wave radiation originating from vegetation, as well as, the routing of atmospheric radiation. TEMP86 offers an extremely robust simulation of solar and long-wave radiation routing through stream side vegetation.

2.1.5 MNSTREM

Sinokrot and Stefan (1993) developed a numerical model based on a finite difference solution to the unsteady heat advection-dispersion equation that predicted hourly water temperature values. It was determined that shallow streams exhibited a strong dynamic behavior and diurnal variations of several degrees Celsius. Solar radiation

was shown to be the most important component of the heat flux across the stream water surface. Shallow streams with little shading were identified as vulnerable to large temperature fluctuations due to a maximal solar heat energy flux and increased stream bed absorption of heat energy. This modeling effort utilized actual stream hydraulic, atmospheric and meteorological, and solar radiation data, which improved accuracy, but limited the portability of the model.

2.2 Stream Temperature Related to Land Use Practices

Non-point source stream temperature increase is directly related to land use and management. Numerous land use activities (i.e. riparian zone vegetation disturbance, altered watershed hydrology, and urbanization) affect the energy relationship that exists between a stream and it's environment. Dam construction, irrigation diversions, timber harvesting and livestock grazing, affect river and stream temperatures.

Riparian vegetation serves to protect and shield the stream from direct solar radiation. Removal or reduction in the quantity and quality of stream side vegetation has been shown to increase summertime stream temperatures (Beschta et. al. 1987). Loss of riparian vegetation due to grazing, logging, or over use activities can be directly linked to an increase in summertime water temperatures due to reduction in quality and quantity of stream shading (Anderson et. al. 1993). Removal of forest cover along stream sides significantly increases the maximum, and in some locations, the minimum stream temperatures during summer months (Rishel et. al. 1982). The literature is uniform in predicting higher summer water temperatures with less stream side vegetation cover

(Gibbons and Salo 1973). Claire and Storch (1977) noted that the average stream temperature of Oregon's Deschutes River through an enclosure that was ungrazed for 10 years was 12° F (6.7° C) lower than stream temperatures in grazed sections.

Altered channel morphology is a secondary response to disturbance of stream side vegetation. Stream side vegetation protects stream banks by reducing erosive energy, by helping deposits build the stream bank, and protecting the stream bank from damaging effects caused by ice, logging and livestock grazing (Platts 1981). Removal of stream side vegetation exposes stream banks to soil erosion. Increased woody vegetation in the riparian area assists bank stability and stream debris provides shade for stream temperature control (Hicks et. al. 1991). Reduced stream side vegetation often promotes widening of the channel, which in turn, increases the stream surface area exposed to solar radiation. Livestock grazing in riparian areas often causes sloughing and collapse of stream banks, reducing bank stability and promoting channel widening (Platts 1981). Wiget and Reichert (Unpublished) found that livestock grazing adjacent to selected Utah streams reduced stream bank stability 59 percent. Marcuson (1977) found that an ungrazed portion of Rock Creek, Montana, had 2.5 times less channel erosion than an adjacent stream section that was grazed.

The cumulative effect of reducing the quality and quantity of stream side vegetation is an immediate increase in the intensity of solar radiation per unit surface area experienced by the stream, and often long term channel widening, increasing stream surface area. An indirect result of degraded stream side vegetation may result in altered subsurface hydrology.

The temperatures of streams has direct impact on the aquatic ecosystem. The ability of water to dissolve oxygen is inversely proportional to water temperature. Elevated stream temperatures decrease the available oxygen available for aquatic biota.

Water temperature controls the composition of aquatic species that rivers and steams support. Stream temperatures have been implicated in declining anadromous fish runs in the Pacific Northwest. High stream temperatures reduce both the survival, growth and reproduction rates of steelhead trout and salmon (Hostetler, S.W. 1991). Stream temperatures for trout should not exceed 65° F (18.3° C) and should be even lower during the critical spawning and incubation periods (Platts 1981).

Aquatic bacteria, some of which are pathogenic to fish, require elevated stream temperatures. A small water temperature increase in the Columbia River allowed for the growth of *Columnaris*, a pathogenic bacteria, which destroys the gill tissue of fish. Brett (1952) found that due to a minor human caused temperature increase in the Columbia river, *Columnaris* was responsible for killing nearly an entire run of sockeye salmon.

Existing temperature standards for the State of Oregon vary by basin, dependent on the natural temperature regime and the limits of aquatic ecosystems. The maximum stream temperature permitted, above which no human caused increase is allowable, ranges from 58° F to 65° F (14.4° C to 18.3° C) (Oregon Department of Environmental Quality 1995). Maximum permissible stream temperatures for selected basins within the state of Oregon are listed in Table 2.1. Streams and rivers that are considered in violation of the standard when daily maximum temperatures are in excess of the standard for seven or more consecutive days.

Western Oregon	14.4° C	58.0° F
Cascade Range	14.4° C	58.0° F
Eastern Oregon	20.0° C	68.0° F
Lower Willamette	22.2° C	72.0° F
Klamath basin (non-salmonid)	22.2° C	72.0° F

Table 2.1. Oregon stream temperature standards.

3. EXPERIMENTAL DESIGN

3.1 Conceptual Model

At any particular instant of time, a defined stream reach is capable of sustaining a particular water column temperature. Stream temperature change that results within a defined reach is explained rather simply. The temperature of a parcel of water that is traversing a stream/river reach enters the reach with a given temperature. If that temperature is greater than that which the defined reach is capable of supporting, the temperature will decrease. If that temperature is less than that which the defined reach is capable of supporting, the temperature will increase. Stream temperature change within a defined reach, is induced by the energy balance between the parcel of water and the surrounding environment. It takes time for the water parcel to traverse the longitudinal distance of the defined reach, during which the energy processes drive stream temperature change. In all natural systems both scenarios occur simultaneously. At any particular instant of time, water that enters the upstream portion of the reach is never exactly the temperature that is supported by the defined reach. And, as the water is transferred downstream, heat energy and hydraulic process that are variable with time and space interact with the water parcel and induce water temperature change. The described modeling scenario is a simplification, however, understanding the basic processes in which stream temperatures change occurs over the course of a defined reach and period of time is essential. Acceptance and understanding of the source of temperature change is mandatory before developing a deeper understanding of stream temperature

thermodynamics. The detailed exploration of stream temperature thermodynamics presented in this research effort serves to explore processes that occur via the basic processes of stream/river thermodynamics.

Model input has been separated into two categories: general inputs and temperature inputs. Each general input is displayed and categorized in Table 3.1 and each temperature input is displayed and categorized in Table 3.2.

General Inputs:	Record Keeping:	Stream/River Name Units Date of Simulation Duration of Simulation River/Stream Mile Elevation Latitude Longitude Time Zone Reach Length
	Atmospheric:	Cloud Cover Relative Humidity Minimum Air Temperature Maximum Air Temperature Time of Minimum Air Time of Maximum Air Wind Speed
	Hydrologic:	Stream Flow Flow Velocity Average Width Stream Bed Slope Percent Bedrock Stream Aspect Stream Bank Slope Topographic Shade Angle
	Shading:	Vegetation Shade Angle Vegetation Height Vegetation Width Canopy Coefficient

Table 3.1. General inputs.

Temperature Inputs:	Sine Wave Estimation:	Hourly Air Temperatures Hourly Upstream Temperatures
	Manual Input:	Hourly Air Temperatures Hourly Upstream Temperatures Hourly Downstream
	Thermistor Data File:	Hourly Air Temperatures Hourly Upstream Temperatures Load Hourly Downstream

Table 3.2. Temperature inputs.

Once all general and temperature inputs are entered the model user has several options in choosing particular evaporation models, and whether to include ground water effects. Further, the time step and distance step values that comprise the finite difference grid may be altered to meet a particular user's need. *Heat Source* will defer to default settings in the event that particular evaporation and groundwater models are not selected and/or the finite difference grid is not altered.

The model is then ready for simulation. *Heat Source* calculates the specific heat energy balance for the stream at every time and distance node. At every time step the implicit difference equations are solved simultaneously. Stream temperature profiles, energy balance values, atmospheric parameters, and, if selected by the user, canopy effects, are generated for each simulation. Model output can either be displayed as text or graphically. All values calculated during simulation may be saved in text format. The general progression of the model is outlined in the model flow chart, Figure 3.1.

Flow Chart

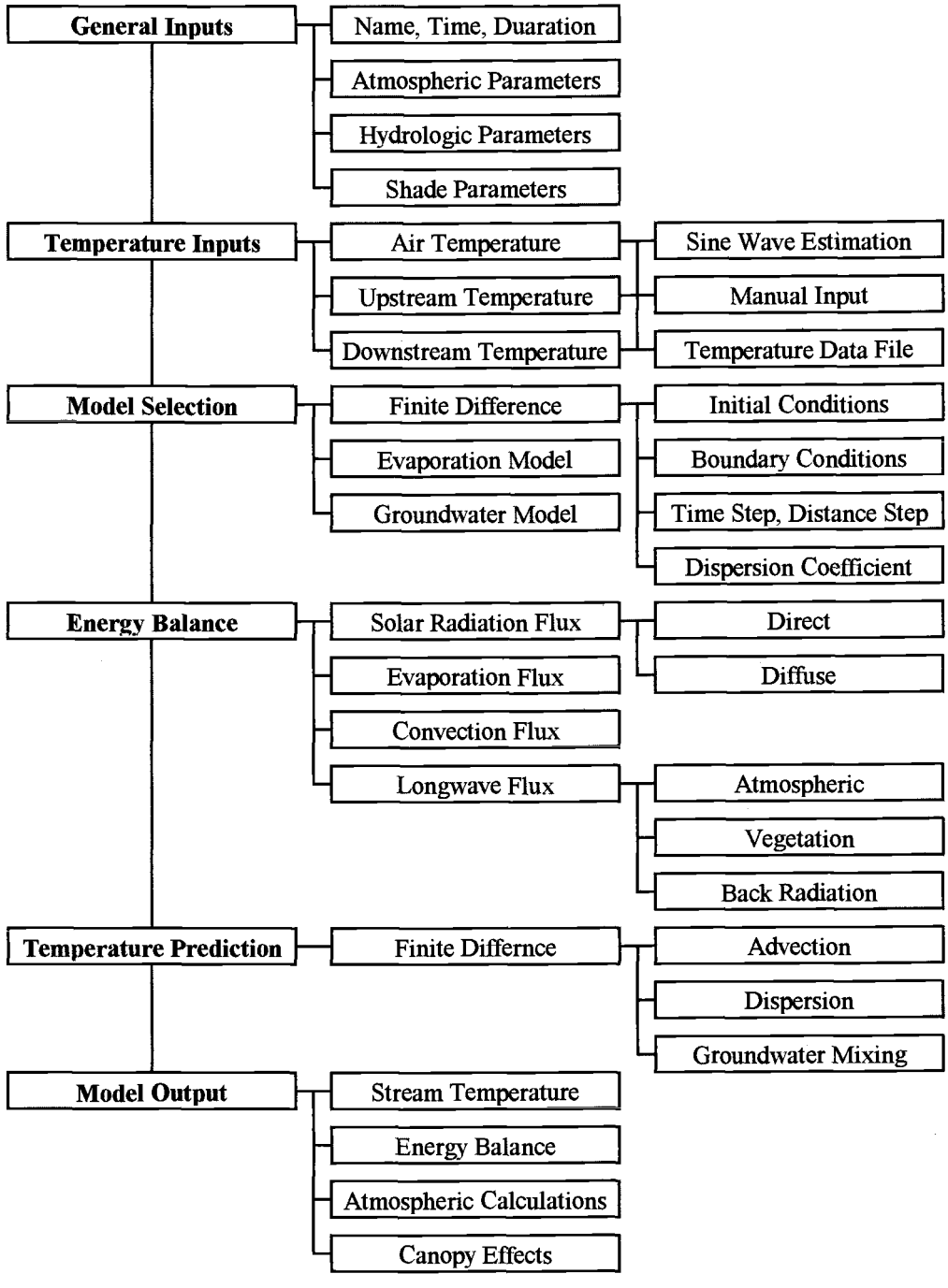

Figure 3.1. Heat Source flow chart

3.1.1 Non-Uniform Heat Energy Transfer Equation

The rate change in stream temperature is driven by the heat energy flux (Φ_i). It is easily shown that a defined volume of water will attain a predictable rate change in temperature, provided an accurate prediction of the heat energy flux. The rate change in stream temperature (T) is calculated as,

$$\frac{\partial T}{dt} = \left(\frac{A_i \cdot \Phi_i}{\rho \cdot c_p \cdot V_i} \right),$$

which reduces to,

Equation 3.1. Rate Change in Temperature (Heat Energy Thermodynamics)

$$\frac{\partial T}{dt} = \left(\frac{\Phi_i}{\rho \cdot c_p \cdot D_i} \right).$$

where,

A_i: cross-sectional area (m^2)
c_p: specific heat of water (cal/kg $\cdot$°C)
D_i: average stream depth (m)
t: time (s)
T: temperature (°C)
V_i: volume (m^3)
Φ_i: total heat energy flux (cal/$m^2 \cdot$s)
ρ: density of water (kg/m^3)

The advective movement of water is a function of the flow velocity (U_x). Advection redistributes heat energy in the positive longitudinal direction. No heat energy is lost or gained by the system during advection, and instead, heat energy is transferred downstream as a function of flow velocity. In the case where flow is uniform, the rate

change in temperature due to advection is expressed in the following first order partial differential equation.

Equation 3.2. Rate Change in Temperature (Advection)

$$\frac{\partial T}{dt} = -U_x \cdot \frac{\partial T}{\partial x}$$

Dispersion processes occur in both the upstream and downstream direction along the longitudinal axis. Heat energy contained in the system is conserved throughout dispersion, and similar to advection, heat energy is simply moved throughout the system. The rate change in temperature due to dispersion is expressed in the following second order partial differential equation.

Equation 3.3. Rate Change in Temperature (Dispersion)

$$\frac{\partial T}{dt} = D_L \cdot \frac{\partial^2 T}{\partial x^2}$$

The dispersion coefficient (D_L) may be calculated by stream dimensions, roughness and flow (Fischer et. al. 1979). In streams that exhibit high flow velocities and low longitudinal temperature gradients, it may be assumed that the system is advection dominated and the dispersion coefficient may be set to zero (Sinokrot and Stefan 1993). In the event that dispersion effects are considered significant, the appropriate value for the dispersion coefficient can be estimated with a practical approach developed and employed in the QUAL 2e model (Brown and Barnwell 1987). An advantage to this approach is that each parameter is easily measured, or in the case of Manning's coefficient (n) and the dispersion constant (K_d), estimated.

Equation 3.4. Physical Dispersion Coefficient (Method 1)

$$D_L = C \cdot K_d \cdot n \cdot U_x \cdot D^{\frac{5}{6}}$$

where,

C: unit conversion
C = 3.82 for English units
C = 1.00 for Metric units
D: average stream depth (m)
D_L: dispersion coefficient (m^2/s)
K_d: dispersion constant (unitless)
n: Manning's coefficient (unitless)
U_x: average flow velocity (m/s)

The longitudinal dispersion coefficient can also be determined from stream dimensions with a relationship developed from roughness and flow (Fischer et. al. 1979).

Equation 3.5. Physical Dispersion Coefficient (Method 2)

$$D_L = C_{eff} \cdot \frac{U_x^2 \cdot W^2}{U_s \cdot D}$$

The implicit numerical solution that is employed will create numerical dispersion equal to the following dispersion constant.

Equation 3.6. Numerical Dispersion Coefficient

$$D_N = \frac{1}{2} \cdot U_x \cdot \Delta x$$

where,

D_N: numerical dispersion (m^2/s)
Δx: distance step defined by finite difference grid (m)
U_x: average flow velocity (m/s)

The simultaneous non-uniform one-dimensional transfer of heat energy is the summation of the rate change in temperature due to heat energy thermodynamics, advection and dispersion. Given that the stream is subject to steady flow conditions and is well mixed, transverse temperature gradients are negligible (Sinokrot and Stefan 1993). An assumption of non-uniform flow implies that cross-sectional area and flow velocity vary with respect to longitudinal position. The following second ordered parabolic partial differential equation describes the rate change in temperature for non-uniform flow.

Equation 3.7. Non-Uniform One-dimensional Heat Energy Transfer

$$\frac{\partial T}{\partial t} = -U_x \cdot \frac{\partial T}{\partial x} + D_L \cdot \frac{\partial^2 T}{\partial x^2} + \frac{\Phi}{c_p \cdot \rho \cdot D_i}$$

Steady Flow: $\frac{\partial U_x}{\partial t} = 0$ Non-Uniform Flow: $\frac{\partial U_x}{\partial x} \neq 0$

The solution to the *one-dimensional heat energy transfer equation* is essentially the summation of thermodynamic heat energy exchange between the stream system and the surrounding environment and physical processes that redistribute heat energy within the stream system. It is important to note that all heat energy introduced into the stream is conserved, with the net result reflected in stream temperature magnitude. Further, heat energy is transient within the stream system, due to longitudinal advective and dispersive transfer of heat energy. The net heat energy flux (Φ) is calculated at every distance step and time step based on physical and empirical formulations developed for each significant energy component. The dispersion coefficient (D_L) may either be specified by the model user, or assumed to equal zero, in which, only numerical dispersion occurs. Efforts to

accurately predict stream temperatures have focused on finite difference solutions to the three modes of heat energy transport and change: advection, dispersion and energy balance.

3.1.2 Non-Uniform Heat Transfer Equation (Implicit Form)

Transformation of the *non-uniform heat transfer equation* into a central difference implicit form will now be demonstrated.

Recall *Equation 3.7.*,

$$\frac{\partial T}{\partial t} = -U_x \cdot \frac{\partial T}{\partial x} + D_L \cdot \frac{\partial^2 T}{\partial x^2} + \frac{\Phi}{c_p \cdot \rho \cdot D_i},$$

which can be expressed as,

$$\frac{\left(T_i^{t+1} - T_i^t\right)}{\Delta t} = \frac{-\left(U_x \cdot T\right)_{i+1}^{t+1} + \left(U_x \cdot T\right)_{i-1}^{t+1}}{2 \cdot \Delta x} + \frac{D_L \cdot \left(T_{i-1}^{t+1} - 2T_i^{t+1} + T_{i+1}^{t+1}\right)}{\Delta x^2} + \frac{\Phi}{c_p \cdot \rho \cdot D_i}.$$

Assume that: $\left(U_x\right)_i = \frac{Q_i}{A_i}$,

substitution yields,

$$\frac{\left(T_i^{t+1} - T_i^t\right)}{\Delta t} = \frac{-\left(\frac{Q}{A} \cdot T\right)_{i+1}^{t+1} + \left(\frac{Q}{A} \cdot T\right)_{i-1}^{t+1}}{2 \cdot \Delta x} + \frac{D_L \cdot \left(T_{i-1}^{t+1} - 2T_i^{t+1} + T_{i+1}^{t+1}\right)}{\Delta x^2} + \frac{\Phi}{c_p \cdot \rho \cdot D_i}$$

which simplifies to,

$$\left(T_i^{t+1} - T_i^t\right) = -\left(\frac{\Delta t \cdot Q_{i+1}}{2 \cdot \Delta x \cdot A_{i+1}} \cdot T_{i+1}^{t+1}\right) + \left(\frac{\Delta t \cdot Q_{i-1}}{2 \cdot \Delta x \cdot A_{i-1}} \cdot T_{i-1}^{t-1}\right) + \frac{\Delta t \cdot D_L}{\Delta x^2} \cdot \left(T_{i-1}^{t+1} - 2T_i^{t+1} + T_{i+1}^{t+1}\right) + \frac{\Delta t \cdot \Phi}{c_p \cdot \rho \cdot D_i}$$

Define: $\delta_i = \frac{\Delta t \cdot Q_i}{2 \cdot \Delta x \cdot A_i}$

$$\lambda = \frac{\Delta t \cdot D_L}{\Delta x^2}$$

Substitution yields,

$$\left(T_i^{t+1} - T_i^t\right) + \left(\delta_{i+1} \cdot T_{i+1}^{t+1}\right) - \left(\delta_{i-1} \cdot T_{i-1}^{t-1}\right) = \lambda \cdot \left(T_{i-1}^{t+1} - 2T_i^{t+1} + T_{i+1}^{t+1}\right) + \frac{\Delta t \cdot \Phi}{cp \cdot \rho \cdot D_i}$$

which simplifies to,

$$T_i^t + \frac{\Delta t \cdot \Phi}{c_p \cdot \rho \cdot D_i} = \left(-\delta_{i-1} - \lambda\right) \cdot T_{i-1}^{t-1} + (1 + 2\lambda) \cdot T_i^{t+1} + \left(\delta_{i+1} - \lambda\right) \cdot T_{i+1}^{t+1}.$$

Define: $a_i = -\delta_{i-1} - \lambda$

$$b_i = 1 + 2\lambda$$

$$c_i = \delta_{i+1} - \lambda$$

$$d_i = T_i^t + \frac{\Delta t \cdot \Phi}{c_p \cdot \rho \cdot D_i}$$

Substitution yields,

Equation 3.8. Non-Uniform Heat Transfer Equation (Implicit Form)

$$d_i = a_i \cdot T_{i-1}^{t+1} + b_i \cdot T_i^{t+1} + c_i \cdot T_{i+1}^{t+1}.$$

3.1.3 Boundary Conditions and Initial Values

Boundary conditions are defined for the finite difference solution and displayed in Figure 3.2. The temperatures at the upstream boundary (i_o) for all time steps (t_o ,$t_{1,}$,..., t_{M-1}, t_M) are supplied by the upstream temperature inputs. At the down steam boundary it is

assumed that temperature remains constant at longitudinal position i_N with respect to time, $\frac{\partial T}{\partial t} = 0$.

It is assumed that initial values of the temperatures at each distance node (i_o ,$i_{1,}$..., i_{N-1}, i_N) occurring at the starting time (t_o) are equal to the boundary condition at time t_o. The initial values can then be stated as: $\frac{\partial T}{\partial x} = 0$ for time t_o.

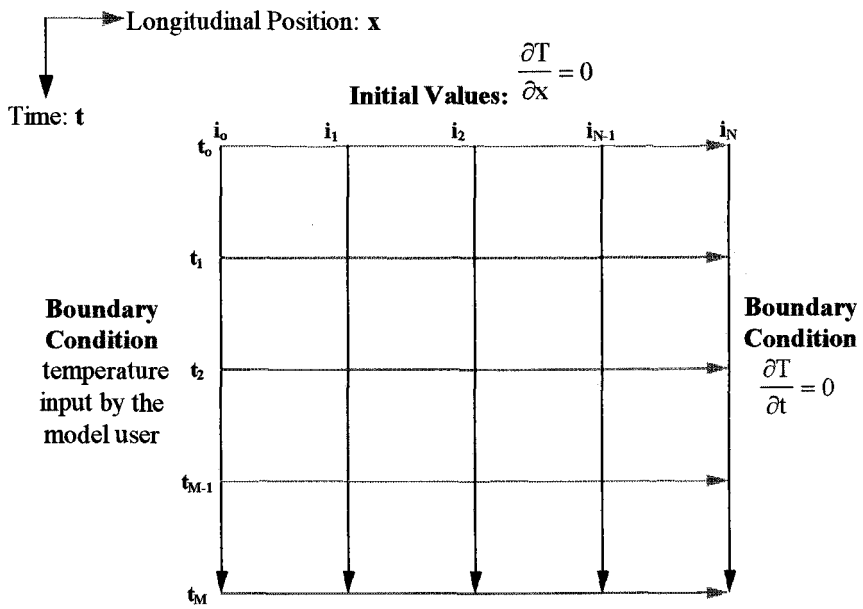

Figure 3.2. Boundary conditions and initial values

3.1.4 Simultaneous Solution

Equation 3.8 is applied to every distance node (i_o ,$i_{1,}$..., i_{N-1}, i_N) for each time step (t_o ,$t_{1,}$..., t_{M-1}, t_M). A series of equations is developed that can be solved simultaneously

using a tri-diagonal matrix method developed by Thomas (1949). The matrix takes the following form.

$$
\begin{aligned}
b_1 T_1^{t+1} + c_1 T_2^{t+1} &= d_1 - a_1 \cdot T_0^{t+1} \\
a_2 T_1^{t+1} + b_2 T_2^{t+1} + c_2 T_3^{t+1} &= d_2 \\
a_3 T_2^{t+1} + b_3 T_3^{t+1} + c_3 T_4^{t+1} &= d_3 \\
a_i T_{i-1}^{t+1} + b_i T_i^{t+1} + c_i T_{i+1}^{t+1} &= d_i \\
a_{N-1} T_{N-2}^{t+1} + b_{N-1} T_{N-1}^{t+1} + c_{N-1} T_N^{t+1} &= d_{N-1} \\
\left(a_N + c_N\right) T_{N-1}^{t+1} + b_N T_N^{t+1} &= d_N
\end{aligned}
$$

All values of a_i, b_i, c_i, and d_i are known. The routine for the simultaneous solution of the tri-diagonal matrix for each time step utilizes the following algorithms (Carnahan et. al. 1969).

$$\beta_1 = b_1 \qquad \beta_i = b_i - \frac{a_i \cdot c_{i-1}}{\beta_{i-1}} \qquad (i = 2,3,4,\ldots,N)$$

$$\gamma_1 = \frac{d_1}{\beta_1} \qquad \gamma_i = \frac{d_i - a_i \cdot \gamma_{i-1}}{\beta_i} \qquad (i = 2,3,4,\ldots,N)$$

$$T_N = \gamma_N \qquad T_i = \gamma_i - \frac{c_i \cdot T_{i+1}}{\beta_i} \qquad (i = N-1, N-2, \ldots, 1)$$

3.1.5 Spatial and Temporal Scale

The length of the defined reach is limited by the assumption that the upstream and downstream portions of the reach are relatively homogenous. For each defined reach the

model user may describe two unique site inputs. *Heat Source* allows the upstream and downstream site description to differ. For each time step, *Heat Source* calculates every distance step, starting at the top of the defined reach, and progressing to the end of the reach. From the top of the reach, the characteristics of the upstream site are assumed. From the mid-point of the reach to the end of the reach, the downstream site characteristics are assumed. As of the time of this writing, no limits to reach length have been established. Theoretically, the only limitations to reach length are that the reach is relatively homogenous and that no surface inflow from merging water bodies occurs in the defined reach.

Heat Source is designed to analyze and predict stream temperature for a duration of one to four days, however, *Heat Source* is primarily concerned with daily prediction of the diurnal energy flux. Prediction time steps are limited by stability considerations for the finite difference solution method.

3.1.6 Atmospheric Parameters

The optical air mass thickness at the site elevation (M) is estimated as a function of the optical air mass at sea level (M_o) and the ratio of air pressure at stream elevation to the air pressure at sea level ($P_{stream:sea}$) (Wunderlich 1972).

Equation 3.9. Optical Air Mass Thickness,

$$M = M_o \cdot P_{stream:sea}$$

Robinson (1966) estimates the value for the optical air mass thickness at sea level (M_o) as a function of the zenith angle (θ_{zenith}) or a function of solar altitude (θ_{sun}).

Equation 3.10. Optical Air Mass at Sea Level

$$M_o = \frac{1}{\cos\theta_{zenith}} = \frac{1}{\sin\theta_{sun}}$$

Total atmospheric pressure (P_{total}) is found as a function of the ratio of the air pressure at the stream surface and the air pressure at sea level ($P_{stream:sea}$).

Equation 3.11. Total Atmospheric Pressure

$$P_{total} = 1000 \cdot P_{stream:sea}$$

where,

P_{total}: atmospheric air pressure (mbar)
$P_{stream:sea}$: ratio of air pressure at stream to sea levels

The ratio of the air pressure at the stream elevation to the air pressure at sea level ($P_{stream:sea}$) is a function of the site elevation (Z) (List 1966).

Equation 3.12. Ratio of Air Pressure at Stream Elevation to that at Sea Level

$$P_{stream:sea} = \left(\frac{288 - 0.0065 \cdot Z}{288}\right)^{5.256}.$$

The Magnus-Tetens formula, as reported by Kleinschmidt (1935), approximates saturation vapor pressure (e_s) as a function of air temperature (T_{air}). This method was developed for application over plane ice or water surfaces at standard atmospheric pressure for air temperature greater than 0° C.

Equation 3.13. Saturation Vapor Pressure

$$e_s = \exp\left[2.3026 \cdot \left(\frac{7.5 \cdot T_{air}}{T_{air}+237.3} + 0.7858\right)\right]$$

where,

e_s: saturation vapor pressure (mbar)
T_{air}: air temperature (°C)

Atmospheric vapor pressure (e_a) is a function of the midday relative humidity (RH) and the saturation vapor pressure (e_s) (Bedient and Huber 1992).

Equation 3.14. Atmospheric Vapor Pressure

$$e_a = \frac{RH \cdot e_s}{100}$$

where,

e_a: air vapor pressure (mbar)
RH: relative humidity (%)

In rare cases, when the vapor gradient in the air exceeds the vapor gradient of water, condensation will occur, representing an energy input to the stream system. If the temperature is below the saturation temperature, then condensation occurs and the vapor pressure of the air becomes the saturation vapor pressure for the given temperature. The temperature at which condensation begins to occur is a function of atmospheric vapor pressure and is estimated in the modified Tabata equation.

Equation 3.15. Modified Tabata Equation

$$T_{sat} = \left\{ \frac{5347.5}{\left[21.382 - \log_e \left(\frac{e_a}{1.01725} \right) \right]} \right\} - 273$$

where,

T_{sat}: saturation temperature: Dew point (°C)
e_a: air vapor pressure (mbar)

When saturation temperature occurs, the vapor pressure of the air (e_a) is equal to that of the saturation vapor pressure (e_s).

$$e_a = e_s$$

It should be noted that *Heat Source* does not include effects of condensation. Condensation may contribute measurable quantities of heat energy to the theoretical stream system when the air temperature is below the dew point for a long duration. The methods for estimating condensation are, however, considered inaccurate and site specific. In the event that *Heat Source* is simulating during periods where the dew point is reached for significant periods, stream temperature prediction errors may result. In summer months it is assumed that the air temperature exceeds the dew point for the majority of the simulation duration and that the water content of the atmosphere is low, making the contribution of heat energy from condensation processes negligible.

The virtual temperature difference is the difference in virtual temperatures of ambient air (VT_{air}) and saturated air (VT_{sat}) at the air-water interface. It is important to account for the virtual temperature difference when the water temperature is high and

wind speed is low because in such situations free convection occurs, allowing the rate of cooling to increase (Trenberth 1992, Beschta 1984).

Equation 3.16. Virtual Temperature Difference

$$VT_{diff} = VT_{sat} - VT_{air}$$

where,

VT_{air}: virtual air temperature (°C)
VT_{diff}: virtual temperature difference (°C)
VT_{sat}: virtual saturation temperature (°C)

Virtual temperature of ambient air directly above the stream is the temperature of the same parcel of air if it were completely dry, but maintaining the same density and total pressure. Virtual air temperature is estimated as a function of atmospheric pressure (P_{total}) and vapor pressure (e_a) (Trenberth 1992, Beschta 1984).

Equation 3.17. Virtual Temperature of Ambient Air

$$VT_{air} = \frac{P_{total}}{\left(P_{total} - 0.378 \cdot e_a\right)} \cdot T_{air}$$

The virtual temperature at the water surface (VT_{sat}) is the predicted temperature of the same parcel of air without vapor present, but with equivalent density and total pressure. Virtual saturation temperature is estimated as a function of atmospheric pressure (P_{total}) and saturation vapor pressure (e_s) (Trenberth 1992, Beschta 1984).

Equation 3.18. Virtual Saturation Temperature

$$VT_{sat} = \frac{P_{total}}{\left(P_{total} - 0.378 \cdot e_s\right)} \cdot T_{air}$$

3.1.7 Solar Parameters

Solar time is based on the rotation of the earth about its axis and the revolution of the earth about the sun. A solar day is the interval of time that the sun appears to complete one full revolution around a point on the earth. It should be noted that the length of one day in solar time may be less than 24 hours. Ibqal (1983) calculates the equation of time (E_t) as a function of the day angle (Γ).

Equation 3.19. Equation of Time

$$E_t = \frac{\left(7.5\cdot 10^{-5} + 0.002\cdot\cos(\Gamma) - 0.032\cdot\sin(\Gamma) - 10.015\cdot\cos(2\Gamma) - 0.041\cdot\sin(2\Gamma)\right)}{0.004363}$$

The day angle (Γ) is calculated in the following equation (Ibqal 1983).

Equation 3.20. Day Angle

$$\Gamma = \frac{2\pi\cdot(d_n - 1)}{365}$$

where,

d_n: day number of the year
Γ: day angle (radians)

A time correction must account for the elliptical shape of the earth, resulting in the difference between the local and standard meridians. The longitude time correction (L_t) is roughly 4 minutes for every degree (Ibqal 1983).

Equation 3.21. Longitude Time Correction

$$L_t = 4\cdot(L_s - L_e)$$

where,

L_e: local Longitude (degrees)
Ls: standard longitude (degrees)
L_t: longitude correction (day fraction)

The corrected solar time (t_{local}) can then be calculated (Ibqal 1983).

Equation 3.22. Corrected Local Solar Time

$$t_{local} = LAT + E_t + L_t$$

where,

E_t: equation of time (day fraction)
LAT: local standard time (day fraction)
t_{local}: local standard time (day fraction)

The hour angle (ω), also referred to as the angular rotation of the earth, is calculated to approximate the position of the sun relative to a fixed position on the earth's surface (Ibqal 1983).

Equation 3.23. Hour Angle Approximation

$$\omega = 2\pi \cdot t_{local}$$

The radius vector (r) is the ratio of the actual distance between the earth and sun to the mean distance between the earth and sun. It is required for the calculation of extra-terrestrial solar radiation (Wunderlich 1972).

Equation 3.24. Radius Vector

$$r = 1 + 0.017 \cdot \cos\left(\frac{2\pi}{365}\left(186 - t_{julian}\right)\right)$$

where,

r: radius vector
t_{julian}: summation of Julian day and fraction of day

Solar declination (δ) is the angle between an imaginary line between the centers of the earth, and sun and the earth's equatorial plane. This angle is constantly changing as a function of time and is estimated with respect to the Julian day number (Iqbal 1983).

Equation 3.25. Solar Declination

$$\delta = 23.45 \cdot \left(\frac{\pi}{180}\right) \cdot \cos\left[\frac{2\pi}{365} \cdot \left(172 - t_{julian}\right)\right]$$

where,

δ: solar declination (radians)
t_{julian}: summation of Julian day and fraction of day

Solar altitude (θ_{sun}), also called solar height, is calculated as a function of local mean time (t_{local}), the angular rotation of the earth (ω), the site specific latitude ($\theta_{latitude}$) and the solar declination (δ) (Iqbal 1983).

Equation 3.26. Solar Altitude

$$\theta_{sun} = \sin^{-1}\left[\left(\cos\theta_{latitude} \cdot \cos\delta \cdot \cos\omega \cdot t_{local}\right) + \left(\sin\theta_{latitude} \cdot \sin\delta\right)\right]$$

where,

$\theta_{latitude}$: latitude (radians)
$\theta_{longitude}$: longitude (radians)
θ_{sun}: solar altitude (radians)
ω: angular rotation of the earth (radians)
δ: solar declination (radians)
t_{local}: solar time (day fraction)

The solar azimuth ($\theta_{azimuth}$), in degrees clockwise from the north, is the angle at the local zenith between the plane of the observer's meridian and the plane of a circle passing through zenith and the sun (Iqbal 1983).

Equation 3.27. Solar Azimuth

$$\theta_{azimuth} = \cos^{-1}\left(\frac{\sin\theta_{sun}\cdot\sin\theta_{latitude} - \sin\delta}{\cos\theta_{sun}\cdot\cos\theta_{latitude}}\right)$$

The zenith angle (θ_{zenith}) is the angle that exists between the angle of the sun and a vector normal to the horizontal surface of the earth and is a function of the solar altitude (θ_{sun}) (Iqbal 1983).

Equation 3.28. Zenith Angle

$$\theta_{zenith} = \cos^{-1}\left(\sin\delta\cdot\sin\theta_{latitude} + \cos\delta\cdot\cos(t\cdot\omega)\right) = 90 - \theta_{sun}$$

The apparent zenith angle ($\theta_{apparent}$) is the angle that exists between the angle of the sun and a vector normal to the stream surface and is a function of solar altitude (θ_{sun}), stream slope (θ_{slope}), stream aspect (θ_{aspect}) in degrees clockwise from the south, and solar azimuth ($\theta_{azimuth}$) (Iqbal 1983).

Equation 3.29. Apparent Zenith Angle

$$\theta_{apparent} = \cos^{-1}\left[\sin\theta_{sun}\cdot\cos\theta_{slope} + \cos\theta_{sun}\cdot\sin\theta_{slope}\cdot\cos\left(\theta_{aspect} - \theta_{azimuth}\right)\right]$$

where,

$\theta_{apparent}$: apparent solar zenith (radians)
θ_{aspect}: stream aspect (radians clockwise from north)
$\theta_{azimuth}$: solar azimuth(radians)
θ_{slope}: stream slope (radians)
θ_{sun}: solar altitude (radians)

3.1.8 Stream Parameters

The reflectivity of the stream surface ($ALBEDO_{stream}$) is estimated as a function of the apparent solar zenith angle ($\theta_{apparent}$) (Sellers 1965).

Equation 3.30. Reflectivity of Stream Surface

For $\left(0^{o} \le \theta_{apparent} \le 80^{o}\right)$,

$$ALBEDO_{stream} = \left(\frac{0.091}{\cos\theta_{apparent}}\right) - 0.0386$$

For $\left(80^{o} \le \theta_{apparent} \le 90^{o}\right)$,

$$ALBEDO_{stream} = \left(0.0515 \cdot \theta_{apparent}\right) - 3.635$$

The stream bed albedo ($ALBEDO_{bed}$), or fraction of incoming heat energy that is reflected from the stream bed surface, is determined as a function of the apparent zenith angle ($\theta_{apparent}$) (Beschta 1984).

Equation 3.31. Stream Bed Albedo

$$ALBEDO_{bed} = \exp\left[\left(0.0214 \cdot \theta_{apparent}\right) - 1.941\right]$$

The efficiency of direct beam solar radiation transmission through a column of stream water along a specified path length (S_3S_4) is calculated as a function of average stream depth ($DEPTH_{ave}$) (Austin and Halikas 1976).

Equation 3.32. Transmissivity of Stream Column

$$TRANS_{stream} = 0.415 - \left[0.194 \cdot \log_{10}(D_i)\right]$$

where,

$TRANS_{stream}$: transmissivity of water column
D_i: average depth of water column (m)

Sellers (1965) showed that as heat energy was transferred to stream bedrock, that a portion of the heat energy was directly transferred back to the stream. The partitioning of heat energy between stream and stream bed, as cited by Beschta (1984) and described by Sellers (1965), is a function of the heat capacity of water (C_{stream}), the thermal diffusivity of the stream (K_{stream}), the heat capacity of bedrock ($C_{bedrock}$) and the thermal diffusivity of bedrock ($K_{bedrock}$).

Equation 3.33. Ratio of Stream and Stream Bed Absorption

$$RATIO_{stream:bedrock} = \frac{\Phi_{stream}}{\Phi_{bedrock}} = \frac{C_{stream} \cdot \left(K_{stream}\right)^{\frac{1}{2}}}{C_{bedrock} \cdot \left(K_{bedrock}\right)^{\frac{1}{2}}} = \frac{1.0 \frac{cal}{cm^3\,^oC} \cdot \left(0.010 \frac{cm^2}{s}\right)^{\frac{1}{2}}}{0.53 \frac{cal}{cm^3\,^oC} \cdot \left(0.045 \frac{cm^2}{s}\right)^{\frac{1}{2}}} \approx 0.9$$

where,

$RATIO_{stream:bedrock}$: ratio of stream water column to stream bed short-wave radiation absorption

$$\left(RATIO_{stream:bedrock} = \frac{\Phi_{stream}}{\Phi_{bedrock}} = 0.9\right)$$

$C_{bedrock}$: heat capacity of bedrock

$$\left(C_{bedrock} = 0.53 \frac{cal}{cm^3\,^oC}\right)$$

$K_{bedrock}$: thermal diffusivity of bedrock

$$\left(K_{bedrock} = 0.045 \frac{cm^2}{s} (quartz)\right)$$

C_{stream}: heat capacity of stream water column

$$\left(C_{stream} = 1.0 \frac{cal}{cm^3 . ^o C}\right)$$

K_{stream}: thermal diffusivity of stream water column

$$\left(K_{stream} = 0.010 \frac{cm^2}{s}\right)$$

The heat energy ratio of stream adsorption and bedrock retention serves to partition the solar radiation flux when it encounters bedrock. Beschta (1984) shows that the fraction of heat energy absorbed by bedrock divided by the fraction of heat energy absorbed by the stream is roughly 53%. In other terms, when one unit of heat energy encounters bedrock material, 47% is absorbed by the water column and 53% is transferred to stream bed material.

Equation 3.34. Fraction of Heat Energy Absorbed by the Stream

$$\lambda_{bedrock} = \frac{BedrockHeat}{StreamHeat} = \frac{1.0}{(1..0 + 0.9)} = 0.53$$

where,

$\lambda_{bedrock}$: fraction of heat energy absorbed by the stream

3.1.9 Stream Side Shading

Once emitted from the sun, photons travel through space to the edge of the atmosphere, at an average intensity referred to as the solar constant (C_{solar}). While passing through the atmosphere solar radiation is absorbed and scattered by ozone, water vapor, dry air and particulates (McCutcheon 1989). Depending on the characteristics of stream

side vegetation and the time of day, an individual photon may or may not encounter a vegetative barrier before arriving at the stream surface.

This brief summary of the sun-stream pathway simplifies the complexity of the atmosphere and stream side vegetation. Further, it relies on the easily predicted position of a particular location on the earth relative to the sun. Simplifying assumptions estimate the atmospheric effects of attenuation and shading while allowing for quantification of stream side vegetation characteristics.

Solar radiation must travel through riparian vegetation where a portion of the incoming solar flux (Φ_{solar}) is scattered and attenuated. Riparian vegetation represents a physical barrier which diminishes the intensity of solar radiation experienced by the stream. Figure 3.3 depicts all possible angles that occur within the positive diurnal solar radiation flux.

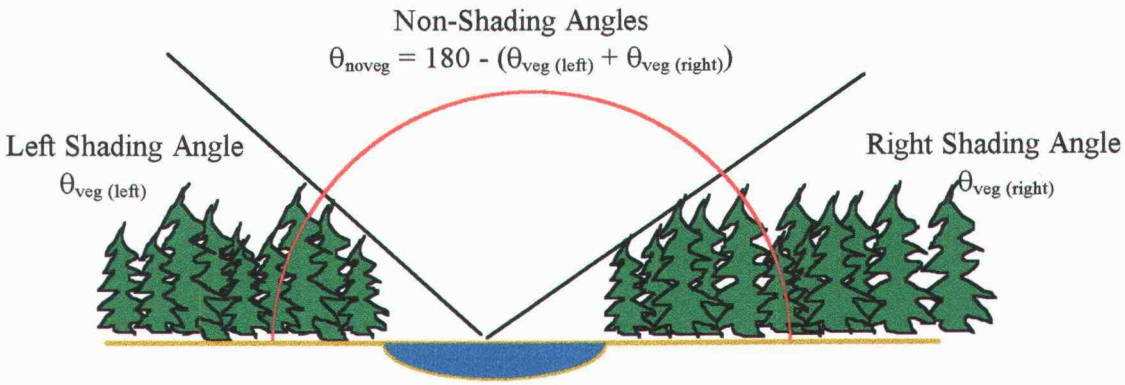

Figure 3.3. Vegetation shading and non-shading angles.

For direct beam radiation, the z-direction solar angle ($\theta_{z\text{-}direction}$),as shown in Figure 3.4, must be determined for routing of direct beam radiation through the vegetation

canopy. The z-direction angle is calculated for each stream bank and used for routing incoming solar radiation through the canopy.

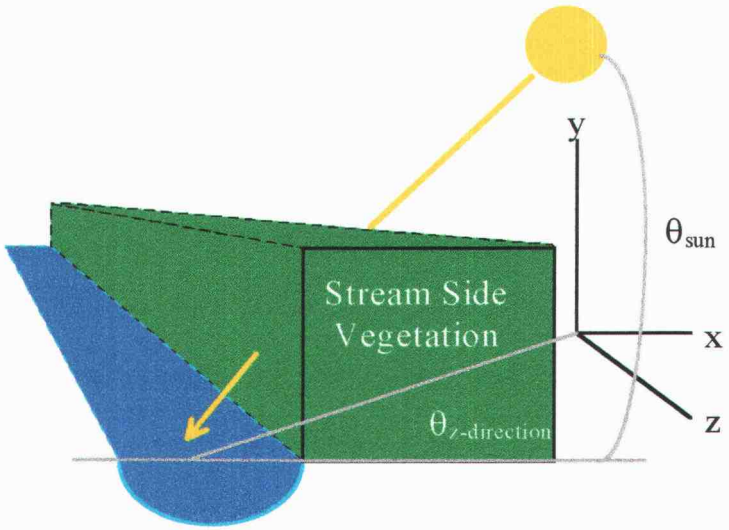

Figure 3.4. Z-Direction Angle

Two parameters of stream side vegetation will control the effectiveness of shading: [1]stream side vegetation density and [2]the path length for which the radiation must pass through stream side vegetation to reach the stream surface. Figure 3.5 depicts the solar angle (θ_{sun}), the stream bank slope (θ_{topo1}), the maximum topographic shading angle (θ_{topo2}), the partial path length from the outer most limits of the earth's atmosphere to the top of the vegetation canopy (S_0S_1), the partial path length through stream side vegetation (S_1S_2), the partial path length from the vegetation canopy to the stream surface (S_2S_3), and partial path length from the stream surface to the stream bed (S_3S_4).

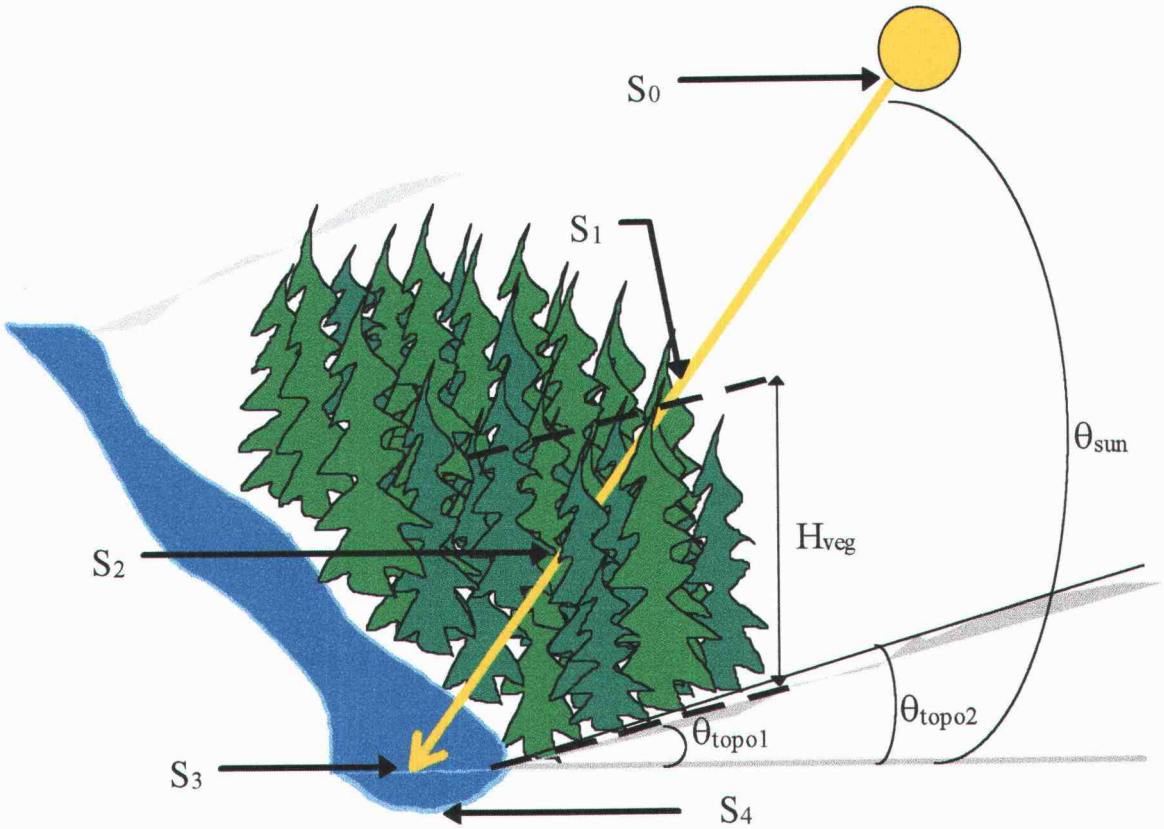

Figure 3.5. Shading angles and partial path lengths.

Several atmospheric and solar parameters are calculated to find the average path length for which incoming solar radiation must travel through the vegetation canopy while en route to the stream. The distance solar radiation must travel through vegetative boundary (S_1S_2) is estimated in the following equation (Beschta 1984).

Equation 3.35. Travel Distance Through Vegetation Canopy

$$S_1S_2 = \left[\frac{H_{veg}}{\left(\tan\theta_{veg} - \tan\theta_{topo1}\right)}\right] \cdot \left[\frac{\cos\theta_{topo1} \cdot \left(\tan\theta_{veg} - \tan\theta_{sun}\right)}{\sin\left(\theta_{sun} - \theta_{topo1}\right)}\right]$$

where,

H_{veg}: height of stream side vegetation (m)
S_1S_2: solar path length through vegetation (m)
θ_{sun}: solar altitude (degrees)
θ_{topo1}: bank slope (degrees)
θ_{veg}: maximum shading angle (degrees)

The distance solar radiation must travel from vegetative boundary to the center of stream (S_2S_3) is estimated in the following equation (Beschta 1984).

Equation 3.36. Travel Distance From Vegetation Canopy to Stream Surface

$$S_2S_3 = \left(\frac{1}{\cos\theta_{sun}}\right) \cdot \left(\frac{H_{veg}}{\tan\theta_{veg} - \tan\theta_{topo1}}\right)$$

Sellers found that 50% of solar heat energy entering pure water at a perpendicular angle of incidence is dissipated in the initial 10 cm of depth. It is, therefore, necessary to calculate the instantaneous path length of incoming direct solar radiation from the stream surface to the stream bed (S_3S_4) as a function of average stream depth (D_i) and the solar zenith angle (q_{zenith}) (Williams 1970).

Equation 3.37. Travel Distance Through Stream Column

$$S_3S_4 = \frac{D_i}{\cot\left(\frac{\sin\theta_{zenith}}{1.333}\right)}$$

where,

D_i: average stream depth (m)
S_3S_4: path length through stream (m)
θ_{zenith}: solar zenith angle (degrees)

The first estimate of the solar radiation path length through the vegetation barrier (SUN_1) is detailed by Beschta (1984).

Equation 3.38. First Estimate of Solar Path length Through Vegetation

$$SUN_1 = \frac{S_1 S_2}{H_{veg}}$$

The second estimate of the solar radiation path length through the vegetation barrier (SUN_2) is also provided by Beschta (1984).

Equation 3.39. Second Estimate of Solar Path length Through Vegetation

$$SUN_2 = SUN_1 + \frac{S_2 S_3}{H_{veg}}.$$

The average solar radiation path length, corrected for the z-direction solar angle ($\theta_{z\text{-direction}}$), is then calculated.

Equation 3.40. Average of Solar Path Length Through Vegetation

$$SUN_{ave} = \left[\frac{(SUN_1 + SUN_2)}{2 \cdot \cos\theta_{z-direction}} \right]$$

The radiation attenuation function is calculated as a function of the canopy coefficient (C_{veg}) and the solar path length through the vegetation canopy (SUN_{ave}). The canopy coefficient (C_{veg}) is the fraction of volume within the vegetation zone which attenuates and/or scatters incoming solar radiation (i.e. 0 - 1). The value of the canopy coefficient is determined by: [1]estimation by model user or [2]model solution by use of energy relationships. The vegetative barrier transmissivity coefficient ($TRANS_{veg}$) is determined as a function of the canopy coefficient (C_{veg}) (Beschta 1984).

Equation 3.41. Vegetation Transmissivity

$$\mathrm{TRANS}_{veg} = 1 - \left(0.9 \cdot \mathrm{C}_{veg}\right)$$

Attenuation of incoming solar radiation (ATTEN) within the vegetation boundary is predicted as a function of vegetation transmissivity (TRANS_{veg}) (Beschta 1984).

Equation 3.42. Vegetation Attenuation of Incoming Solar Radiation

$$\mathrm{ATTEN} = \left[\mathrm{TRANS}_{veg}\right]^{\mathrm{SUN}_{ave}}$$

There is no solar energy flux through topographic barriers; the incoming direct beam solar flux is completely attenuated. Local dawn and dusk, and therefore, the timing of the local diurnal solar radiation cycle, are controlled by the topographic shading angles, as shown in Figure 3.6.

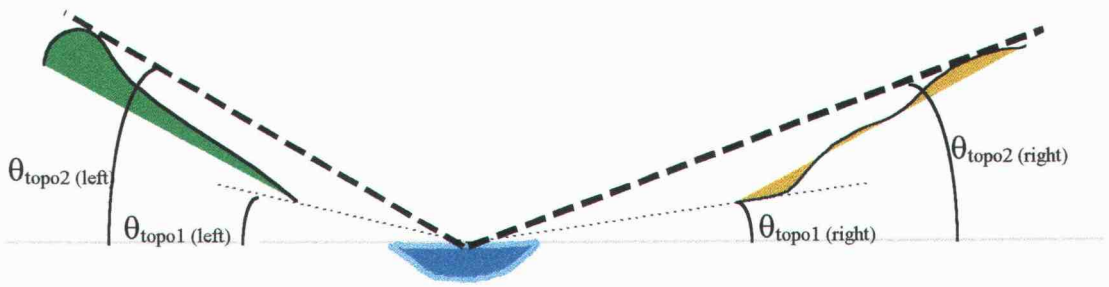

Figure 3.6. Topographic shading angles.

The diurnal positive solar radiation flux begins when the angle of incoming solar radiation is greater than the topographic shading angle at local dawn ($\theta_{sun} \geq \theta_{topo2}$). Conversely, local dusk occurs when the angle of incoming solar radiation is less than the topographic shading angle ($\theta_{sun} \leq \theta_{topo2}$).

By definition, local sunrise occurs when the center of the sun, from which the solar angle is estimated, is equal to that of the eastern topographic horizon. At sunrise the sun

is east of the local upper celestial meridian and is estimated using a modification of the solar altitude equation (Wunderlich 1972).

Equation 3.43. Hour Angle at Sunrise Approximation

$$\cos\omega_{sr} = \frac{\sin\theta_{topo2(east)} - (\sin\theta_{latitude} \cdot \sin\delta)}{(\cos\theta_{latitude} \cdot \cos\delta)} = \cos\omega_{sr}'$$

where,

ω_{sr}: hour angle at sunrise, measured westward from upper celestial meridian: $\pi < \omega_{sr} < 2\pi$ (radians)

ω_{sr}': complimentary sunrise angle: $\omega_{sr}' < \pi/2$ (radians)

If $\omega_{sr}' < 0$ then,

$$\omega_{sr} = \pi + |\omega_{sr}'|$$

If $\omega_{sr}' \geq 0$ then,

$$\omega_{sr} = 2\pi - \omega_{sr}'$$ (Wunderlich 1972)

$\theta_{topo2(east)}$: eastern topographic shade angle: solar altitude at sunrise (radians)

$\theta_{latitude}$: local latitude (radians)

δ: solar declination (radians)

For general approximation it is assumed that the sunset solar angle is equal to the western topographic shading angle, which allows estimation of the hour angle at sunset (ω_{ss}) (Wunderlich 1972).

Equation 3.44. Hour Angle at Sunset Approximation

$$\cos\omega_{sr} = \frac{\sin\theta_{topo2(east)} - (\sin\theta_{latitude} \cdot \sin\delta)}{(\cos\theta_{latitude} \cdot \cos\delta)} = \cos\omega_{sr}'$$

The relationship between corrected local solar time and the hour angle allow estimation of local standard time of both sunrise and sunset.

Equation 3.45. Standard Local Time Determination

$$LAT = \frac{\omega}{2\pi} - E_t - L_t$$

where,

E_t: equation of time (day fraction)
LAT: local standard time (day fraction)
L_t: longitude correction (day fraction)
ω: generic hour angle: $\omega = \omega_{sr}$ or $\omega = \omega_{ss}$ (day fraction)

Day length determination becomes trivial after the standard local time is determined for both sunrise and sunset hour angles.

Equation 3.46. Day Length Determination

$$t_{day} = LAT_{ss} - LAT_{sr}$$

where,

t_{day}: day length (day fraction)
LAT_{sr}: sunrise local standard time (day fraction)
LAT_{ss}: sunset local standard time (day fraction)

3.1.10 Stream/River System Energy Balance

In general, the net energy flux experienced by all stream/river systems follows two cycles: a seasonal cycle and a diurnal cycle. In the Pacific Northwest, the seasonal net energy cycle experiences a maximum positive flux during summer months (July and August), while the minimum seasonal flux occurs in winter months (December and January). The diurnal net energy cycle experiences a daily maximum flux that occurs at or near the sun's zenith angle, while the daily minimum flux often occurs during the late night or the early morning. It should be noted, however, that the diurnal heat energy cycle may be inconsistent with past or future daily stream temperature profiles when meteorological

conditions are variable. Cloud cover and precipitation seriously alter the energy relationship between the stream and its environment.

Water has a relatively high heat capacity ($c_w = 10^3$ cal·kg^{-1}·K^{-1}) (Scatterlund and Adams 1992). Conceptually, water is a heat sink. Heat energy that is gained by the stream is retained and only slowly released back to the surrounding environment, represented by the cooling flux ($\Phi_{cooling}$). Heating periods occur when the net energy flux (Φ_{total}) is positive: ($\Phi_{heating} > \Phi_{cooling}$).

Equation 3.47. Heat Energy Continuity

$$\Phi_{total} = \Phi_{heating} - \Phi_{cooling}$$

where,

Φ_{total}: Net heat energy flux (cal/m^2·s)
$\Phi_{heating}$: Positive heat energy flux (cal/m^2·s)
$\Phi_{cooling}$: Negative heat energy flux (cal/m^2·s)

Water temperature is a function of the total heat energy contained in a discrete volume and may be described in terms of energy per unit volume $\left(\frac{E_i}{V_i}\right)$:

Equation 3.48. Heat Energy per Unit Volume

$$\frac{E_i}{V_i} = T_W \cdot \rho \cdot c_W = \frac{\text{energy}}{\text{volume}} = \frac{\text{cal}}{m^3}.$$

where,

c_w: Specific heat capacity of water (1000 cal/kg ·K)
E_i: Heat energy (cal)
ρ: Water density (1000 kg/m^3)
T_w: Water temperature (°C)
V_i: Volume (m^3)

It follows that large volume streams are less responsive to temperature change, and conversely, low flow streams will exhibit greater temperature sensitivity.

The net heat energy flux (Φ_{total}) consists of several individual thermodynamic energy flux components, as depicted in Figure 3.7, namely: solar radiation (Φ_{solar}), long-wave radiation ($\Phi_{longwave}$), conduction ($\Phi_{conduction}$), groundwater exchange ($\Phi_{groundwater}$) and evaporation ($\Phi_{evaporationl}$).

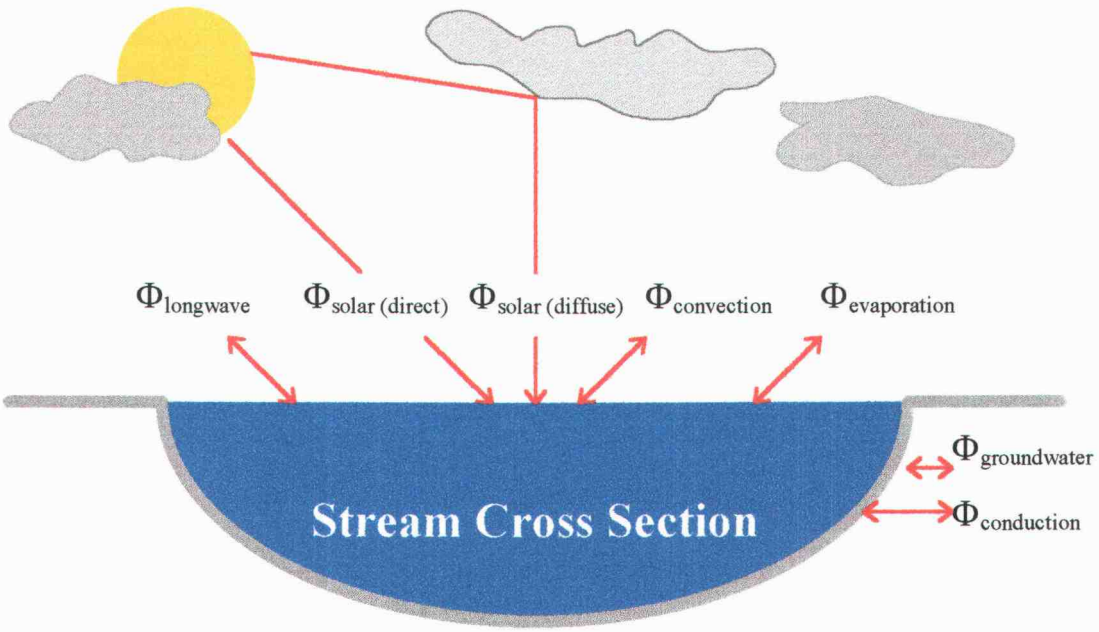

Figure 3.7. Components of the net energy flux.

The ultimate source of heat energy is solar radiation, both diffuse and direct. Secondary sources of heat energy include long-wave radiation, from both the atmosphere and stream side vegetation, stream bed conduction and in some cases, groundwater exchange at the water-stream bed interface. Several processes dissipate heat energy at the air-water interface, namely: evaporation, convection and back radiation. Heat energy is

acquired by the stream system when the flux of heat energy entering the stream is greater than the flux of heat energy leaving. The net energy flux provides the rate at which energy is gained or lost per unit area and is represented as the instantaneous summation of all heat energy components.

Equation 3.49. Net Heat Energy Continuity Equation

$$\Phi_{total} = \Phi_{solar} + \Phi_{longwave} + \Phi_{convection} + \Phi_{evaporation} + \Phi_{streambed} + \Phi_{groundwater}$$

3.1.10.1 Net Solar Radiation Flux: Φ_{solar}

Solar heat energy is treated sequentially in four steps: solar radiation flux experienced at the top of the outer fringe of the atmosphere, solar radiation flux received at the top of the vegetation canopy surrounding the stream, solar radiation flux transmitted to the stream surface and solar radiation flux transmitted through the stream water column. Solar radiation experienced at the outer limits of the earth's atmosphere, also referred to as extra-terrestrial solar radiation, is based on measured values of radiation emitted from the sun and the trigonomic relationship which accounts for the direct solar beam intensity on a tangential plane (Wunderlich 1972). With the accurate prediction of extra-terrestrial radiation, clear sky solar radiation experienced directly above the vegetation canopy surrounding the stream is a function of atmospheric transmittance. Clouded sky transmittance becomes difficult to model due to the great variability of cloud albedo and distribution. The accuracy of solar radiation flux prediction is seriously compromised in a clouded sky situation due to the extreme variability of atmospheric transmittance. Routing the solar radiation flux through the vegetation canopy relies on the

geometry of the vegetation, the transmittance of the vegetation and the path from the sun to the stream surface. The solar radiation flux then encounters the stream surface where radiation received will either reflect off the stream due to the stream albedo or penetrate the surface where the solar radiation is routed through the stream column as a function of stream morphology and water column transmittance.

The solar radiation flux (Φ_{solar}) is the summation of direct beam solar radiation flux (Φ_{direct}) and diffuse radiation flux ($\Phi_{diffuse}$), minus the solar energy flux that is absorbed by the stream bed ($\Phi_{absorbed}$):

Equation 3.50. Solar Radiation Continuity

$$\Phi_{solar} = \Phi_{direct} + \Phi_{diffuse} - \Phi_{absorbed}$$

where,

Φ_{solar}: solar radiation flux experienced by stream (cal/m^2 s)
Φ_{direct}: direct beam solar radiation flux penetrating stream surface (cal/m^2 s)
$\Phi_{diffuse}$: diffuse solar radiation flux penetrating stream surface (cal/m^2 s)
$\Phi_{absorbed}$: solar radiation flux which is absorbed by stream bed (cal/m^2 s)

Extra-terrestrial solar radiation intensity is the solar radiation flux that is experienced by the outer limits of the atmosphere and can be approximated given that the radius vector and the solar altitude are known (Wunderlich 1972).

Equation 3.51. Solar Flux Experienced at Outer Edge of Atmosphere

$$\Phi_{direct0} = \frac{\Phi_{constant}}{r^2} \sin\theta_{solar}$$

where,

$\Phi_{direct0}$: extra-terrestrial solar radiation flux (cal/m^2 sec)
$\Phi_{constant}$: solar radiation flux constant (333.33 cal/m^2 sec) (Wunderlich 1972)
r: radius vector
θ_{solar}: solar altitude (radians)

The flux of direct beam solar radiation available above stream side vegetation must account for attenuation and scattering induced by atmospheric transmissivity (τ_{atm}) along an instantaneous path length (Iqbal 1983).

Equation 3.52. Solar Radiation Flux Experienced at Top of Vegetation Canopy

$$\Phi_{direct1} = \Phi_{direct0} \cdot \tau_{atm}^{M} \cdot \cos\theta_{zenith}$$

where,

$\Phi_{direct1}$: direct beam solar radiation flux directly above vegetation canopy (cal/m^2 sec)
$\Phi_{direct0}$: extra-terrestrial solar radiation flux (cal/m^2 sec)
M: optical air mass thickness
τ_{atm}: atmospheric transmissivity
θ_{zenith}: solar zenith angle (radians)

Prediction of the direct solar radiation flux experienced directly above the stream surface must account for vegetative transmissivity (τ_{veg}) which induces attenuation and scattering effects. It is assumed that direct solar radiation follows a straight path from the sun to the stream surface. If the angle of solar incidence (θ_{solar}) is less than the maximum angle of vegetative shading, but greater than the maximum topographic shading angle, the solar path length is routed through a portion of the vegetative boundary ($\theta_{topo1} < \theta_{sun} < \theta_{veg}$).

Equation 3.53. Solar Radiation Flux Experienced by Stream Surface

$$\Phi_{direct2} = \Phi_{direct1} \cdot \tau_{veg}^{SUN}$$

where,

$\Phi_{direct2}$: direct beam solar radiation flux directly above stream surface (cal/m^2 sec)
$\Phi_{direct1}$: direct beam solar radiation flux directly above vegetation canopy (cal/m^2 sec)
SUN: solar path length through stream side vegetation (meters)
τ_{veg}: vegetation transmissivity

When the angle of solar incidence is greater than that of the maximum vegetation shading angle, the solar path length does not encounter the vegetative barrier and is routed directly to the stream surface ($\theta_{veg} < \theta_{sun}$).

$$\Phi_{direct2} = \Phi_{direct1}$$

The quantity of direct beam solar radiation delivered to the stream system, while accounting for the reflectivity of the stream surface (ψ_{stream}), is calculated as:

Equation 3.54. Net Solar Flux Experienced by Stream Surface

$$\Phi_{direct3} = \Phi_{direct2} \cdot (1 - \psi_{stream}).$$

where,

$\Phi_{direct3}$: direct beam solar radiation flux experienced by stream (cal/m^2 sec)
$\Phi_{direct2}$: direct beam solar radiation flux directly above stream surface (cal/m^2 sec)
ψ_{stream}: stream surface albedo

Diffuse solar radiation experienced at the top of the vegetative barrier as reported by Beschta (1984) is a function of an empirically based ratio between the direct beam solar radiation and diffuse solar radiation (Brooks 1959).

Equation 3.55. Diffuse Solar Radiation Flux at Top of the Vegetation Canopy

$$\Phi_{diffuse1} = \lambda_{direct:diffuse} \cdot \Phi_{direct1}$$

where,

$\Phi_{diffuse1}$: diffuse solar radiation flux at top of the vegetation canopy (cal/m^2 sec)
$\Phi_{direct1}$: direct beam solar radiation flux directly above vegetation canopy (cal/m^2 sec)
$\lambda_{direct:diffuse}$: ratio of direct to diffuse solar radiation

Diffuse radiation can be estimated as a function of the direct solar radiation for a cloudless atmosphere and is a function of the zenith angle (θ_{zenith}) as developed by Brooks (1959) and reported in Reifsnyder and Lull (1965).

Equation 3.56. Ratio of Direct to Diffuse Solar Radiation Flux

$$\lambda_{direct:diffuse} = 0.0167 + \left[0.1072 \cdot \left(\frac{1}{\cos\theta_{zenith}} \right) \right]$$

where,

$\lambda_{direct:diffuse}$: Ratio of direct to diffuse solar radiation
θ_{zenith}: Solar zenith angle (radians)

Diffuse unobstructed ($\Phi_{diffuse2M}$) radiation experienced by the surface of the stream arrives at the stream surface through the stream side canopy opening and is quantified by methods presented by Beschta (1984).

Equation 3.57. Unobstructed Diffuse Solar Radiation Flux

$$\Phi_{diffuse2M} = \Phi_{diffuse1} \cdot \left[\frac{\frac{\pi}{2} - \left(\theta_{veg(left)} + \theta_{veg(right)} \right)}{\frac{\pi}{2}} \right]$$

where,

$\Phi_{diffuse2M}$: diffuse solar radiation flux arriving at stream surface through vegetation canopy opening (cal/m^2 s)
$\Phi_{diffuse1}$: diffuse solar radiation flux experienced at the top of vegetation canopy (cal/m^2 s)
$\theta_{veg(left)}$: maximum left bank vegetation shading angle (radians)
$\theta_{veg(right)}$: maximum right bank vegetation shading angle (radians)

Obstructed diffuse radiation is routed through the vegetation barrier and experiences loss in magnitude due to the scattering and attenuation effects induced by stream side vegetation.

Equation 3.58. Obstructed Diffuse Radiation Flux (Left)

$$\Phi_{diffuse2L} = \frac{2}{\pi} \cdot \left[\left(\theta_{veg(left)} - \theta_{topo1(left)} \right) \cdot \left(\Phi_{diffuse1} \right) \cdot \left(\tau_{veg(left)} \right)^{SUN_{ave(left)}} \right]$$

where,

$\Phi_{diffuse2L}$: diffuse solar radiation flux arriving at stream surface through left bank stream side canopy (cal/m^2 s)
$\Phi_{diffuse1}$: diffuse solar radiation flux experienced at the top of vegetation canopy (cal/m^2 s)
$\theta_{veg(left)}$: maximum left bank vegetation shading angle (radians)
$\theta_{topo1(left)}$: maximum left bank slope (radians)
$\tau_{veg(left)}$: transmissivity of left bank vegetation
$SUN_{ave(left)}$: average solar path length through left bank vegetation (meters)

Equation 3.59. Obstructed Diffuse Radiation Flux (Right)

$$\Phi_{diffuse2R} = \frac{2}{\pi} \cdot \left[\left(\theta_{veg(right)} - \theta_{topo1(rightt)} \right) \cdot \left(\Phi_{diffuse(S_1)} \right) \cdot \left(\tau_{veg(right)} \right)^{SUN_{ave(right)}} \right]$$

where,

$\Phi_{diffuse2R}$: diffuse solar radiation flux arriving at stream surface through right bank stream side canopy (cal/m^2 s)
$\Phi_{diffuse1}$: diffuse solar radiation flux experienced at the top of vegetation canopy (cal/m^2 s)
$\theta_{veg(right)}$: maximum right bank vegetation shading angle (radians)
$\theta_{topo1(right)}$: maximum right bank slope (radians)
$\tau_{veg(right)}$: transmissivity of right bank vegetation
$SUN_{ave(right)}$: average solar path length through right bank vegetation (meters)

The diffuse solar radiation flux experienced by the stream surface ($\Phi_{diffuse3}$) is the summation of unobstructed diffuse radiation passing through the vegetation opening ($\Phi_{diffuse2M}$) and the obstructed diffuse radiation passing through streamside vegetation, while accounting for the scattering and attenuation effects of the vegetation ($\Phi_{diffuse2L}$ + $\Phi_{diffuse2R}$). The stream albedo is incorporated to account for the reflectivity of the stream surface.

Equation 3.60. Diffuse Solar Radiation Flux at Stream Surface

$$\Phi_{diffuse3} = (1 - \psi_{stream}) \cdot (\Phi_{diffuse2M} + \Phi_{diffuse2L} + \Phi_{diffuse2R})$$

where,

$\Phi_{diffuse3}$: diffuse solar radiation flux experienced by stream (cal/m^2 s)
$\Phi_{diffuse2M}$: diffuse solar radiation flux arriving at stream surface through canopy opening (cal/m^2 s)
$\Phi_{diffuse2L}$: diffuse solar radiation flux arriving at stream surface through left bank streamside canopy (cal/m^2 s)
$\Phi_{diffuse2R}$: diffuse solar radiation flux arriving at stream surface through right bank streamside canopy (cal/m^2 s)
ψ_{stream}: albedo of the stream surface

The net solar radiation flux (Φ_{solar3}) that enters the stream is the sum of the direct and diffuse solar radiation flux components experienced by the stream surface.

Equation 3.61. Net Solar Radiation Flux Entering Stream Surface

$$\Phi_{solar3} = \Phi_{direct3} + \Phi_{diffuse3}$$

where,

Φ_{solar3}: net solar radiation flux experienced by stream (cal/m^2 s)
$\Phi_{direct3}$: direct solar radiation flux experienced by stream (cal/m^2 s)
$\Phi_{diffuse3}$: diffuse solar radiation flux experienced by stream (cal/m^2 s)

The solar radiation flux experienced at the stream bed (Φ_{solar4}) is calculated as the product of the flux exerted on the stream surface (Φ_{solar3}) and the transmissivity of the water column (τ_{stream}).

Equation 3.62. Solar Radiation Flux Experienced at Stream Bed

$$\Phi_{solar4} = \Phi_{solar3} \cdot \left(\tau_{stream}\right)^{SUN_{H2O}}$$

where,

Φ_{solar4}: solar radiation flux arriving at stream bed (cal/m^2 s)
Φ_{solar3}: solar radiation flux penetrating stream surface (cal/m^2 s)
τ_{stream}: tranmissivity of water column
SUN_{H2O}: path length through water column (meters)

The solar flux that is experienced by the stream bed (Φ_{solar5}) is calculated as the product of the solar flux at depth (Φ_{solar4}) and the portion of the solar flux that is absorbed ($1-\psi_{bed}$).

Equation 3.63. Solar Radiation Flux Initially Absorbed by Stream Bed

$$\Phi_{solar5} = \Phi_{solar4} \cdot \left(1 - \psi_{bed}\right)$$

where,

Φ_{solar5}: solar radiation flux experienced by stream bed (cal/m^2 s)
Φ_{solar4}: solar radiation flux arriving at stream bed (cal/m^2 s)
ψ_{bed}: stream bed albedo

To accurately conserve heat energy, consideration for stream bed material absorption of heat energy (Φ_{solar5}) represents a partial transfer of the solar flux to the stream bed. However, a portion of the solar flux that is transferred to stream bed material is immediately returned to the stream. The energy flux absorbed by bedrock is calculated as:

Equation 3.64. Solar Radiation Flux Absorbed by Stream Bed

$$\Phi_{absorbed} = \left(\frac{\lambda_{bedrock} \cdot BEDROCK \cdot \Phi_{solar5}}{100} \right).$$

where,

$\Phi_{absorbed}$: solar radiation flux absorbed by stream bed (cal/m^2 s)
Φ_{solar5} solar radiation flux experienced by stream bed (cal/m^2 s)
$\lambda_{bedrock}$: bedrock absorption coefficient: $\lambda_{bedrock} \approx 0.53$
BEDROCK: percent of bedrock that is greater than 25 cm diameter (%)

The net solar radiation heat energy flux experienced by the stream column is then easily determined as:

Equation 3.65. Net Solar Radiation Flux

$$\Phi_{solar} = \Phi_{direct} + \Phi_{diffuse} - \Phi_{absorbed}.$$

In summary, this equation represents heat energy gained from the direct beam and diffuse solar radiation flux, minus the heat energy flux absorbed by the stream bed.

3.1.10.2 Stream Bed Conduction Flux: $\Phi_{conduction}$

Heat energy conduction between the stream bed and stream is driven by a heat gradient. Stream bed characteristics affect the solar absorption properties of a stream, especially in shallow streams. Solid rock, in particular, will absorb solar energy, which will conduct to the stream during and after solar radiation has diminished for the day. Conductive heat from the stream bed will broaden the temperature profile, rather than increase the maximum daily water temperature (Beschta 1984).

The heat energy available for absorption by stream bed material is a function of stream depth. Brown (1969) shows that the stream bed conduction is negligible for average stream depths greater than 20 cm. When average depth is less than 20 cm, the solar flux exerted on the stream bed results in accumulation and storage of heat energy within the bedrock (E_{stored}).

Equation 3.66. Heat Energy Stored in Stream Bed Material

$$E_{stored} = AREA_{streambed} \cdot \int_{t_o}^{t} \left(\Phi_{absorb} - \Phi_{conduction}\right)$$

where,

E_{stored}: energy stored in stream bed (cal)
$AREA_{streambed}$: surface area of stream bed (m^2)
Φ_{absorb}: solar radiation flux absorbed by stream bed ($cal \cdot m^{-2} \cdot s^{-1}$)
$\Phi_{conduction}$: stream bed conduction flux experienced by stream column ($cal \cdot m^{-2} \cdot s^{-1}$)

Heat energy gained by the stream bed is conducted to the stream over a specific time period. The time in which the heat energy of the stream bed is conducted to the stream's volume of water is a function of the particle size of the stream bed materials. For

particle sizes of less than 25 cm in diameter, the heat energy gained by the stream bed is immediately returned to the stream volume of water. In cases where the particle diameter is greater than 25 cm, heat energy is stored, and released at a time adjusted rate that dissipates all stored heat over an eight hour interval.

Equation 3.67. Stream Bed Conduction Flux

$$\Phi_{conduction} = \frac{E_{stored}}{W_{stream(i)} \cdot dx \cdot 28{,}800}$$

where,

$\Phi_{conduction}$: bedrock conduction flux ($cal \cdot m^{-2} \cdot s^{-1}$)
E_{stored}: energy stored in stream bed (cal)
$W_{stream(n)}$: width of stream bed at node i (m)
dx: distance step: length of parcel (m)

It should be noted that all solar heat energy is conserved. In effect, a portion of solar heat energy is routed through the bedrock material, but eventually is returned to the stream system. Bedrock conduction does not occur when: [1]there is not bedrock present with a diameter of 25 cm or greater and/or [2]the average stream depth is greater than 20 cm.

3.1.10.3 Long-Wave Radiation: $\Phi_{longwave}$

The long wave radiation flux is comprised of a positive component and a negative component. The intensity of incoming long wave radiation ($\Phi_{longwave(+)}$) experienced by the stream surface is proportional to atmospheric moisture (Anderson 1954). Humidity and air temperature influence long-wave radiation greatly, while carbon dioxide and other molecules in the atmosphere have less of an influence. Further, Anderson (1954) found

that the height of cloud cover effects the intensity of long-wave radiation. A water surface generally reflects 3% of incoming long wave radiation, while the remaining 97% is absorbed (McCutcheon 1989). Bowie et. al. (1985) found that Brundt's formula provided the most accurate estimation of long-wave radiation for latitudes between 26° 13' N to 47° 45' N and elevations between -30 meters and 3342 meters.

Equation 3.68. Brundt's formula

$$\Phi_{longwave1} = \sigma \cdot \varepsilon_{atm} \cdot (T_{air} + 273)^4 \cdot (1.0 + 0.17 \cdot C_L^{\,2})$$

where,

$\Phi_{longwave1}$: long-wave radiation emitted from the atmosphere experienced above the vegetation canopy (cal m^{-2} s^{-1})
C_L: cloudiness coefficient
T_{air}: air temperature (°C)
σ: Stefan-Boltzman constant ($1.355 \cdot 10^{-8}$ cal·m^{-2}·s^{-1}·K^{-4})
ε_{atm}: atmosphere emissivity

The incoming long wave radiation flux must be routed through streamside vegetation ($\Phi_{longwave2L}$, $\Phi_{longwave2R}$), as well through non-vegetated areas above the stream surface ($\Phi_{longwave2M}$).

Equation 3.69. Atmospheric Long-Wave Radiation Flux (Left)

$$\Phi_{longwave2L} = \frac{2}{\pi} \cdot \left[\left(\theta_{veg(left)} - \theta_{topo1(left)} \right) \cdot \left(\Phi_{longwave1} \right) \cdot \left(\tau_{veg(left)} \right)^{SUN_{ave(left)}} \right]$$

where,

$\Phi_{longwave2L}$: atmospheric long-wave flux penetrating left bank vegetation (cal m^{-2} s^{-1})
$\Phi_{longwave1}$: atmospheric long-wave flux at top of vegetation canopy (cal m^{-2} s^{-1})
$\theta_{veg(left)}$: left bank vegetation shade angle (radians)
$\theta_{topo1(left)}$: left bank slope shade angle (radians)
$\tau_{veg(left)}$: transmissivity of left bank vegetation
$SUN_{ave(left)}$: average path length through left bank vegetation (maters)

Equation 3.70. Atmospheric Long-Wave Radiation Flux (Right)

$$\Phi_{longwave2R} = \frac{2}{\pi} \cdot \left[\left(\theta_{veg(right)} - \theta_{topo1(right)} \right) \cdot \left(\Phi_{longwave1} \right) \cdot \left(\tau_{veg(right)} \right)^{SUN_{ave(right)}} \right]$$

where,

$\Phi_{longwave2R}$: atmospheric long-wave flux penetrating right bank vegetation (cal m^{-2} s^{-1})
$\Phi_{longwave1}$: atmospheric long-wave flux at top of vegetation canopy (cal m^{-2} s^{-1})
$\theta_{veg(right)}$: right bank vegetation shade angle (radians)
$\theta_{topo1(right)}$: right bank slope shade angle (radians)
$\tau_{veg(right)}$: transmissivity of right bank vegetation
$SUN_{ave(right)}$: average path length through right bank vegetation (maters)

Equation 3.71. Atmospheric Long-Wave Radiation Flux (Canopy Opening)

$$\Phi_{longwave2M} = \frac{2}{\pi} \cdot \left[\frac{\pi}{2} - \left(\theta_{veg(right)} + \theta_{veg(left)} \right) \right] \cdot \left(\Phi_{longwave1} \right)$$

The vegetation canopy is assumed to emit long wave radiation that is readily absorbed by the stream surface. The radiating surface of the streamside vegetation is a function of the maximum angles of vegetation and average path length through vegetation on both banks and the canopy transmissivity.

Equation 3.72. Radiating Surface Area of Stream Side Vegetation

$$AREA_{veg} = \frac{2}{\pi} \cdot \left[\left(\theta_{veg(left)} \cdot \left(1 - \left(\tau_{veg(left)} \right)^{SUN_{ave(left)}} \right) \right) + \left(\theta_{veg(right)} \cdot \left(1 - \left(\tau_{veg(right)} \right)^{SUN_{ave(right)}} \right) \right) \right]$$

where,

$AREA_{veg}$: estimated radiating surface area of vegetation canopy
$\theta_{veg(left)}$: left bank vegetation shade angle (radians)
$\theta_{topo1(left)}$: left bank slope shade angle (radians)
$SUN_{ave(left)}$: average path length through left bank vegetation (meters)
$\tau_{veg(left)}$: transmissivity of left bank vegetation
$\theta_{veg(right)}$: right bank vegetation shade angle (radians)
$\theta_{topo1(right)}$: right bank slope shade angle (radians)
$SUN_{ave(right)}$: average path length through right bank vegetation (meters)
$\tau_{veg(right)}$: transmissivity of right bank vegetation

Long wave radiation directed downward from the canopy is the product of the canopy radiating surface area ($AREA_{veg}$), canopy emissivity (ε_{veg}), Stefan-Boltzmann constant (σ) and the air temperature (T_{air}), which is assumed to be equal to that of the canopy (Beschta 1984).

Equation 3.73. Vegetation Long-Wave Radiation Flux

$$\Phi_{longwave(veg)} = \left(AREA_{veg} \cdot \varepsilon_{veg} \cdot \sigma \cdot \left(T_{air} + 273.15\right)^4\right)$$

where,

$\Phi_{longwave(veg)}$: long-wave radiation flux originating from vegetation canopy (cal m^{-2} s^{-1})
$AREA_{veg}$: estimated surface area of vegetation canopy
ε_{veg}: vegetation canopy emissivity ($\varepsilon_{veg} \approx 0.95$) (Beschta 1984)
σ: Stefan-Boltzmann constant ($1.355 \cdot 10^{-8}$ cal m^{-2} s^{-1} K^{-4})
T_{air}: air temperature (°C)

Incoming long-wave heat energy originating from the atmosphere and experienced by the stream surface ($\Phi_{longwave(+)}$) is simply the summation of incoming long-wave flux components multiplied by the reflectance of the stream surface.

Equation 3.74. Incoming Long-Wave Flux Experienced by Stream Surface

$$\Phi_{longwave(+)} = (1 - C_R) \cdot (\Phi_{longwave2M} + \Phi_{longwave2L} + \Phi_{longwave2R} + \Phi_{longwave(veg)})$$

where,

$\Phi_{longwave(+)}$: net long-wave radiation flux entering stream surface (cal m^{-2} s^{-1})
C_R: reflection coefficient ($C_R \approx 0.03$) (Beschta 1984)
$\Phi_{longwave2M}$: long-wave radiation flux through canopy opening (cal m^{-2} s^{-1})
$\Phi_{longwave2L}$: long-wave radiation flux through left bank vegetation (cal m^{-2} s^{-1})
$\Phi_{longwave2R}$: long-wave radiation flux through right bank vegetation (cal m^{-2} s^{-1})

Long-wave emission from the surface of the stream ($\Phi_{longwave(-)}$), termed back radiation, is the second most important component in dissipating heat energy from the stream system (Parker & Krenkal 1969). The emissivity of the water is best described by the Stefan-Boltzmann, Fourth Power, Radiation Law for a blackbody (McCutcheon 1989). The negative long wave radiation flux becomes the product of stream emissivity (ε_{H20}), the Stefan-Boltzmann constant (σ) and stream temperature (T_{H20}):

Equation 3.75. Back Radiation Flux

$$\Phi_{longwave(-)} = -\varepsilon_{H2O} \cdot \sigma \cdot (T_{H20} + 273)^4$$

where,

$\Phi_{longwave(-)}$: back radiation flux originating from stream surface (cal·m^{-2}·s^{-1})
ε_{H2O}: emissivity of stream surface ($\varepsilon_{H2O} \approx 0.97$) (Beschta 1984)
σ: Stefan-Boltzmann constant ($1.355 \cdot 10^{-8}$ cal·m^{-2}·s^{-1}·K^{-4})
T_{H2O}: stream temperature (°C)

The net long wave radiation flux ($\Phi_{longwave}$) is then simply calculated as the sum of the positive and negative long wave flux.

Equation 3.76. Net Long-Wave Radiation Flux

$$\Phi_{longwave} = \Phi_{longwave(+)} + \Phi_{longwave(-)}$$

3.1.10.4 Evaporation Flux: $\Phi_{evaporation}$

Molecular motion in a liquid phase is related to heat energy; as heat energy increases, so does molecular motion. As the molecular motion of a water molecule in the liquid phase increases, in response to increased heat energy, it begins to overcome the molecular attraction to liquid water, causing water molecules to escape as water vapor. When the vapor pressure of the air above the stream is low, the released water vapor from the stream has a lower chance of colliding with other molecules in the air, and thus, a greater chance of remaining in the gaseous phase as water vapor. If the vapor pressure is high, the chance of molecular collisions is greater, with an increased tendency for the water vapor to be forced back into the liquid phase. Saturation vapor pressure results when the rate of water molecules leaving the stream surface is equal to the rate of water molecules being introduced back to the liquid phase of the stream.

Water molecules in the liquid phase require energy to overcome the molecular bonds that bind the liquid molecules. The energy needed to change water from a liquid to gaseous phase is known as *the latent heat of vaporization*. Heat energy necessary for the evaporative process is furnished by the stream system and transferred to the surrounding air mass, representing a net heat energy loss.

The evaporative heat flux across the air-water interface is generally the most significant factor in dissipation of stream heat (Parker & Krenkel 1969). Special

consideration must be taken in addressing evaporation. The evaporation flux is the energy process in which streams lose most heat energy, and therefore, contributes most to decrease stream temperature. Further, the evaporation flux is utilized by the Bowen ratio to approximate the convective heat energy flux, and thus, the accuracy of the convection flux is dependent on accurate estimation of the evaporation energy flux. Unfortunately, the evaporation flux is often the most difficult heat transfer process to model.

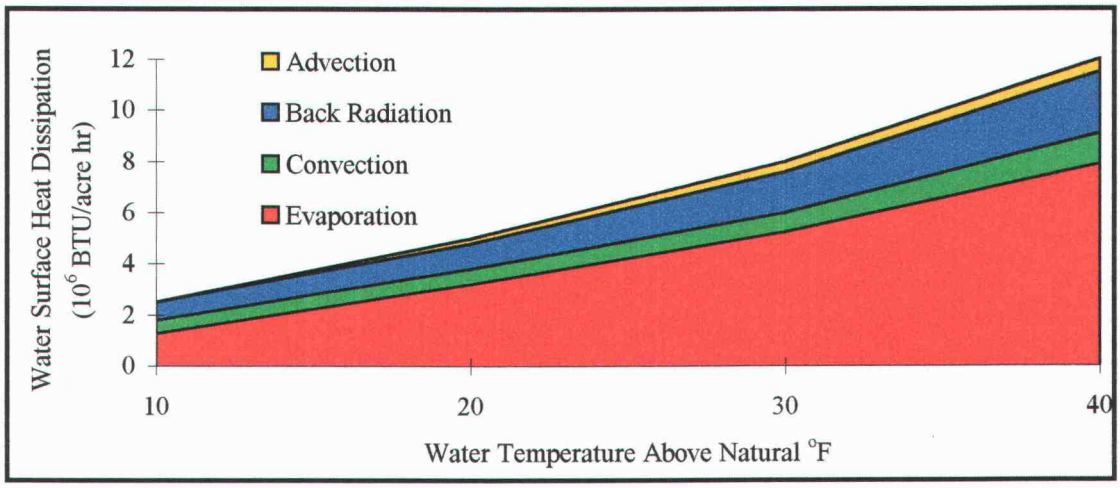

Figure 3.8. Heat dissipation from water surface by evaporation, back radiation, convection and advection during June (data taken from Parker and Krenkel 1969).

Evaporation, the vaporization of water molecules, is driven by a vapor pressure gradient between the water surface (e_s)and the air (e_a) directly above the stream: $e_a < e_s$. Only when the air is saturated does evaporation cease to occur. In rare cases, the air may become supersaturated and condensation results: $e_a \geq e_s$.

The evaporative flux is found using a Dalton type equation which calculates the summation of the sensible heat carried with the water vapor when evaporation occurs (Q_v)

and the product of the latent heat of evaporation (LHV), density of water (ρ_{water}) and the rate of evaporation (E). Brown and Barnwell (1987) found that for practical modeling applications the sensible heat term (Q_v) is negligible.

Equation 3.77. Evaporation Flux

$$\Phi_{evaporation} = \rho_{water} \cdot LHV \cdot E$$

where,

$\Phi_{evaporation}$: evaporation flux emitted from stream surface ($cal \cdot m^{-2} \cdot s^{-1}$)
ρ_{water}: density of water (kg/m^3)
LHV: latent heat of vaporization (cal/kg)
E: evaporation rate (m/s)

The energy needed for water to change from a liquid to a gas, the latent heat of vaporization (LHV), is a function of water temperature (McCutcheon 1989):

Equation 3.78. Latent Heat of Vaporization

$$LHV = 595 - (0.56 \cdot T_{H2O})$$

The rate of evaporation (E) is derived by assuming that turbulent mixing is responsible for the transport of momentum, heat and water vapor in the atmospheric boundary layer directly above the stream surface (McCutcheon 1989). Evaporation rate approximation is a function of the vapor gradient (e_s - e_a), the movement of the air directly above the water surface and the evaporation coefficient (ϕ).

Equation 3.79. Evaporation Rate

$$E = u \cdot \phi \cdot (e_s - e_a)$$

where,

E: evaporation rate (m/s)
u: wind speed (m/s)
ϕ: evaporation coefficient
e_s: saturation vapor pressure (mbar)
e_a: vapor pressure (mbar)

Using the *energy balance method* for evaporation rates experienced in the San Diego Aqueduct, Bowie et. al. (1985) tested various approximations and determined that the following form was the most suit approximation for open channel flow.

Equation 3.80. Bowie Evaporation Rate Model

$$\dot{E} = \frac{\left(2.664 + \left(0.505 \cdot u\right)\right) \cdot \left(e_s - e_a\right)}{100}$$

Several other evaporation models that have been developed for lakes and reservoirs are available to the user. Table 3.3 lists the various evaporation models and the water body for which it was developed.

Equation 3.81. Penman Evaporation Rate Model

$$\dot{E} = \frac{\left(0.50 + \left(0.24 \cdot u\right)\right) \cdot \left(e_s - e_a\right)}{38.09}$$

Equation 3.82. Ryan and Harleman Evaporation Rate Model

$$\dot{E} = \left[\left(1.123 \cdot 10^{-2} \cdot u\right) + \left(9.504 \cdot 10^{-3} \cdot VT_{diff}^{\frac{1}{3}}\right)\right] \cdot \left(e_s - e_a\right)$$

Equation 3.83. Zaykov Evaporation Rate Model

$$\dot{E} = \left(0.015 \cdot 0.0108 \cdot u\right) \cdot \left(e_s - e_a\right)$$

Equation 3.84. Meyer Evaporation Rate Model

$$\dot{E} = 2.42 \cdot 10^{-2} \cdot (1.0 + 0.1 \cdot u) \cdot (e_s - e_a)$$

Equation 3.85. Harbeck Evaporation Rate Model

$$\dot{E} = (5.8505 \cdot 10^{-3} \cdot u) \cdot (e_s - e_a)$$

Equation 3.86. Turner Evaporation Rate Model

$$\dot{E} = (9.144 \cdot 10^{-3} \cdot u) \cdot (e_s - e_a)$$

Equation 3.87. Fry Evaporation Rate Model

$$\dot{E} = (9.9728 \cdot 10^{-3} \cdot u) \cdot (e_s - e_a)$$

where,

E: evaporation rate (m/s)
u: wind speed (m/s)
e_s: saturation vapor pressure (mbar)
e_a: vapor pressure (mbar)

Investigator	**Water Body**
Bowie	San Diego Aqueduct
Penman	Various lakes
Ryan and Harleman	Small lakes and reservoirs
Zaykav	Ponds and small reservoirs
Meyer	Small lakes and reservoirs
Harbeck	Lake Mead, Nevada
Turner	Lake Michie, North Carolina
Fry	Small lakes

Table 3.3. Evaporation models developed for specific water bodies.

3.1.10.5 Convection Flux: $\Phi_{convection}$

The convective heat energy flux across the air-water interface is the result of turbulent and molecular heat exchange which occurs in response to a heat energy gradient (Beschta 1984). Sensible heat will be transferred across the air-water interface when the respective temperatures of the stream and ambient air are different. From Furrier's heat transfer studies, the rate of heat energy transfer is proportional to the heat gradient (McCutcheon 1989). The Bowen ratio is a constant of proportionality between the convection flux and the evaporation flux at the air-water interface, and is therefore, a function of stream and air temperature and vapor pressure (Bowen 1926).

Equation 3.88. Bowen's Ratio

$$BOWEN_{ratio} = \frac{\Phi_{convection}}{\Phi_{evaporation}} = 0.01 \cdot \left[\frac{(T_{stream} - T_{air})}{(e_s - e_a)}\right] \cdot \left[\frac{P_{total}}{29.92}\right]$$

It follows that the convective heat flux at the air-water interface is the product of the Bowen ratio and the evaporative heat flux.

Equation 3.89. Convection Flux

$$\Phi_{convection} = BOWEN_{ratio} \cdot \Phi_{evaporation}$$

3.1.10.6 Groundwater Energy Exchange

A particular stream reach must be classified as gaining, losing or impermeable by comparing the magnitude of upstream and downstream flow. Often flow loss due to evapo-transpiration is negligible. Constantz et. al. (1993) found that a 160 m reach on St.

Kevin Gulch, Colorado lost 2-3 m^3/day due to evapo-transpiration. The losses attributed to seepage loss for the same reach was 300 m^3/day.

A volume of water that supplements the stream flow, adds heat energy proportional to the temperature of the groundwater. Gaining and losing reaches must be determined by the difference in flow between the two monitoring sites. Influent groundwater seepage flow yields an energy input to the stream system. Effluent groundwater seepage flow yields an energy output from the stream system. An energy relationship is easily developed to account for stream-groundwater temperature mixing.

Equation 3.90. Stream Temperature After Groundwater Mixing

$$T_{H2O(t+dt,n)} = \frac{\left(T_{H2O(t,n)} \cdot Q_{stream}\right) + \left(T_{gw} \cdot Q_{gw}\right)}{\left(Q_{stream} + Q_{gw}\right)}$$

where,

$T_{H2O(t+dt,n)}$: adjusted stream temperature (°C)
$T_{H20(t,n)}$: stream temperature (°C)
Q_{stream}: average stream flow (cms)
T_{gw}: groundwater temperature (°C)
Q_{gw}: groundwater exchange volume $\left(Q_{gw} = \frac{dx}{L_{reach}}\left(Q_{up} - Q_{dn}\right)\right)$ (cms)

3.2 Data Collection

3.2.1 Stream Temperature Data

Many of the past attempts to measure stream temperature have failed to consider the importance of the site specific characteristics of the stream reach. All stream temperature measurement should focus on relatively homogenous stream reaches. This author acknowledges that natural water bodies are inherently heterogeneous with respect to distance and time. A relatively homogenous reach must contain the following characteristics: no major changes in vegetation shading structure, no major changes in topographic shade structure, no surface inflow at any portion of the defined reach and no flow hindrance (i.e. reservoirs, beaver ponds, pools with zero velocity).

Two different Hobo® thermistor types are commonly used to measure stream and air temperatures. Model number HTEA-05+37 is an external thermistor and model number HTI-05+37 is an internal thermistor. Both measure temperature with a resolution of ±0.18° - 0.36° F (± 0.10° - 0.20° C), as listed by the manufacturer. The internal thermistors are placed inside a water proofed PVC capsule, that is then submerged in the stream. The external thermistor pigtail is placed directly in the water column. By conducting experimental analysis, the two Hobo® thermistor types were analyzed for accuracy and response-time.

Both types of thermistor units have a filtering device that omits the noise that would be expected with the ± 0.1° -0.2° C temperature resolution. The result is that the temperature changes in steps, rarely less than 0.2° C (0.36° F). In general, the device

does not register a change in temperature unless the magnitude of the change is greater than the resolution.

Internal Encapsulated Thermistors	°F	°C
Average Deviation	0.0531	0.0295
Standard Deviation	0.0750	0.0417
95% Confidence Interval	0.1039	0.0577
External Thermistors	°F	°C
Average Deviation	0.0602	0.0344
Standard Deviation	0.0850	0.0422
95% Confidence Interval	0.1178	0.0654

Table 3.4. Statistical analysis of Hobo® thermistors

Five encapsulated internal thermistors and five external thermistors were placed in a water bath that experienced a 15° F temperature change over a time period of one day. The encapsulated internal thermistors had a slightly lower standard deviation (0.075° F) than the external thermistors (0.085° F), which is probably due to the dampening effect of the capsule. The external thermistor registered the effects of differential heating in the water bath that were not experienced by the encapsulated thermistors. Regardless, the thermistors in their respective environments tend to agree with each other, which is extremely important for the purpose of this research project. It is paramount that the thermistors provide the same output when they are in the same environment, and it appears that they do just that. From the data provided, the thermistors have a 95% confidence interval between ±0.104° F - 0.118° F (± 0.0577° C - 0.0654° C).

When the thermistors are placed inside of the PVC capsule, the temperature measurements are not occurring in real-time. There is a considerable lag-time between the

stream temperature measured by the external thermistor unit and the stream temperature experienced by the encapsulated thermistor. Figure 3.9 displays a temperature profile that was measured by both an internal and external thermistor. Both temperature profiles are similar in magnitude, but lag-time is noticeable.

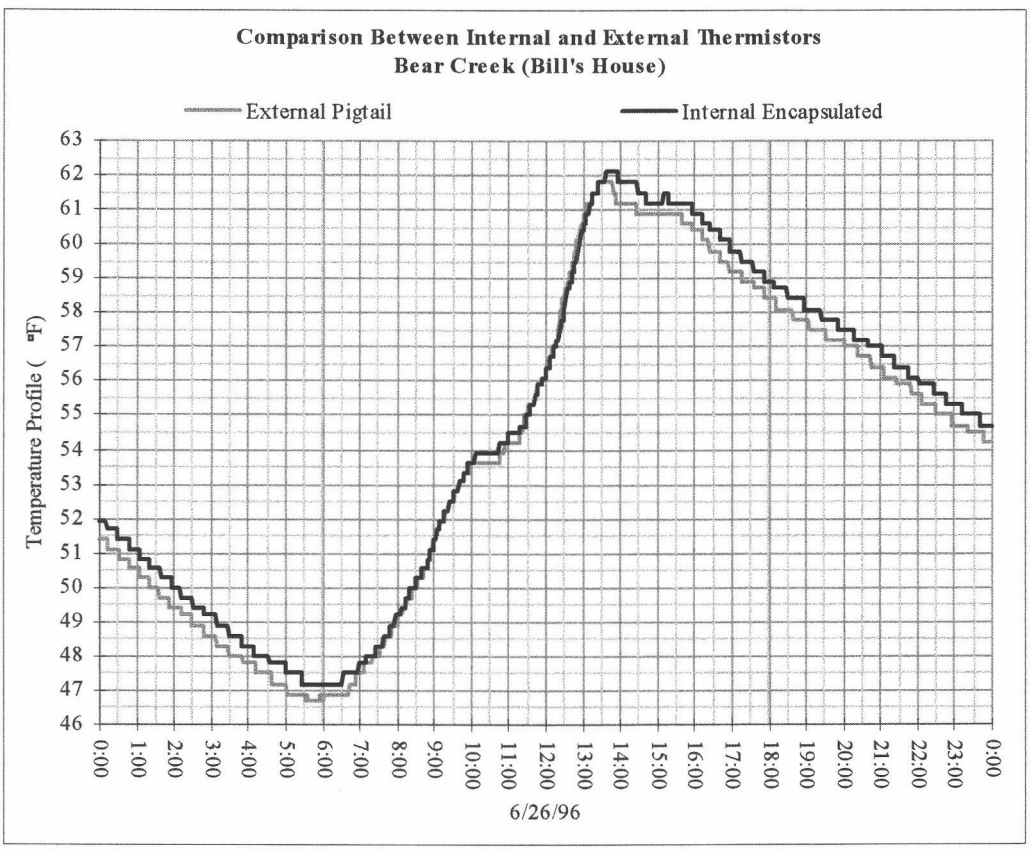

Figure 3.9. Comparison between internal and external thermistors for one full day (6/26/96).

Using the same data set, Figure 3.10 narrows the time interval to eight hours. The resulting graph of the temperature profiles from 1:00 am to 9:00 am clearly shows a lag-time ranging from fifteen to forty-five minutes. It was commonly found that lag-time increased as the rate change of temperature increased.

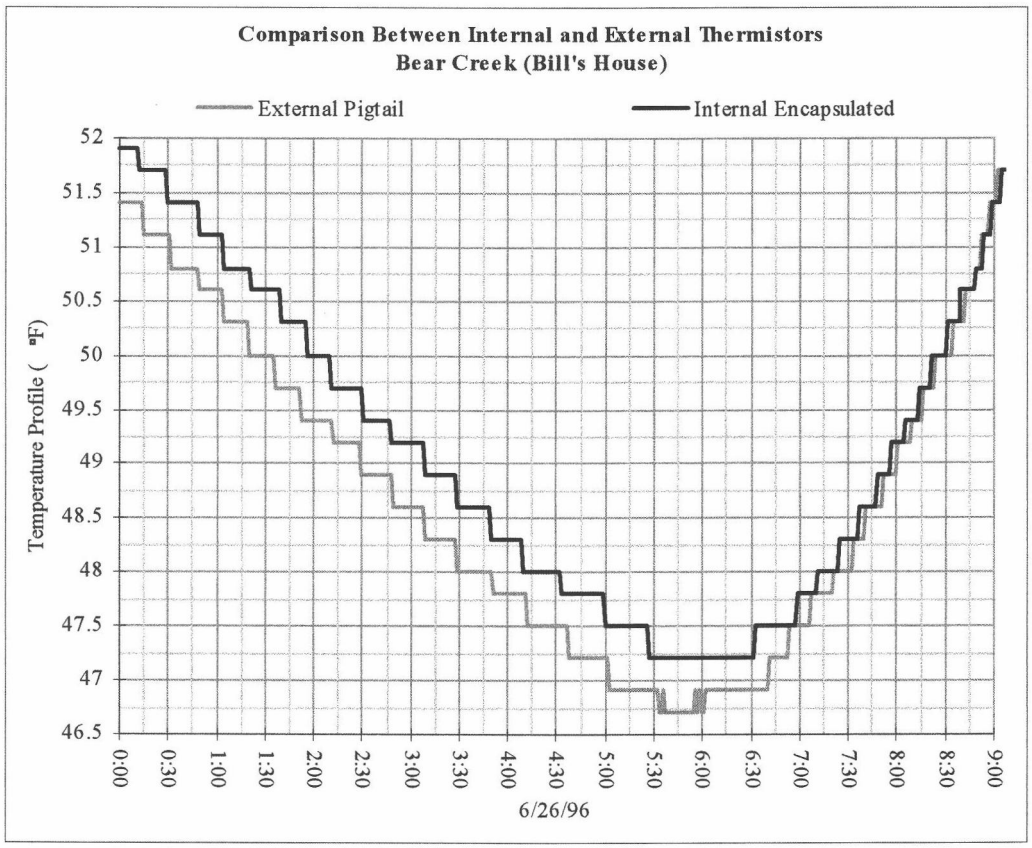

Figure 3.10. Comparison between internal and external thermistors from 1:00 am to 9:00 am (6/26/96).

Lag-time limits the usability of data collected with the internal thermistor units because *Heat Source* requires that stream temperature data correlate with the timing of the diurnal solar cycle. External thermistors were, therefore, exclusively used to measure stream temperature. Due to the differential heating that each type of thermistor experiences, the external and internal thermistors should never be used together. It is recommended that future stream temperature measurements should rely on the external thermistor units.

Stream temperature were measured at the bottom of the stream and, when possible, in shade. Care was taken to ensure that the thermistor units were placed in the center of the flow field. Air temperature was always measured at four feet above the stream surface and in shade. It was found that the thermistor units place in direct sunlight recorded elevated and inaccurate air temperatures.

3.2.2 Hydraulic Data

Stream flow was measured with the standard current meter method. Stream velocity was measured with Flow Mate current meter, model 2000, which has a ±0.01 foot per second resolution, as listed by the manufacturer. Cross-sections were selected for straightness and uniformity with a flow field that had relatively parallel stream lines. The two point method (0.2 x depth, 0.8 x depth) was used to measure velocity in streams when depth exceeded one foot and the one point method (0.6 x depth) was used to measure velocity in streams when depth was less than one foot. The area weight averaged velocity was used for a model input. Stream width was measured at the sampling site. Depth is automatically calculated by the model from the flow volume, flow velocity and stream surface width.

$$\text{Depth} = \frac{\text{Flow}}{\text{Velocity} \cdot \text{Width}}$$

Percent bedrock is an estimate made by the model user. Bed slope was determined from U.S.G.S. topographic maps. Stream aspect was found using a compass.

3.2.3 Atmospheric Data

Wind speed was either estimated by the model user or determined from the nearest weather station or airport. The cloud cover was assumed to be zero for all simulations. Relative humidity was determined from the nearest weather station or airport.

3.2.4 Shade Data

Vegetation shade angles and bank slope were calculated as a function of height and the distance to the center of the stream. The topographic shade angle was measured using a protractor. Vegetation height and width were measured with a thirty foot tape. In the cases where vegetation height was to high too measure, estimates were used. When vegetation width exceeded 100 feet, 100 feet was used as an input. The canopy density was estimated by the model user.

4. RESULTS

4.1 Model Validation

Eight different sampling sites were selected from which fifteen data sets were collected and used for simulation purposes. The diverse topography of Oregon provided varied types of sampling sites. The data collected and presented ranged from the Coastal Mountains of Western Oregon, to the Willamette Valley, to the high desert of Central Oregon.

Actual upstream, actual downstream and predicted downstream temperature profiles are plotted for each simulation. The stream temperature change, both actual and predicted, that occurred over the defined reach is also plotted for each simulation. The model output is statistically analyzed to determine the Pearson product moment (R^2), which were rounded to the nearest one hundredth, and the standard error (S.E.).

The selection of sampling sites was intended only to provide varied settings to test the performance of *Heat Source*. Inference as to the correlation of stream parameters and shading levels to stream temperature magnitude is left to the discretion of the reader. The following simulations are performed to validate *Heat Source* and to establish statistical model accuracy.

4.1.1 Klochman Creek (Sample Site 1)

Located roughly 40 miles southeast of Prineville, Oregon, Klochman Creek flows from east/southeast to west/northwest. The stream bank vegetation at sample site 1

consists of grass, roughly 1 - 1.5 feet in height. Flow volume is small and flow velocity ranges from slow to medium speeds. At sample site 1, Klochman Creek is shallow, with an average depth of 8 to 9 inches. The length of the defined reach is 900 feet and exhibits little change in channel morphology, however, due to the topography at the downstream sampling site, the shading characteristics vary with respect to longitudinal position. Wind speed was considered negligible for June 29 and June 30, however, wind was present for July 2 and July 3. No clouds were present during simulation.

Record Keeping				
Units	English			
Date of Simulation	6/29/96, 6/30/96, 7/2/96, 7/3/96 1:00 am			
Duration of Simulation	1 days			
Elevation	3900 feet			
Latitude	44°			
Longitude	120.75°			
Time Zone	Pacific			
Reach Length	900 feet			
Atmospheric Parameters				
Wind Speed	0 mph (6/29, 2/30) 2.5 mph (7/2, 7/3)			
Cloud Cover	clear (0%)			
Relative Humidity	20 %			
Hydraulic Parameters	Upstream		Downstream	
Flow Velocity	0.9 feet/second		0.9 feet/second	
Stream Flow	1.06 cubic feet per second		1.10 cubic feet per second	
Average Width	1.6 feet		1.8 feet	
Stream Bed Slope	0.01		0.01	
Percent Bedrock	25 %		25 %	
Stream Aspect	210° from North		190° from North	
Shade Parameters	Upstream		Downstream	
	Left	Right	Left	Right
Topographic Shade Angle	12°	5°	10°	55°
Vegetation Shade Angle	35°	40°	35°	30°
Stream Bank Slope	0.1	0.1	0.1	2.0
Vegetation Height	1.0 feet	1.0 feet	1.5 feet	1.5 feet
Vegetation Width	10 feet	10 feet	15 feet	15 feet
Canopy Coefficient	0.3	0.3	0.3	0.3

Table 4.1. Input Parameters for Klochman Creek (Sample Site 1 - 6/29/96, 6/30/96, 7/2/96, 7/3/96).

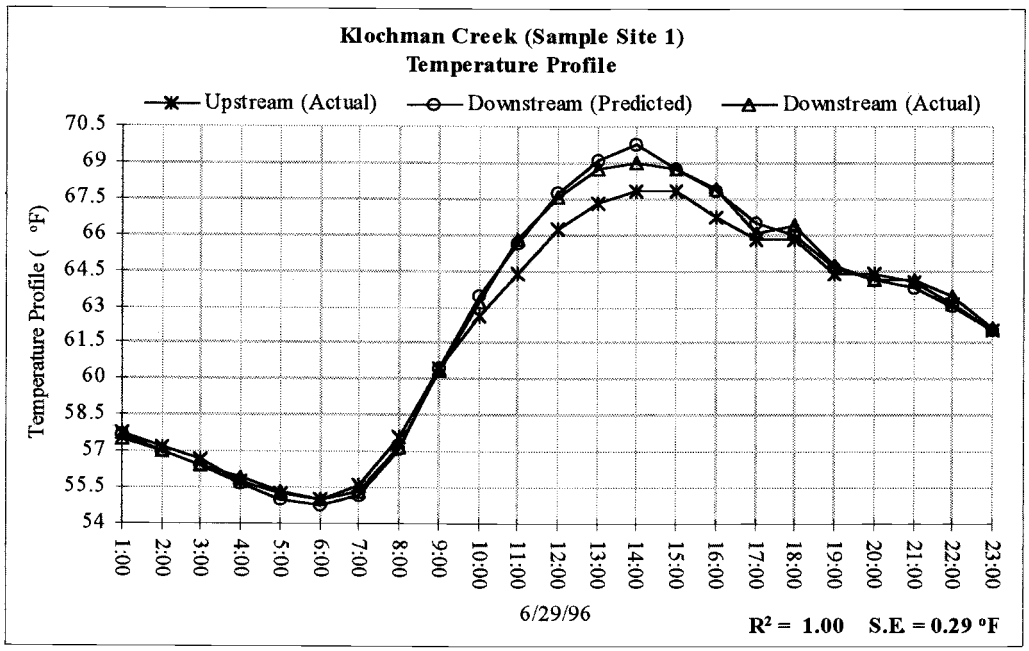

Figure 4.1. Klochman Creek (Sample Site 1) temperature profile for 6/29/96.

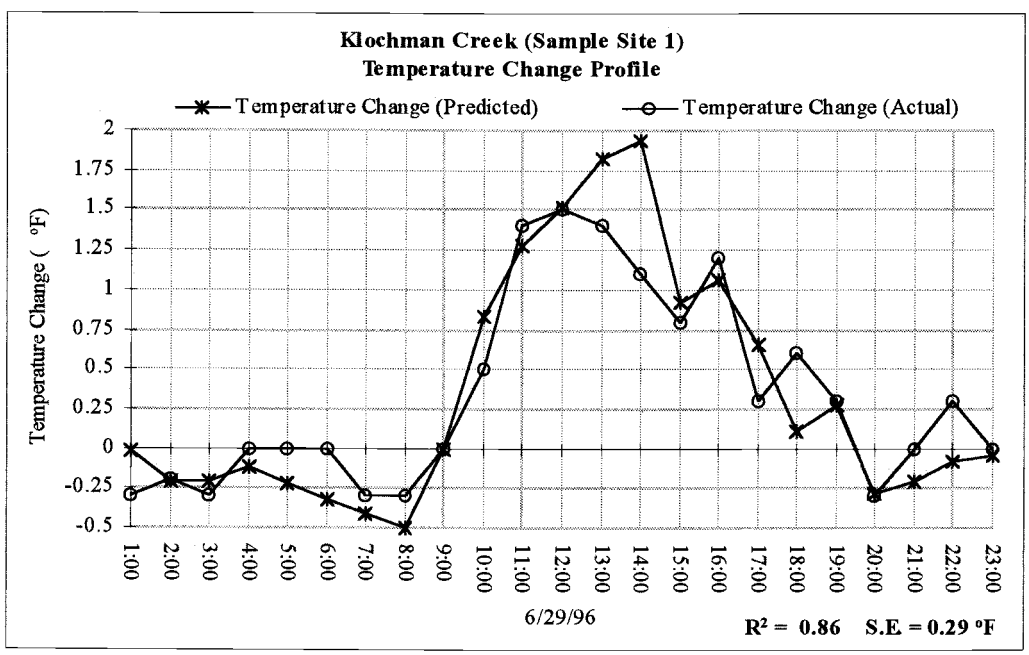

Figure 4.2. Klochman Creek (Sample Site 1) temperature change profile for 6/29/96.

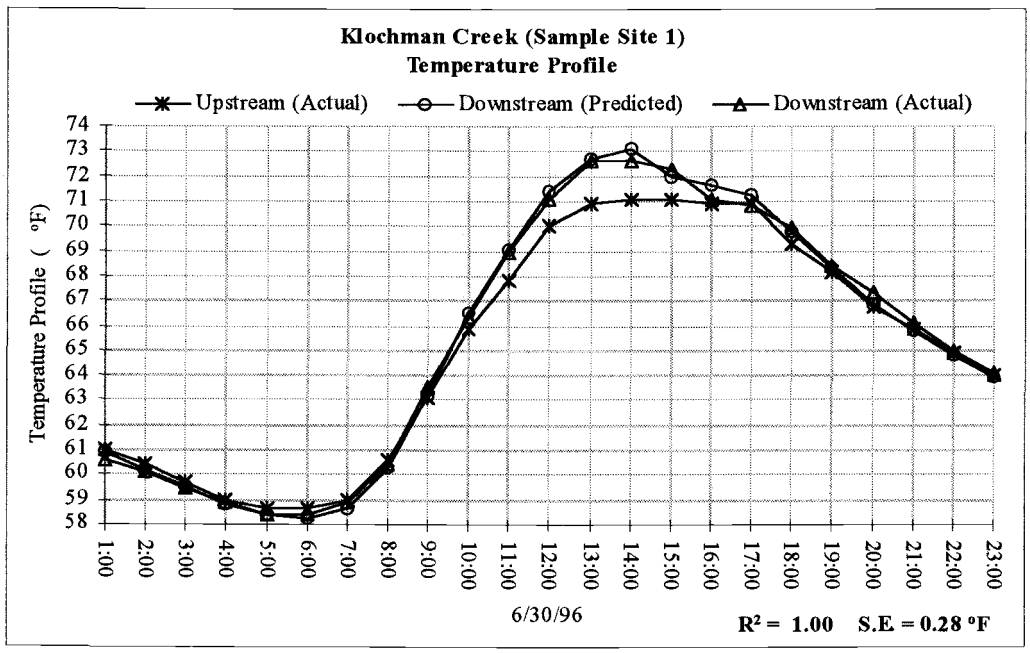

Figure 4.3. Klochman Creek (Sample Site 1) temperature profile for 6/30/96.

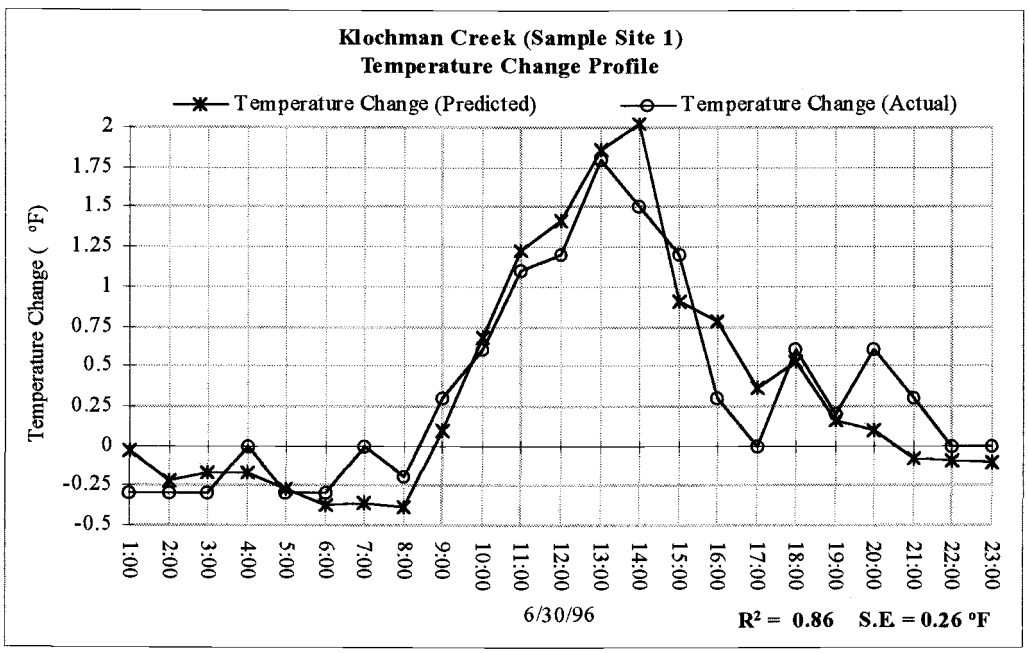

Figure 4.4. Klochman Creek (Sample Site 1) temperature change profile for 6/30/96.

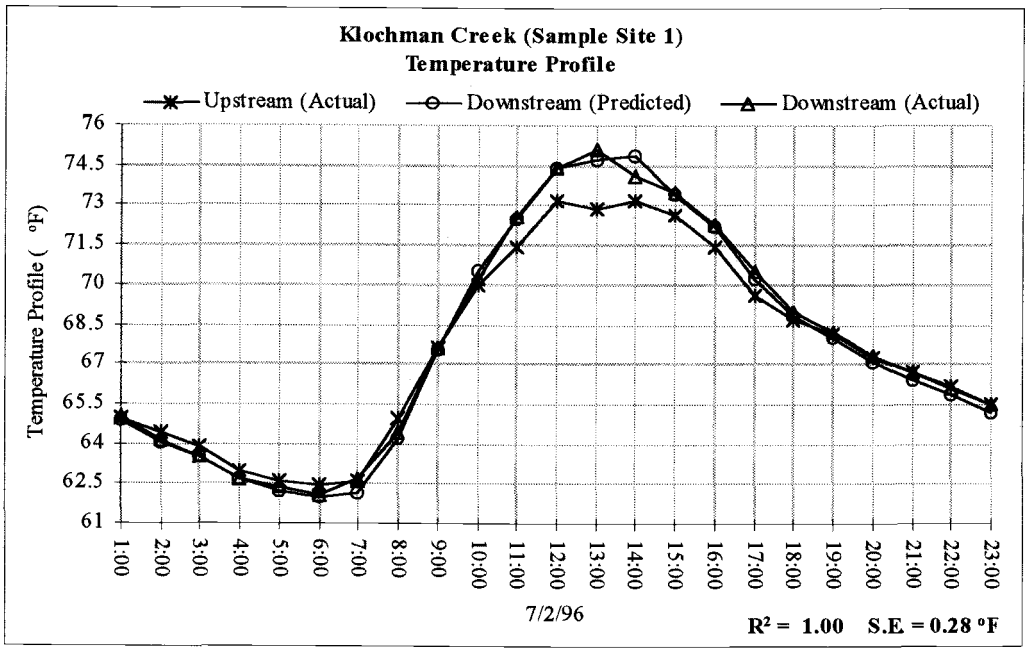

Figure 4.5. Klochman Creek (Sample Site 1) temperature profile for 7/2/96.

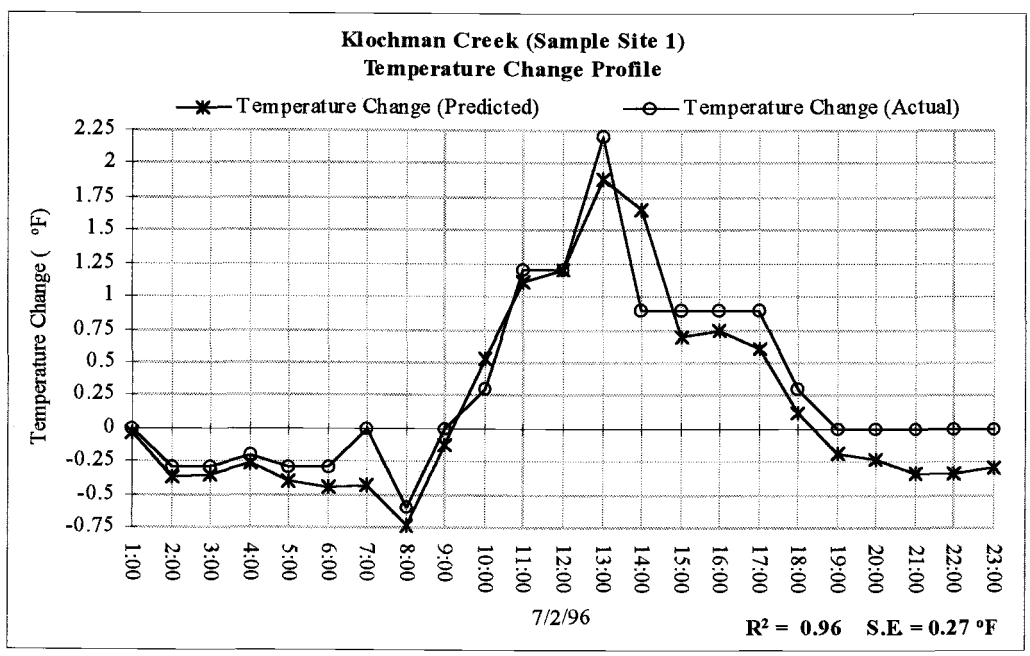

Figure 4.6. Klochman Creek (Sample Site 1) temperature change profile for 7/2/96.

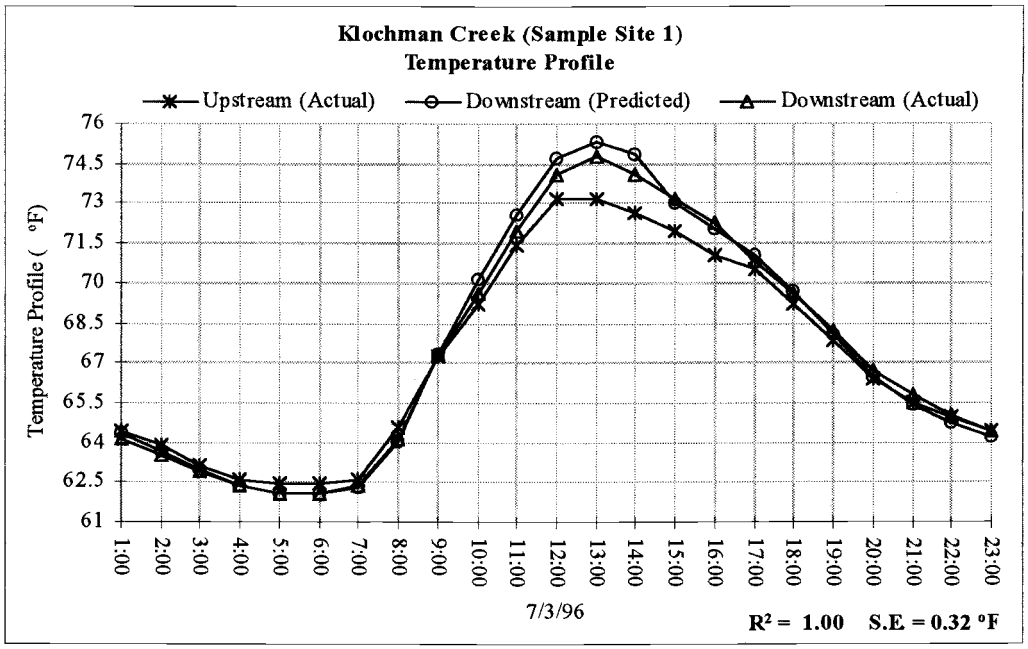

Figure 4.7. Klochman Creek (Sample Site 1) temperature profile for 7/3/96.

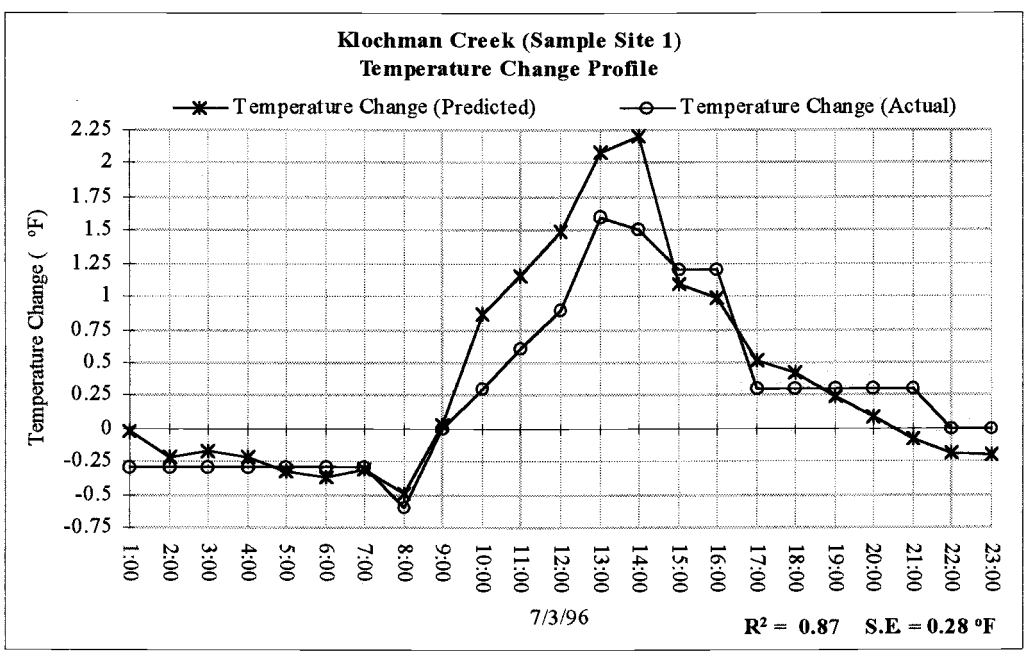

Figure 4.8. Klochman Creek (Sample Site 1) temperature change profile for 7/3/96.

4.1.2 Klochman Creek (Sample Site 2)

Sample site 2 utilized the downstream boundary of sample site 1, but increased the distance of the defined reach 900 feet in the upstream direction, resulting in a total reach length of 1800 feet. Stream bank vegetation at the upstream boundary consisted of well spaced, medium sized juniper trees and the downstream portion of the reach consisted of grass, roughly one foot in height, along the stream bank.

Record Keeping				
Units	English			
Date of Simulation	7/2/96 1:00 am			
Duration of Simulation	1 days			
Elevation	3900 feet			
Latitude	44°			
Longitude	120.75 °			
Time Zone	Pacific			
Reach Length	1800 feet			
Atmospheric Parameters				
Wind Speed	2.5 mph			
Cloud Cover	clear (0%)			
Relative Humidity	20 %			
Hydraulic Parameters	Upstream		Downstream	
Flow Velocity	0.9 feet/second		0.9 feet/second	
Stream Flow	0.98 cubic feet per second		1.10 cubic feet per second	
Average Width	1.2 feet		1.8 feet	
Stream Bed Slope	0.01		0.01	
Percent Bedrock	25 %		25 %	
Stream Aspect	220° from North		190° from North	
Shade Parameters	Upstream		Downstream	
	Left	Right	Left	Right
Topographic Shade Angle	15°	10°	10°	55°
Vegetation Shade Angle	60°	55°	35°	30°
Stream Bank Slope	0.1	0.1	0.1	2.0
Vegetation Height	15.0 feet	15.0 feet	1.5 feet	1.5 feet
Vegetation Width	45 feet	45 feet	15 feet	15 feet
Canopy Coefficient	0.3	0.3	0.3	0.3

Table 4.2. Input Parameters for Klochman Creek (Sample Site 2 - 7/2/96).

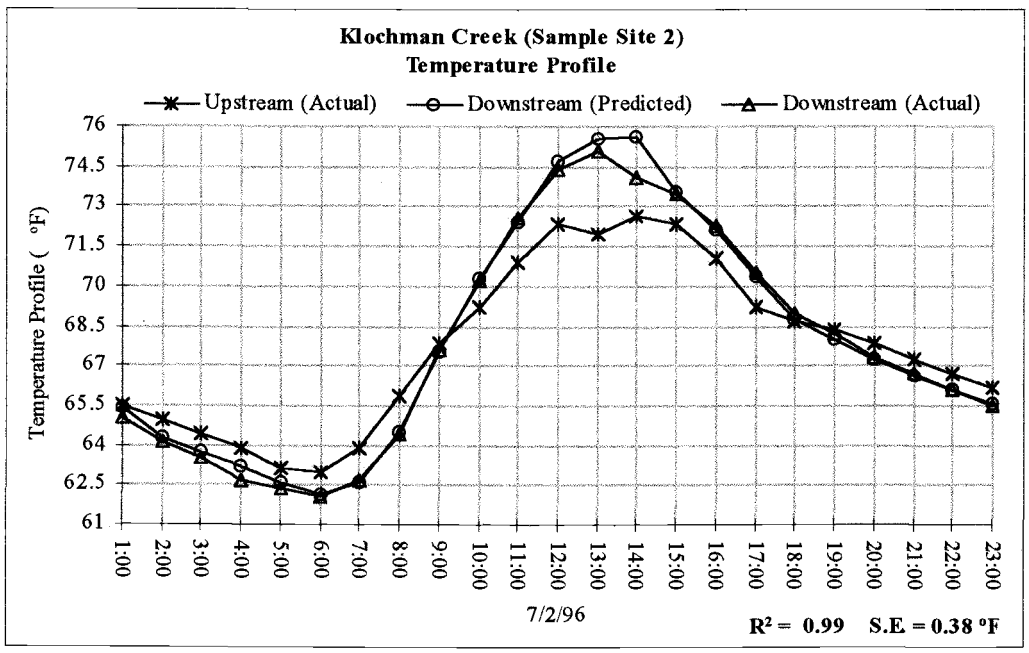

Figure 4.9. Klochman Creek (Sample Site 2) temperature profile for 7/2/96.

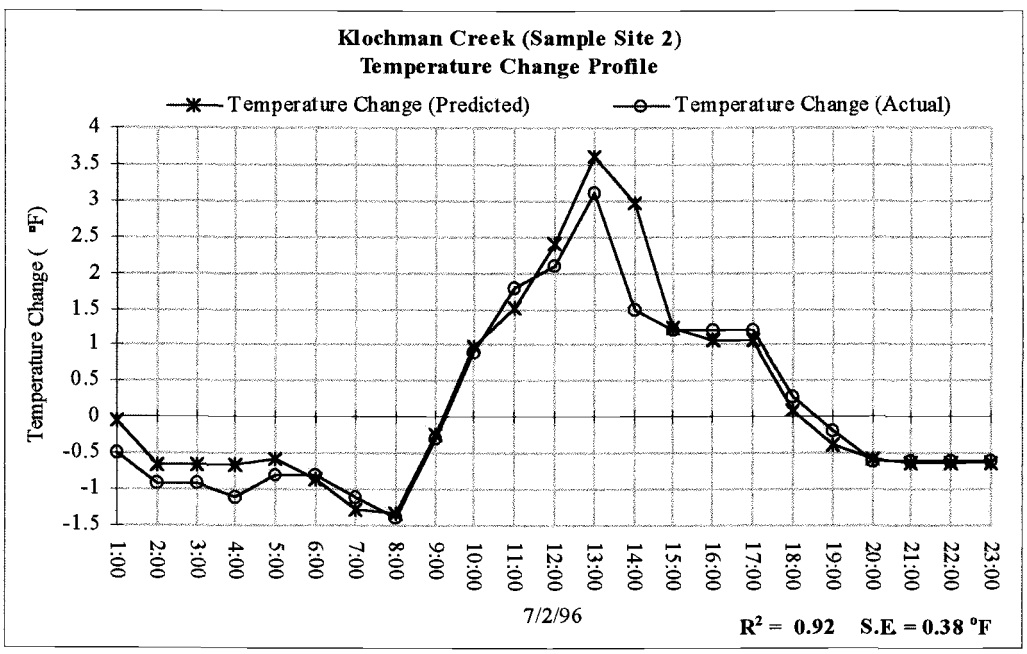

Figure 4.10. Klochman Creek (Sample Site 2) temperature change profile for 7/2/96.

4.1.3 Klochman Creek (Sample Site 3)

Well spaced juniper trees provided some shade along the stream banks of the upper portions of the reach, while the downstream portion of the reach mainly consisted of grass. Stream flow was roughly one cubic foot per second and flow velocity was roughly one foot per second. Stream width increases in the downstream direction from 1.2 feet to 2.5 feet. The defined reach was 900 feet in length.

Record Keeping				
Units	English			
Date of Simulation	7/2/96 1:00 am			
Duration of Simulation	1 days			
Elevation	3900 feet			
Latitude	44°			
Longitude	120.75 °			
Time Zone	Pacific			
Reach Length	900 feet			
Atmospheric Parameters				
Wind Speed	5.0 mph			
Cloud Cover	clear (0%)			
Relative Humidity	20 %			
Hydraulic Parameters	Upstream		Downstream	
Flow Velocity	0.9 feet/second		0.9 feet/second	
Stream Flow	0.98 cubic feet per second		1.10 cubic feet per second	
Average Width	1.2 feet		2.5 feet	
Stream Bed Slope	0.01		0.01	
Percent Bedrock	25 %		25 %	
Stream Aspect	220° from North		190° from North	
Shade Parameters	Upstream		Downstream	
	Left	Right	Left	Right
Topographic Shade Angle	15°	10°	12°	5°
Vegetation Shade Angle	60°	55°	35°	30°
Stream Bank Slope	0.1	2.0	0.1	0.1
Vegetation Height	15.0 feet	15.0 feet	1.5 feet	1.5 feet
Vegetation Width	45 feet	45 feet	10 feet	10 feet
Canopy Coefficient	0.3	0.3	0.3	0.3

Table 4.3. Input Parameters for Klochman Creek (Sample Site 3 - 7/2/96, 7/3/96).

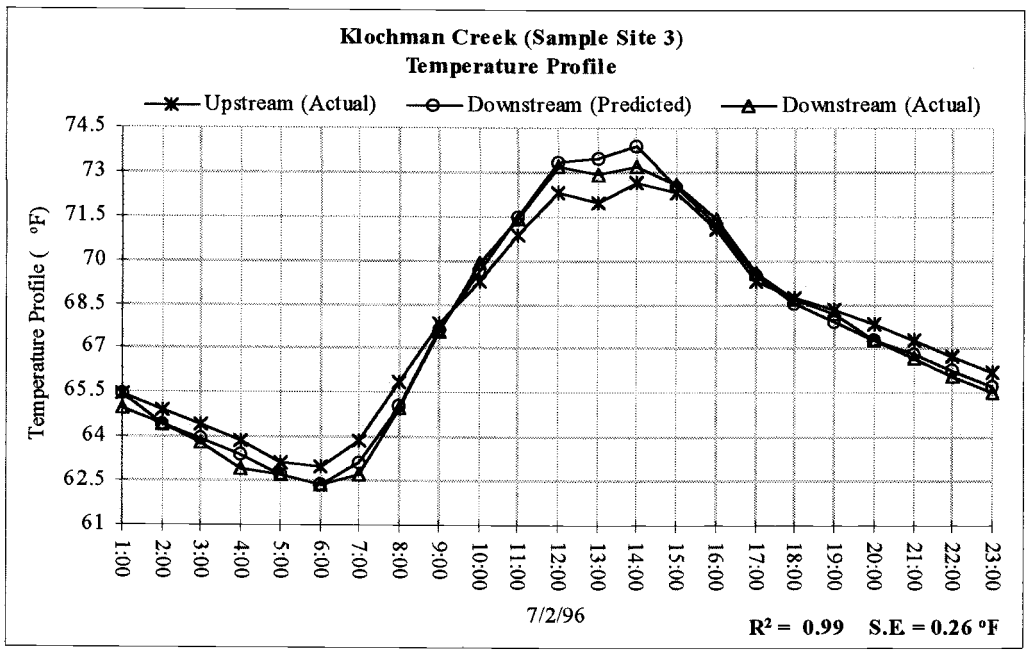

Figure 4.11. Klochman Creek (Sample Site 3) temperature profile for 7/2/96.

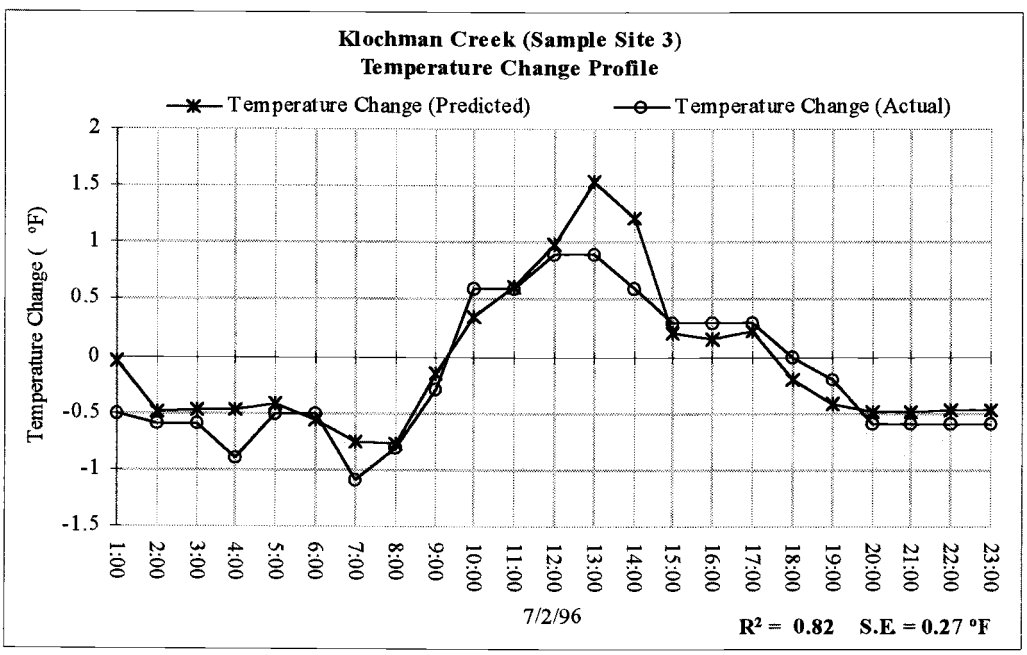

Figure 4.12. Klochman Creek (Sample Site 3) temperature change profile for 7/2/96.

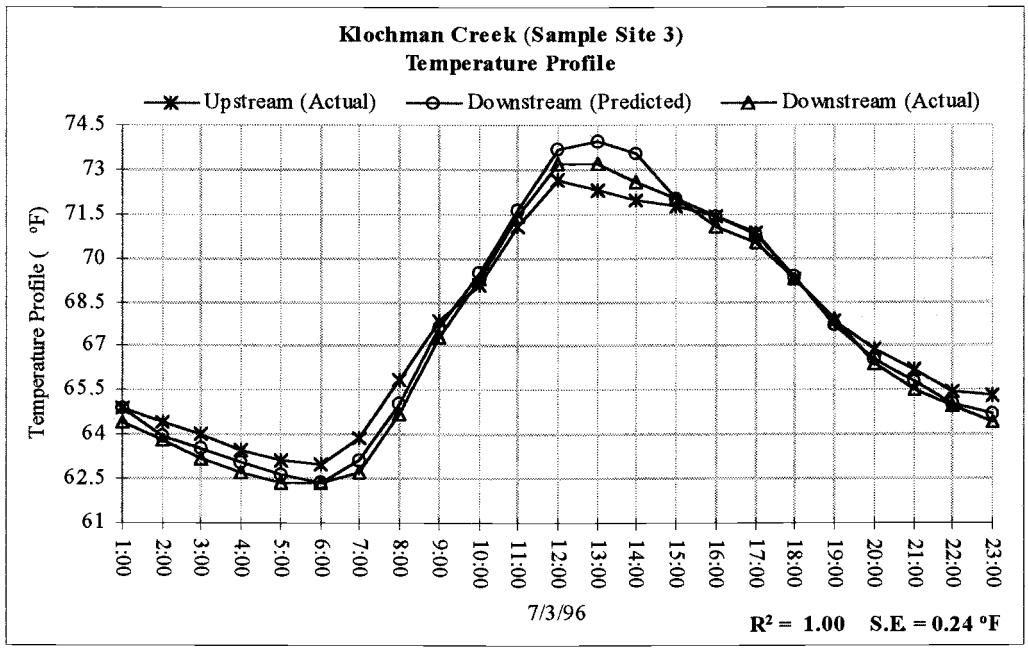

Figure 4.13. Klochman Creek (Sample Site 3) temperature profile for 7/3/96.

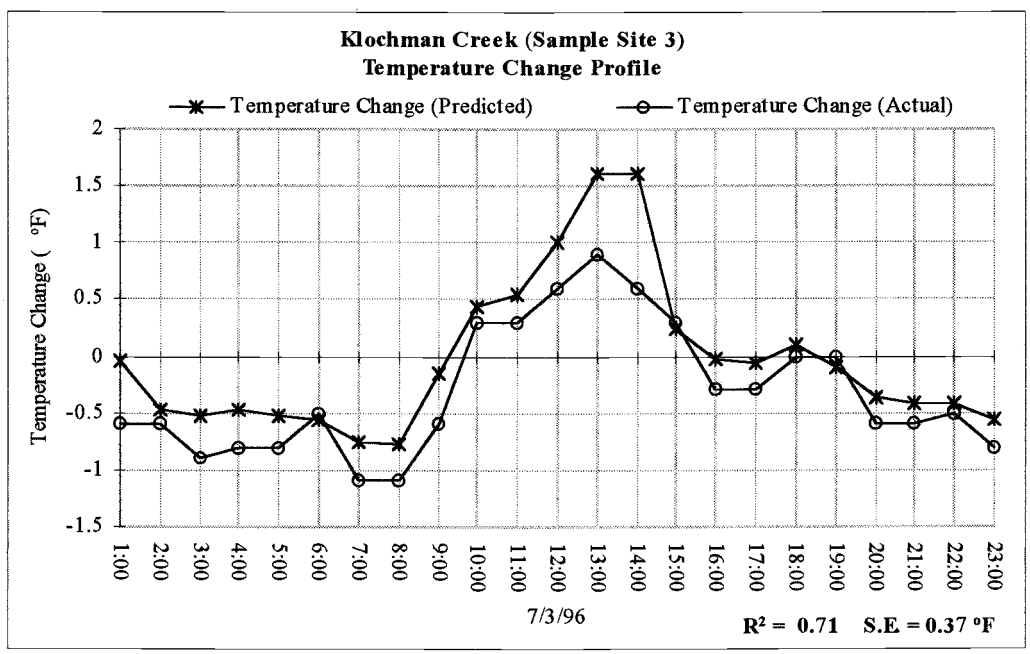

Figure 4.14. Klochman Creek (Sample Site 3) temperature change profile for 7/3/96.

4.1.4 Klochman Creek (Sample Site 4)

The stream bank vegetation consisted of well spaced juniper trees, fifteen feet in height, and grass, one foot in height. Stream flow volume was three cubic feet per second. The stream was shallow, with an average depth of ten to eleven inches. The length of the defined reach was 600 feet, over which the stream exhibited little change in channel morphology. Wind speed was considered negligible for June 29, however, a wind was present for July 1 and July 2. No clouds were present during simulation.

Record Keeping				
Units	English			
Date of Simulation	6/29/96, 7/1/96, 7/2/96 1:00 am			
Duration of Simulation	1 days			
Elevation	3900 feet			
Latitude	44°			
Longitude	120.75°			
Time Zone	Pacific			
Reach Length	600 feet			
Atmospheric Parameters				
Wind Speed	0 mph (6/29), 2.5 mph (7/1, 7/2)			
Cloud Cover	clear (0%)			
Relative Humidity	20 %			
Hydraulic Parameters	Upstream		Downstream	
Flow Velocity	0.81 feet/second		0.81 feet/second	
Stream Flow	3.09 cubic feet per second		3.27 cubic feet per second	
Average Width	4.3 feet		4.5 feet	
Stream Bed Slope	0.01		0.01	
Percent Bedrock	25 %		25 %	
Stream Aspect	273° from North		158° from North	
Shade Parameters	Upstream		Downstream	
	Left	Right	Left	Right
Topographic Shade Angle	10°	15°	5°	10°
Vegetation Shade Angle	25°	20°	50°	45°
Stream Bank Slope	0.1	0.1	0.1	0.1
Vegetation Height	1.0 feet	1.0 feet	1.5 feet	1.5 feet
Vegetation Width	10 feet	10 feet	15 feet	15 feet
Canopy Coefficient	0.3	0.3	0.3	0.3

Table 4.4. Input Parameters for Klochman Creek (Sample Site 4 - 6/29/96, 7/1/96, 7/2/96).

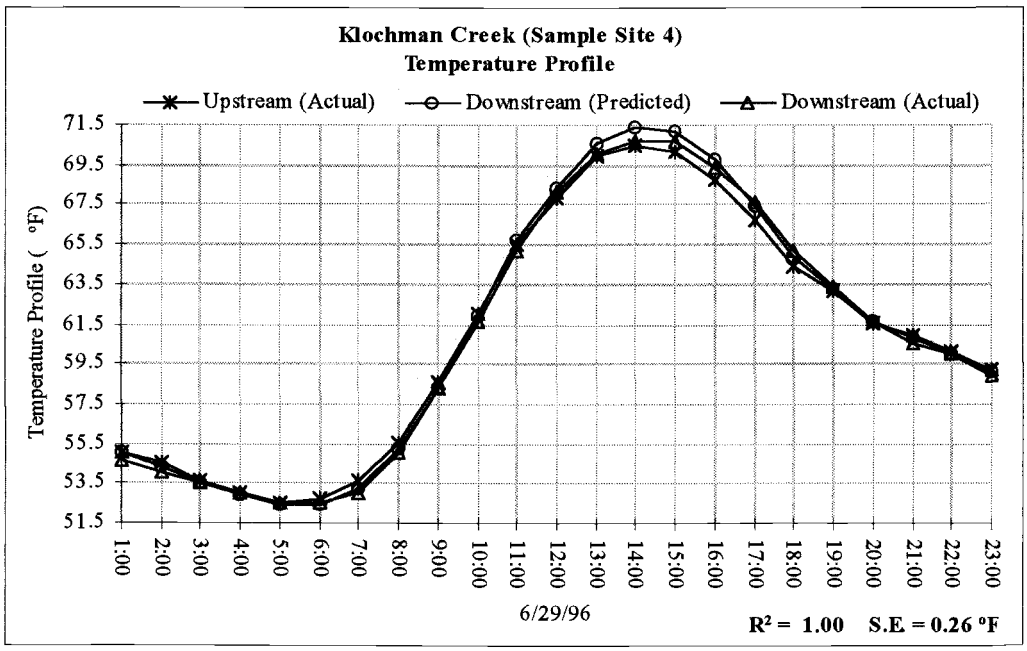

Figure 4.15. Klochman Creek (Sample Site 4) temperature profile for 6/29/96.

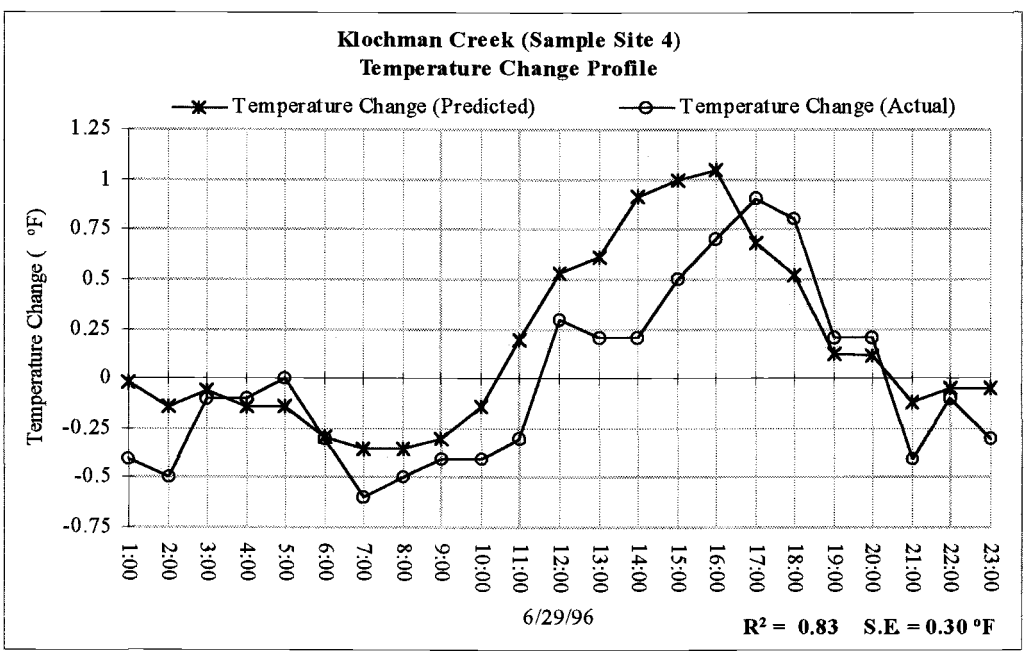

Figure 4.16. Klochman Creek (Sample Site 4) temperature change profile for 6/29/96.

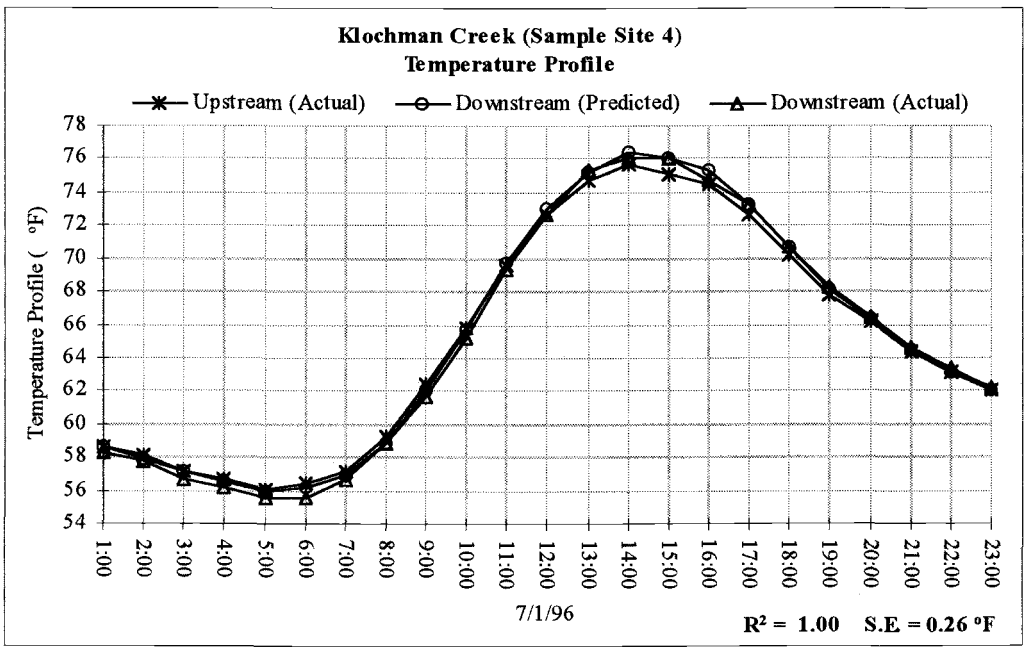

Figure 4.17. Klochman Creek (Sample Site 4) temperature profile for 7/1/96.

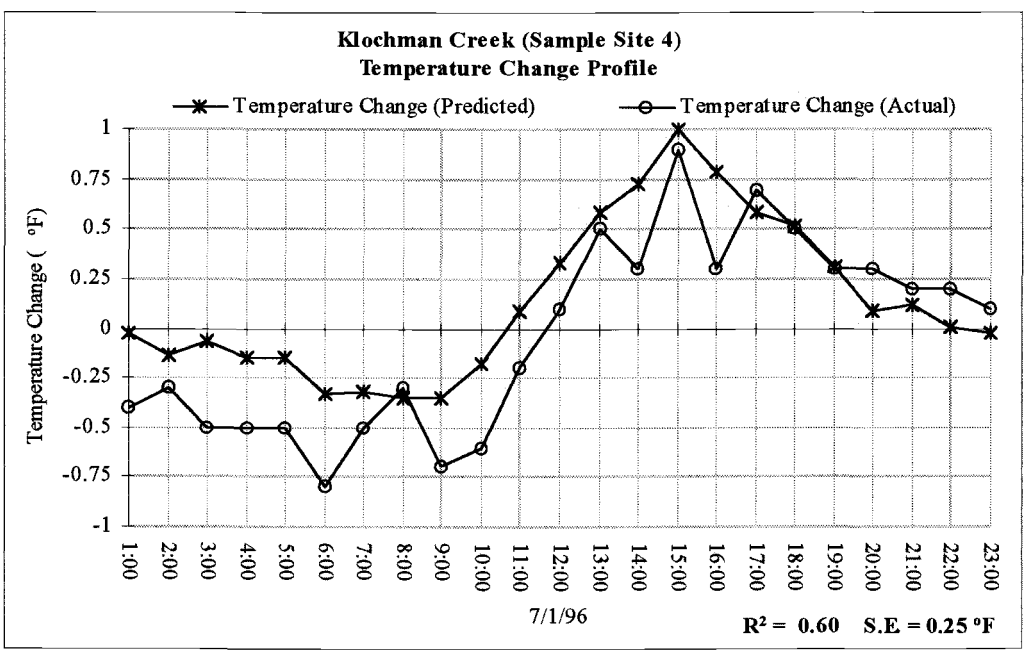

Figure 4.18. Klochman Creek (Sample Site 4) temperature change profile for 7/1/96.

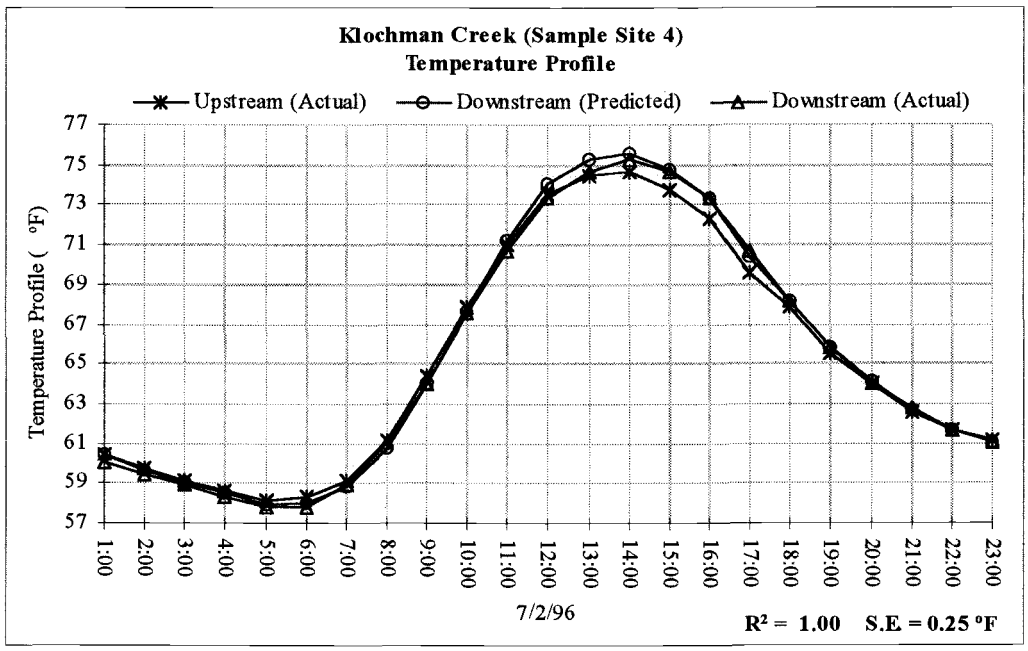

Figure 4.19. Klochman Creek (Sample Site 4) temperature profile for 7/2/96.

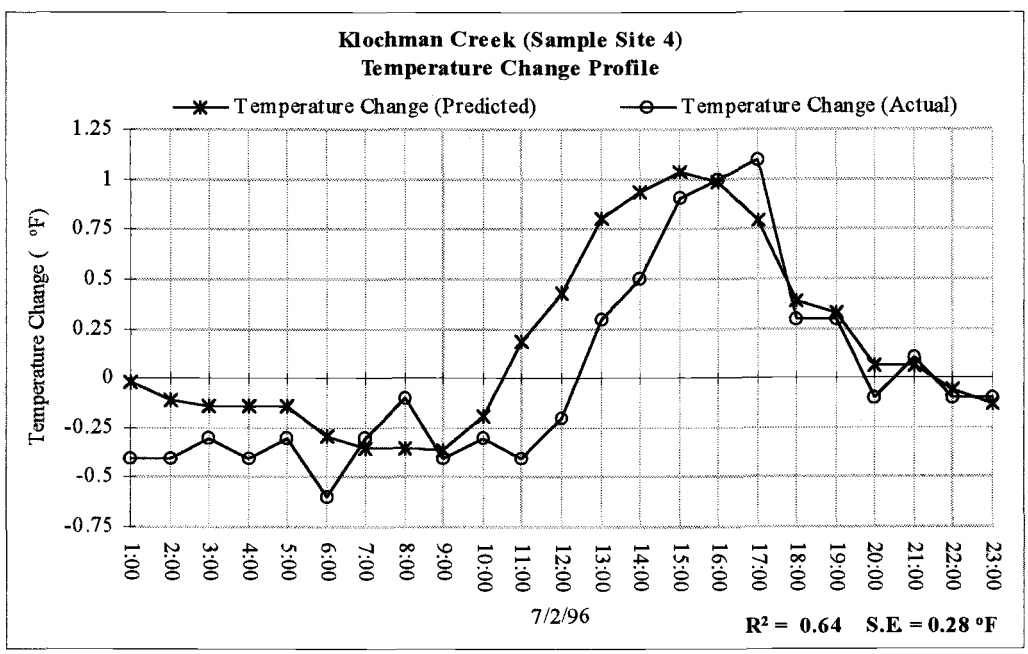

Figure 4.20. Klochman Creek (Sample Site 4) temperature change profile for 7/2/96.

4.1.5 Klochman Creek (Sample Site 5)

The stream bank vegetation at the upstream boundary consisted of well spaced juniper trees, fifteen feet in height, while the downstream portion of the reach was mainly grass, one foot in height. Stream flow volume was just over three cubic feet per second. The stream is shallow, with an average depth of nine to eleven inches. The length of the defined reach was 2600 feet. Wind speed was considered negligible for June 29, however, a wind was present for July 1. No clouds were present during simulation.

Record Keeping				
Units	English			
Date of Simulation	6/29/96, 7/1/96 1:00 am			
Duration of Simulation	1 days			
Elevation	3900 feet			
Latitude	44°			
Longitude	120.75°			
Time Zone	Pacific			
Reach Length	2600 feet			
Atmospheric Parameters				
Wind Speed	0 mph (6/29), 2.5 mph (7/1)			
Cloud Cover	clear (0%)			
Relative Humidity	20 %			
Hydraulic Parameters	Upstream		Downstream	
Flow Velocity	0.96 feet/second		0.96 feet/second	
Stream Flow	3.27 cubic feet per second		3.35 cubic feet per second	
Average Width	4.5 feet		4.2 feet	
Stream Bed Slope	0.01		0.01	
Percent Bedrock	25 %		25 %	
Stream Aspect	158° from North		210° from North	
Shade Parameters	Upstream		Downstream	
	Left	Right	Left	Right
Topographic Shade Angle	5°	10°	5°	10°
Vegetation Shade Angle	50°	45°	50°	45°
Stream Bank Slope	0.1	0.1	0.1	0.1
Vegetation Height	15.0 feet	15.0 feet	1.5 feet	1.0 feet
Vegetation Width	45.0 feet	30.0 feet	15.0 feet	30.0 feet
Canopy Coefficient	0.3	0.3	0.3	0.3

Table 4.5. Input Parameters for Klochman Creek (Sample Site 5 - 6/29/96, 7/1/96).

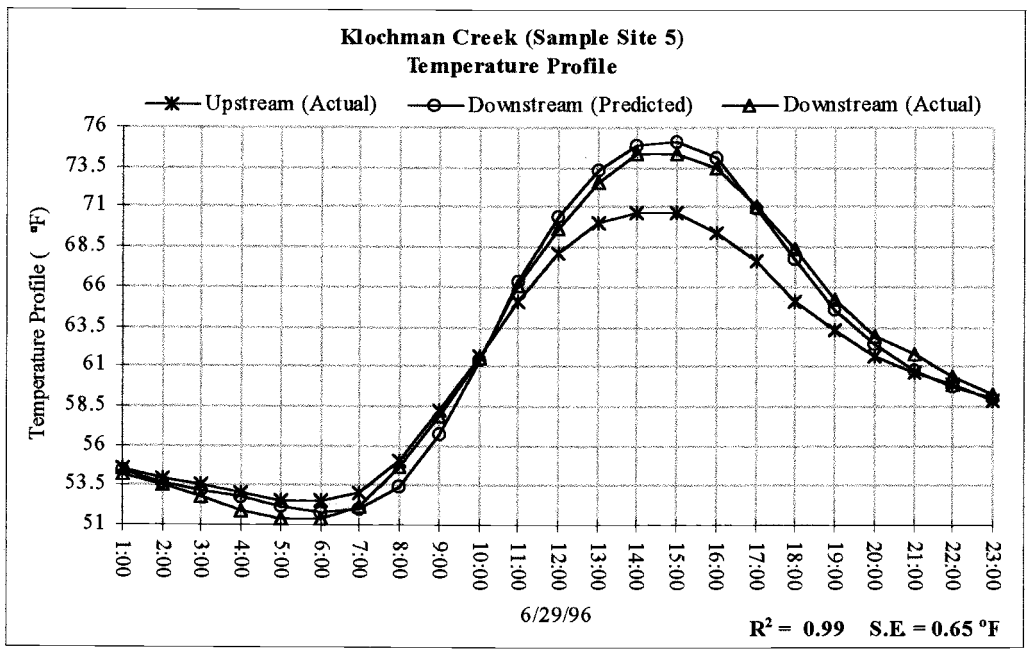

Figure 4.21. Klochman Creek (Sample Site 5) temperature profile for 6/29/96.

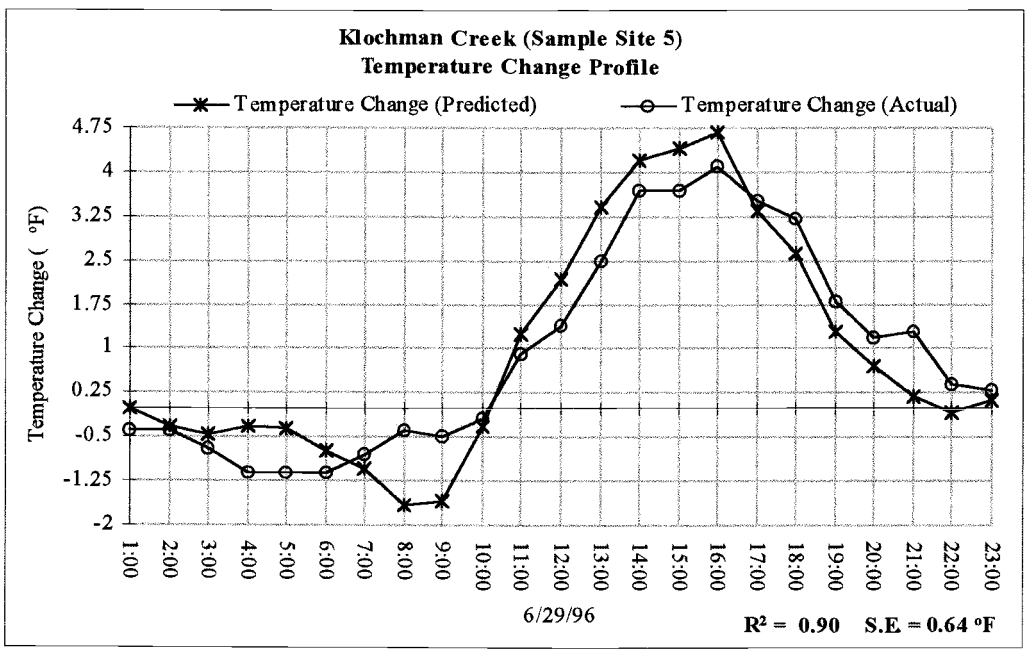

Figure 4.22. Klochman Creek (Sample Site 5) temperature change profile for 6/29/96.

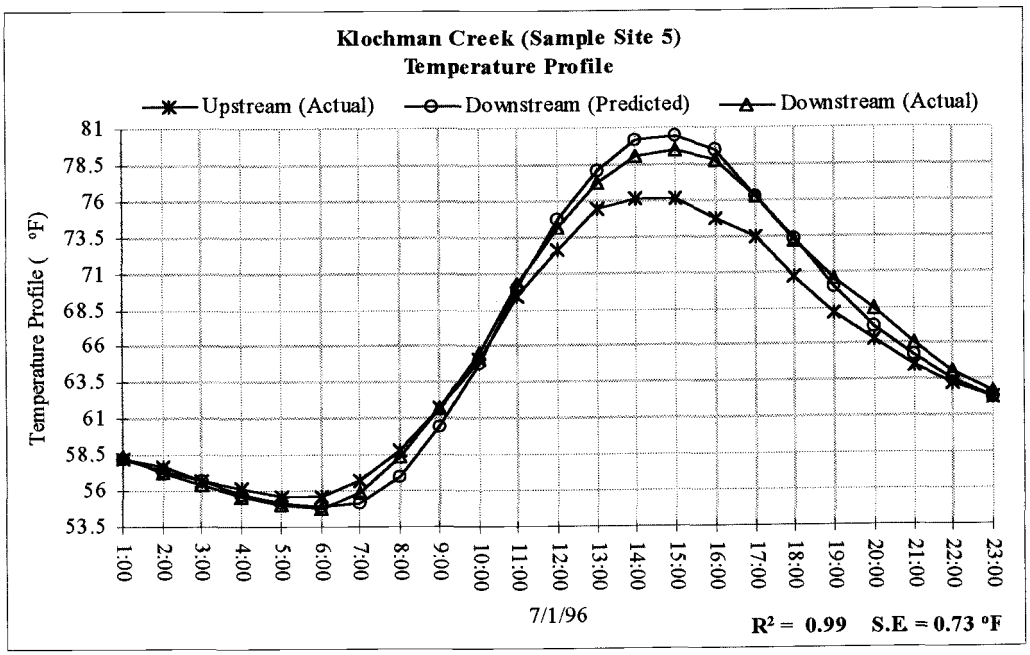

Figure 4.23. Klochman Creek (Sample Site 5) temperature profile for 7/1/96.

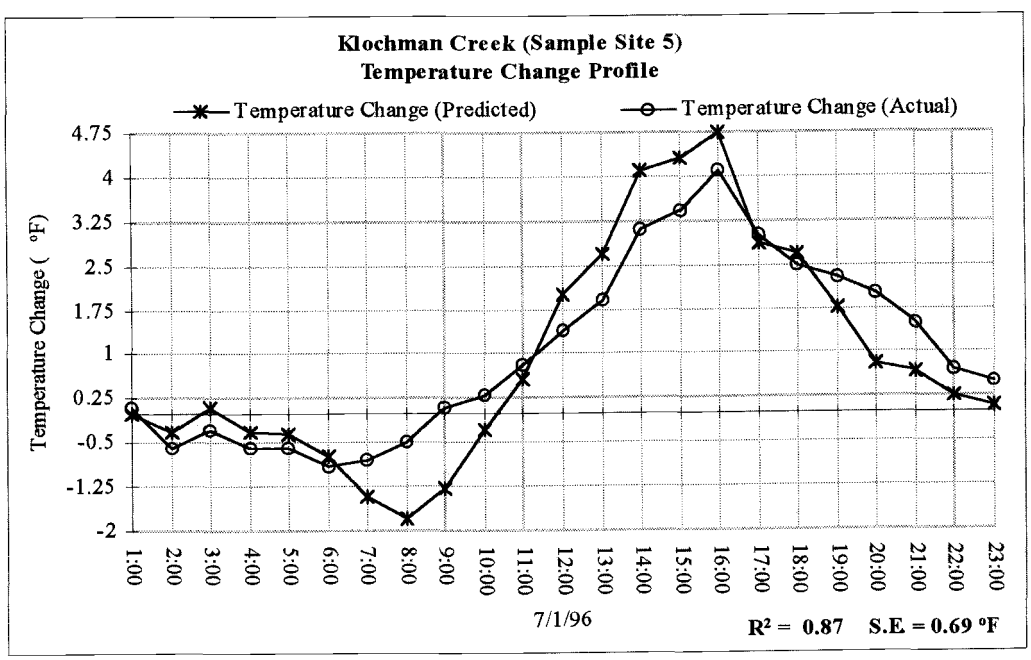

Figure 4.24. Klochman Creek (Sample Site 5) temperature change profile for 7/1/96.

4.1.6 Bear Creek (Sample Site 6)

Located roughly 40 miles southeast of Prineville, Oregon, Bear Creek flows from east/southeast to west/northwest. The stream bank vegetation was grass, one foot or less in height, and was uniform over the entire reach. Vegetation and topographic shading angles were low. Stream flow volume was about three cubic feet per second. The stream is shallow, with an average depth of four to ten inches. The length of the defined reach was 800 feet. Wind was present for July 4. No clouds were present during simulation.

Record Keeping				
Units	English			
Date of Simulation	7/4/96 1:00 am			
Duration of Simulation	1 days			
Elevation	3800 feet			
Latitude	44°			
Longitude	120.75 °			
Time Zone	Pacific			
Reach Length	800 feet			
Atmospheric Parameters				
Wind Speed	2.5 mph			
Cloud Cover	clear (0%)			
Relative Humidity	20 %			
Hydraulic Parameters	Upstream		Downstream	
Flow Velocity	1.10 feet/second		1.10 feet/second	
Stream Flow	2.96 cubic feet per second		3.12 cubic feet per second	
Average Width	6.7 feet		7.1 feet	
Stream Bed Slope	0.01		0.01	
Percent Bedrock	25 %		25 %	
Stream Aspect	210° from North		220° from North	
Shade Parameters	Upstream		Downstream	
	Left	Right	Left	Right
Topographic Shade Angle	5°	15°	10°	15°
Vegetation Shade Angle	24°	24°	24°	24°
Stream Bank Slope	0.1	0.1	0.1	0.1
Vegetation Height	1.0 foot	1.0 foot	1.0 foot	1.0 foot
Vegetation Width	10.0 feet	10.0 feet	15.0 feet	15.0 feet
Canopy Coefficient	0.3	0.3	0.3	0.3

Table 4.6. Input Parameters for Bear Creek (Sample Site 1 - 7/4/96).

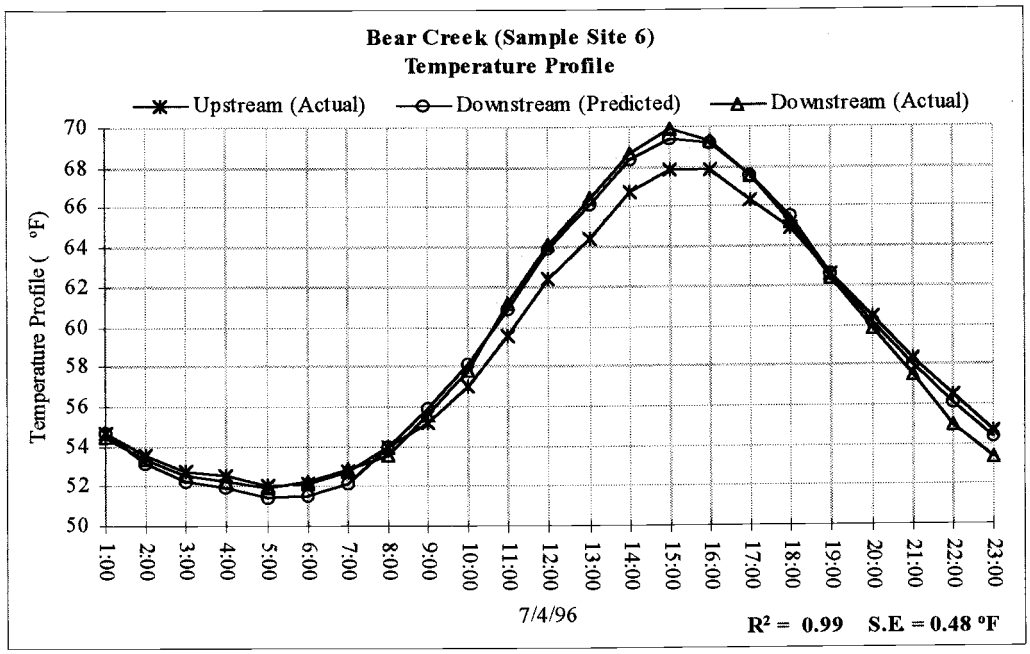

Figure 4.25. Bear Creek (Sample Site 6) temperature profile for 7/4/96.

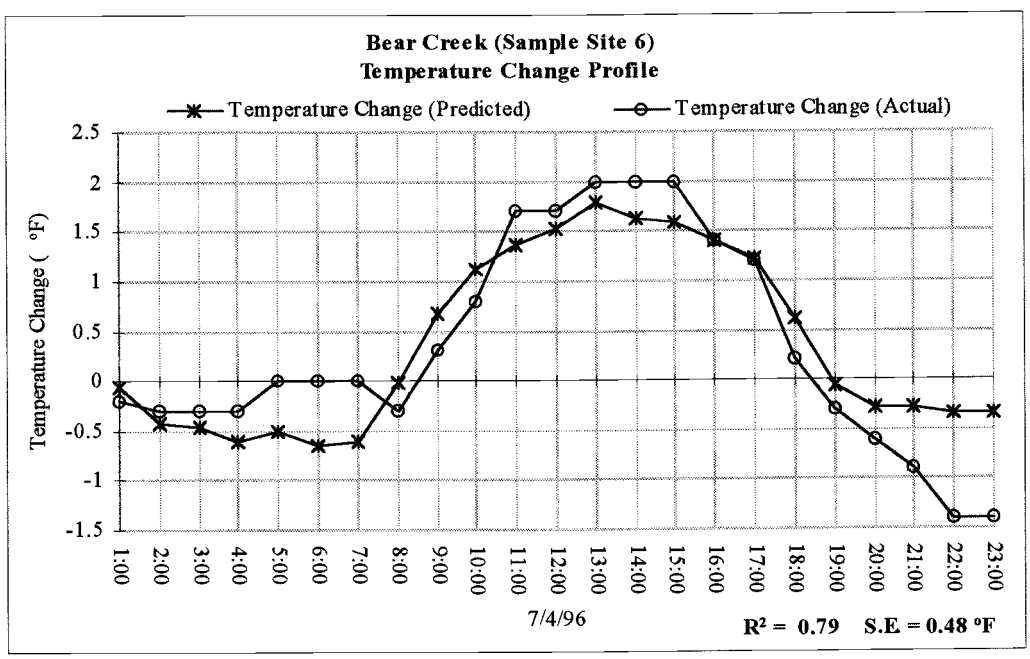

Figure 4.26. Bear Creek (Sample Site 6) temperature change profile for 7/4/96.

4.1.7 Rock Creek (Sample Site 7)

Rock Creek is located in the foot-hills to Mary's Peak, near Philomath, Oregon, and flows from Northeast to Southwest. The vegetation canopy provides high shading levels to the stream. Flow volume is high and velocities are moderate. The stream is shallow, with an average depth of 10 to 11 inches. Bed rock consists of 100% large gravel, cobble and boulders. The length of the defined reach was 505 feet and exhibited little change in channel morphology with respect to position. Wind speed was negligible and no clouds were present during simulation.

Record Keeping				
Units	English			
Date of Simulation	6/6/96 1:00 am			
Duration of Simulation	1 days			
Elevation	500 feet			
Latitude	44.5°			
Longitude	123.5°			
Time Zone	Pacific			
Reach Length	505 feet			
Atmospheric Parameters				
Wind Speed	0 mph			
Cloud Cover	clear (0%)			
Relative Humidity	25 %			
Hydraulic Parameters	Upstream		Downstream	
Flow Velocity	1.25 feet/second		1.25 feet/second	
Stream Flow	13.4 cubic feet per second		13.4 cubic feet per second	
Average Width	12 feet		12 feet	
Stream Bed Slope	0.01		0.01	
Percent Bedrock	100%		100%	
Stream Aspect	175° from North		170° from North	
Shade Parameters	Upstream		Downstream	
	Left	Right	Left	Right
Topographic Shade Angle	0°	0°	0°	0°
Vegetation Shade Angle	65°	45°	70°	40°
Stream Bank Slope	0.1	0.1	0.1	0.1
Vegetation Height	20 feet	20 feet	20 feet	20 feet
Vegetation Width	30 feet	30 feet	30 feet	30 feet
Canopy Coefficient	0.4	0.4	0.4	0.3

Table 4.7. Input Parameters for Rock Creek (Sample Site 7 - 6/6/96).

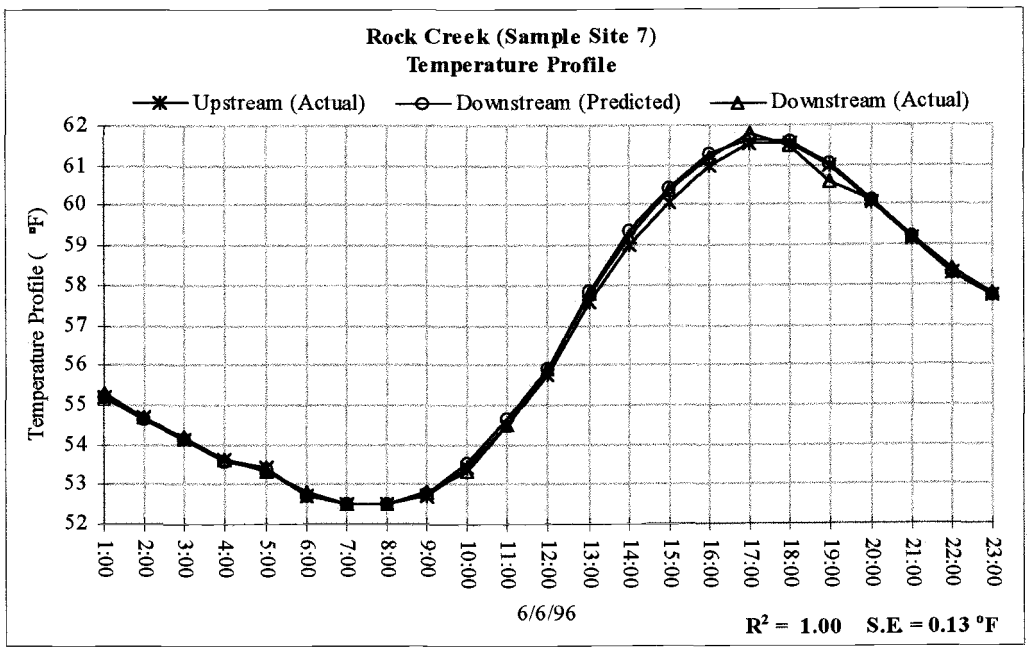

Figure 4.27. Rock Creek (Sample Site 7) temperature profile for 6/6/96.

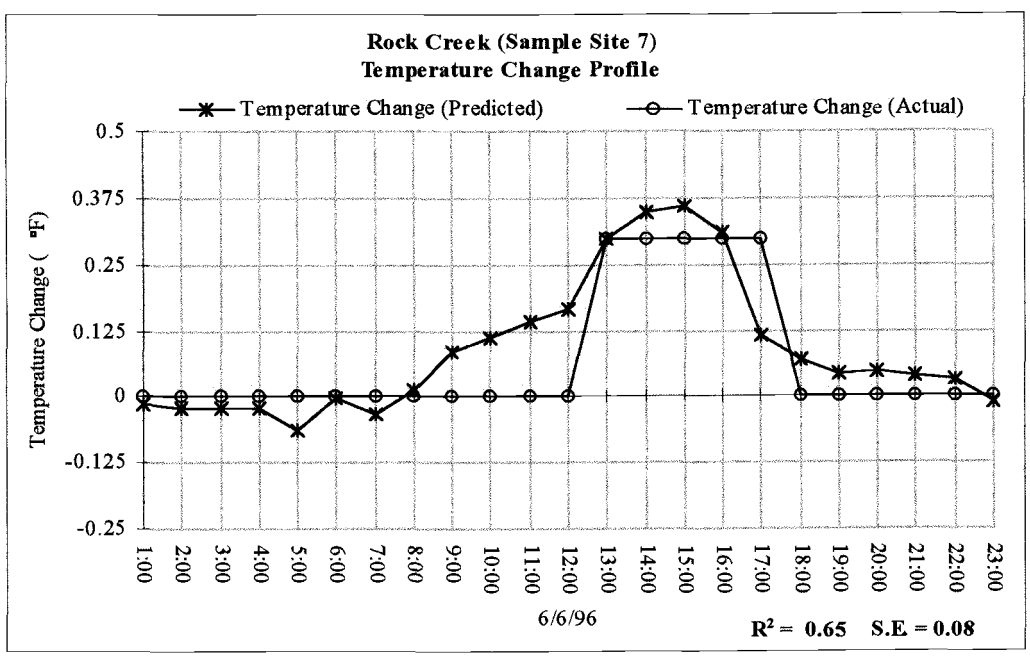

Figure 4.28. Rock Creek (Sample Site 7) temperature change profile for 6/6/96.

4.1.8 Moore Creek (Sample Site 8)

Located near Corvallis, Oregon, Moore Creek flows from southwest to northeast. A few small trees were located on the stream banks, but in general, the stream bank vegetation consisted of tall grass. Flow volume is small and velocity is slow. The stream is shallow, with an average depth of 6 to 7 inches. The length of the defined reach was 715 feet and exhibited little change in channel morphology and shading characteristics with respect to position. Wind speed was negligible and no clouds were present during simulation.

Record Keeping				
Units	English			
Date of Simulation	6/8/96 1:00 am			
Duration of Simulation	1 days			
Elevation	250 feet			
Latitude	45°			
Longitude	123 °			
Time Zone	Pacific			
Reach Length	715 feet			
Atmospheric Parameters				
Wind Speed	0 mph			
Cloud Cover	clear (0%)			
Relative Humidity	53 %			
Hydraulic Parameters	Upstream		Downstream	
Flow Velocity	0.8 feet/second		0.8 feet/second	
Stream Flow	0.7 cubic feet per second		0.7 cubic feet per second	
Average Width	2.25 feet		2.25 feet	
Stream Bed Slope	0.01		0.01	
Percent Bedrock	10 %		10 %	
Stream Aspect	46° from North		48° from North	
Shade Parameters	Upstream		Downstream	
	Left	Right	Left	Right
Topographic Shade Angle	5°	0°	5°	0°
Vegetation Shade Angle	59°	59°	59°	59°
Stream Bank Slope	0.1	0.1	0.1	0.1
Vegetation Height	3 feet	3 feet	3 feet	3 feet
Vegetation Width	20 feet	20 feet	20 feet	20 feet
Canopy Coefficient	0.2	0.2	0.2	0.2

Table 4.8. Input Parameters for Moore Creek (Sample Site 8 - 6/8/96).

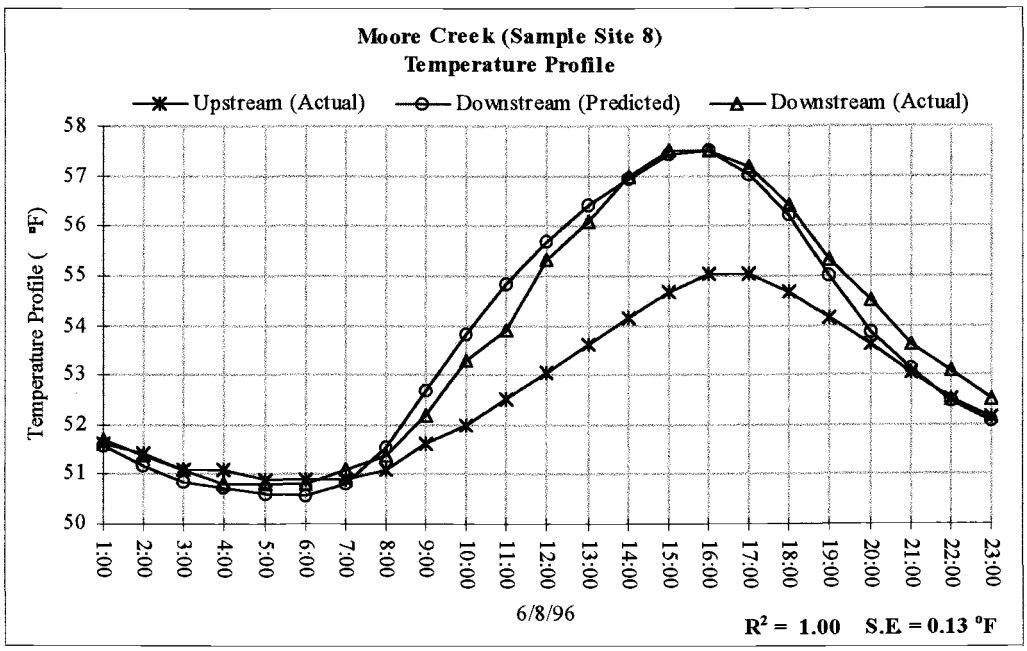

Figure 4.29. Moore Creek (Sample Site 8) temperature profile for 6/8/96.

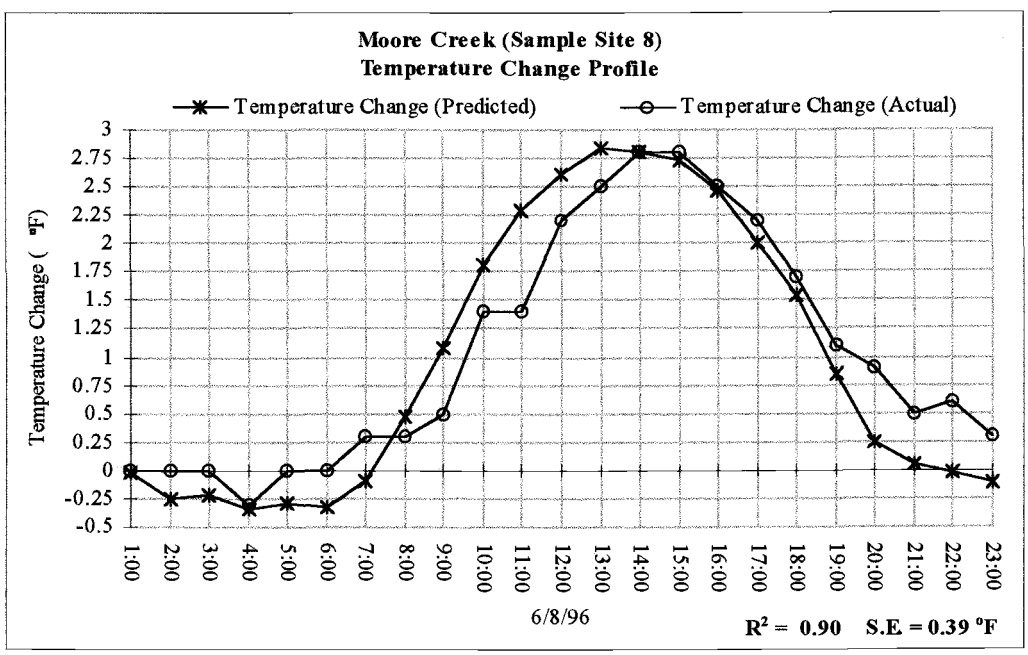

Figure 4.30. Moore Creek (Sample Site 8) temperature change profile for 6/8/96.

4.1.9 Summary of Model Accuracy

Table 4.9 summarizes the model accuracy for each of the preceding simulations.

		Temperature Profile		Temperature Change	
Sample Site	**Date**	**R^2**	**S.E.**	**R^2**	**S.E.**
1	6/29/96	1.00	0.29 °F	0.86	0.29 °F
1	6/30/96	1.00	0.28 °F	0.86	0.26 °F
1	7/2/96	1.00	0.28 °F	0.96	0.27 °F
1	7/3/96	1.00	0.32 °F	0.87	0.28 °F
2	7/2/96	0.99	0.38 °F	0.92	0.38 °F
3	7/2/96	0.99	0.26 °F	0.82	0.27 °F
3	7/3/96	1.00	0.24 °F	0.71	0.37 °F
4	6/29/96	1.00	0.26 °F	0.83	0.30 °F
4	7/1/96	1.00	0.26 °F	0.60	0.25 °F
4	7/2/96	1.00	0.25 °F	0.64	0.28 °F
5	6/29/96	0.99	0.65 °F	0.90	0.64 °F
5	7/1/96	0.99	0.73 °F	0.87	0.69 °F
6	7/4/96	0.99	0.48 °F	0.79	0.48 °F
7	6/6/96	1.00	0.13 °F	0.65	0.08 °F
8	6/8/96	1.00	0.13 °F	0.90	0.39 °F
	Average:	**1.00**	**0.33 °F**	**0.82**	**0.35 °F**

Table 4.9. Summary of model accuracy.

4.2 Sensitivity Analysis

Model sensitivity to input parameter change was tested by using the input values, listed in Table 4.10, for an imaginary stream system.

Record Keeping				
Date of Simulation	7/20/96 1:00 am			
Duration of Simulation	1 days			
Elevation	3000 feet			
Latitude	45 °			
Longitude	121 °			
Time Zone	Pacific			
Reach Length	800 feet			
Atmospheric Parameters				
Wind Speed	5 mph			
Cloud Cover	clear (0%)			
Relative Humidity	25 %			
Hydraulic Parameters	Upstream		Downstream	
Flow Velocity	1.5 feet/second		1.5 feet/second	
Stream Flow	2.0 cubic feet per second		2.0 cubic feet per second	
Average Width	3 feet		3 feet	
Stream Bed Slope	0.01		0.01	
Percent Bedrock	50 %		50 %	
Stream Aspect	180° from North		180° from North	
Shade Parameters	Upstream		Downstream	
	Left	Right	Left	Right
Topographic Shade Angle	5°	5°	5°	5°
Vegetation Shade Angle	45°	45°	45°	45°
Stream Bank Slope	0.1	0.1	0.1	0.1
Vegetation Height	10 feet	10 feet	10 feet	10 feet
Vegetation Width	20 feet	20 feet	20 feet	20 feet
Canopy Coefficient	0.5	0.5	0.5	0.5
Temperature Data	Minimum	Time	Maximum	Time
Air Temperature	45 °F	4:00 am	80 °F	5:00 PM
Upstream Temperature	50 °F	6:00 am	65 °F	4:00 PM

Table 4.10. Listing of input parameters for sensitivity analysis.

Each input parameter was incrementally changed between a minimum of -100% and a maximum of +100%, where 0% represents no change. The maximum stream temperature change incurred over the defined reach was then recorded. All other input

values where constant during the testing of each input. Maximum stream temperature sensitivity to each input parameter was then ranked and classified as either high (greater than 67%), moderate (33% to 67%) or low (less than 33%). The testing of model sensitivity not only put *Heat Source* through rigorous simulation scenarios, but also provided insight as to how stream system thermodynamics react to the various atmospheric, hydrologic and shading input parameters.

Atmospheric input parameters, displayed in Figure 4.31, generally exhibit low sensitivity. Wind speed, varied from 0 mph (-100%) to 10 mph (+100%), was inversely linearly proportional to stream temperature change. Evaporation is a linear function of wind speed, which explains the linearity of the stream temperature response to changing wind speed input values. The model sensitivity to wind speed is consistent with the general understanding of the stream system and the algorithms employed.

Stream temperature sensitivity to a maximum daily air temperature, ranging from 32.0° F (-60%) to 120.0° F (+50%), displays a slightly non-linear relationship to stream temperature change (Figure 4.31). Air temperature is utilized in the heat energy balance for atmospheric long-wave flux, vegetation long-wave flux, convection flux and vapor pressure calculations. Even though air temperature values are heavily used by this methodology, the sensitivity of the stream system to maximum daily air temperature is considered low. Simulation for a maximum daily air temperature of 40.0° F (-50%), yielded a 18% decrease in maximum stream temperature change. Further, simulation for a maximum daily air temperature of 120.0° F (+50%), yielded a 10% increase in maximum stream temperature change.

Sensitivity results for relative humidity are consistent with the understanding of the physics of evaporation and the algorithms used to describe the vapor gradient between the surface of the stream and the air directly above the stream surface. The maximum daily stream temperature change was ±10% corresponding to a ±50% change in relative humidity (Figure 4.31) and the sensitivity was low.

Maximum daily stream temperature sensitivity to elevation was extremely low (Figure 4.31). The values tested ranged from 0 feet (-100%) to 6000 feet (+100%). Elevation is used to calculate the optical air mass of the atmosphere, which is then utilized in solar flux calculations. Elevation is also used to calculate barometric pressure, which then is utilized for virtual temperature calculations.

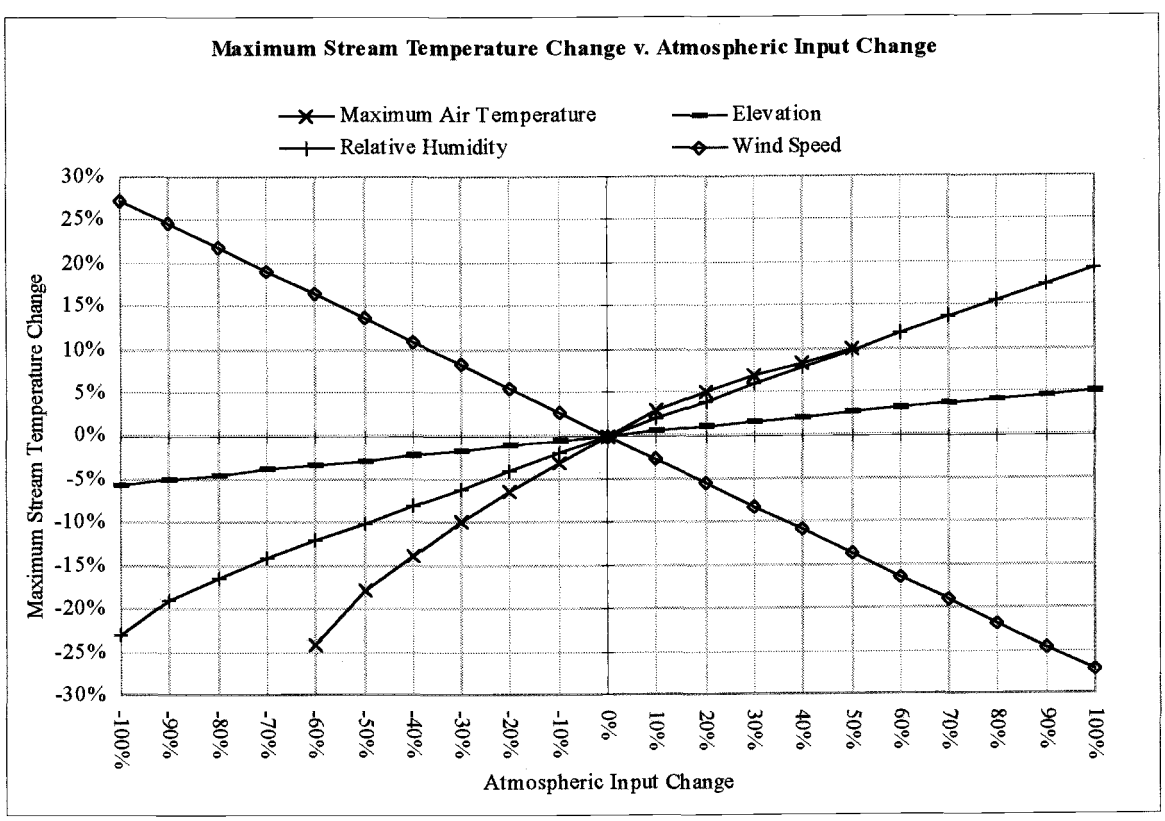

Figure 4.31. Maximum stream temperature sensitivity analysis for atmospheric input parameters.

Maximum stream temperature sensitivity to channel width is considered to be very high. As channel width increases, the surface area of the stream increases, providing a greater surface area for heat energy exchange between the stream and the atmosphere, namely: short and long-wave radiation processes. Given that flow is steady and the flow volume is conserved, an increase in channel width implies a decrease in stream depth. The rate change of stream temperature is proportional to channel width and inversely proportional to stream depth. Channel width was varied from .3 feet (-90%), where stream depth equaled 4.44 feet, to 6 feet (+100%), where stream depth equaled 0.22 feet. Maximum stream temperature sensitivity to channel width is displayed in Figure 4.32.

The temperature of the water entering the defined reach greatly affects the stream temperature change that occurs within the defined reach. The high sensitivity of the maximum daily stream temperature to the upstream maximum temperature is easily explained. At any instant of time, a defined stream reach is capable of sustaining a particular water column temperature. If the temperature entering a stream reach is greater than that which is supported by energy processes inherent to that reach at a specific time, the temperature will decrease. If the temperature entering a stream reach is less than that which is supported by energy processes inherent to that reach at a specific time, the temperature will increase.

Up stream maximum daily temperatures ranged from 32.5° F (-50%) to 123.5° F (+90%) and are displayed in Figure 4.32. At the lower extreme, the temperature of the water entering the defined reach is significantly lower than the stream system is capable of sustaining, and therefore, a large change in stream temperature occurs over the defined reach. At the highest maximum upstream temperature extreme, the water is entering the

defined reach with a temperature that greatly exceeds that which is supported by the defined reach, and a significant negative temperature change results. Such stream temperature response is commonly experienced with natural stream systems with sudden changes in the stream environment, namely: varying quality and quantity of shade and channel morphology.

By varying the composition of the stream bed material with respect to grain size, the maximum daily stream temperature change sensitivity was found to be low (Figure 4.32). These sensitivity results imply that a reduction in the d_{50} of stream bed material resulted in a small temperature increase, while an increase in the d_{50} of stream bed material resulted in small stream temperature decrease. These results are an artifact of the modeling methodology, and no verification research has been conducted. The stream bed increasingly accepts energy from solar and long-wave radiation as a function of increasing grain size. Increasing the grain size of stream bed materiel will increase radiation absorption. Heat energy is slowly released to the water column based on the conductance of quartz. All energy is conserved, resulting in less heat energy delivered to the water column at maximum radiation periods, but more heat energy delivered to the water column at later periods of the day. Streams with large grain size bed material experience a smaller instantaneous radiation heat energy flux because a portion of the radiation flux is diverted to the stream bed material. Such streams cool at a slower rate because the bulk of the energy stored in the stream bed is released in the late afternoon and evening when the quantity of heat energy stored in the stream bed is greatest.

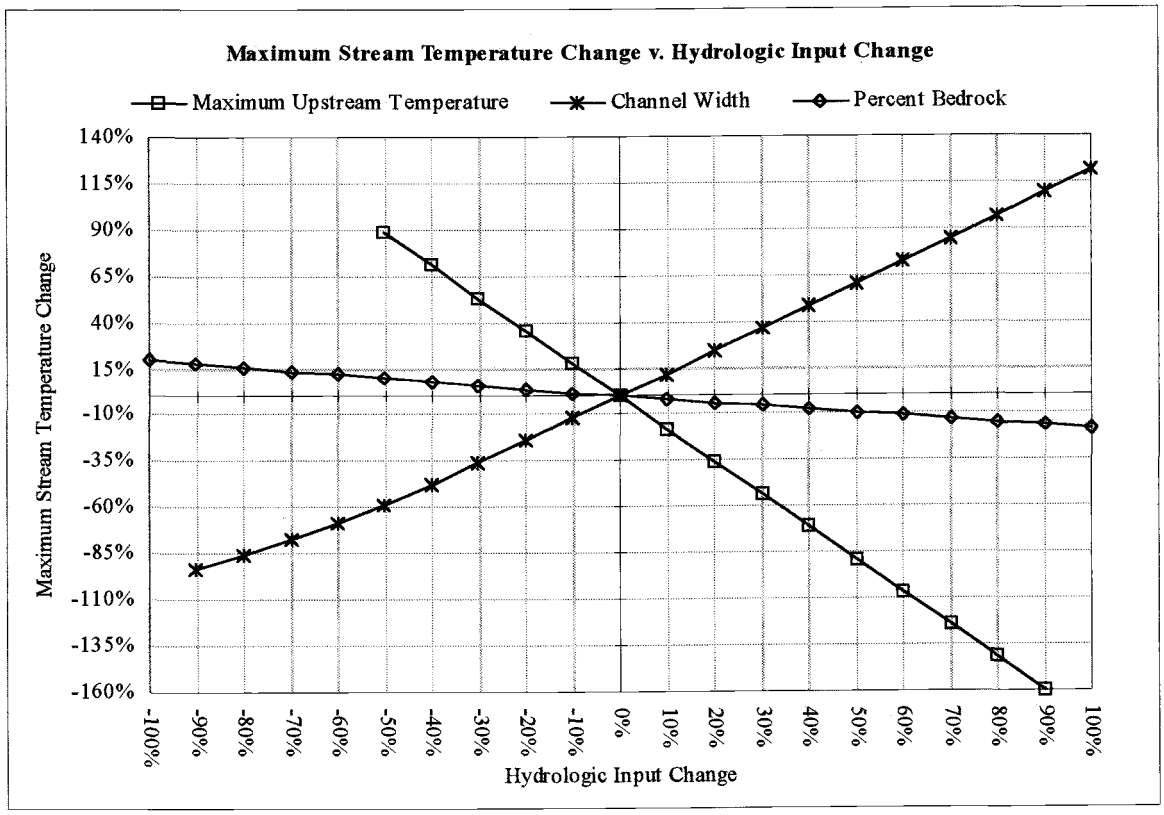

Figure 4.32. Maximum stream temperature sensitivity analysis for hydraulic input parameters.

Maximum stream temperature change was found to highly sensitive to stream flow for inducing a positive temperature change (Figure 4.33). It is widely accepted that low flow streams are highly sensitive to temperature change, while high volume streams and rivers exhibit lower temperature sensitivity. The magnitude of sensitivity serves as a reminder that effort for reducing excessive water temperatures should focus on low volume streams.

The induced maximum daily stream temperature change displayed little sensitivity to flow velocity. Slower velocities serve to increase the duration that the water parcel is exposed to the energy processes contained in the reach. In the case of this particular

reach, the increased time that the water parcel was exposed to the energy balance did not seriously alter the temperature change incurred over the reach distance (Figure 4.33).

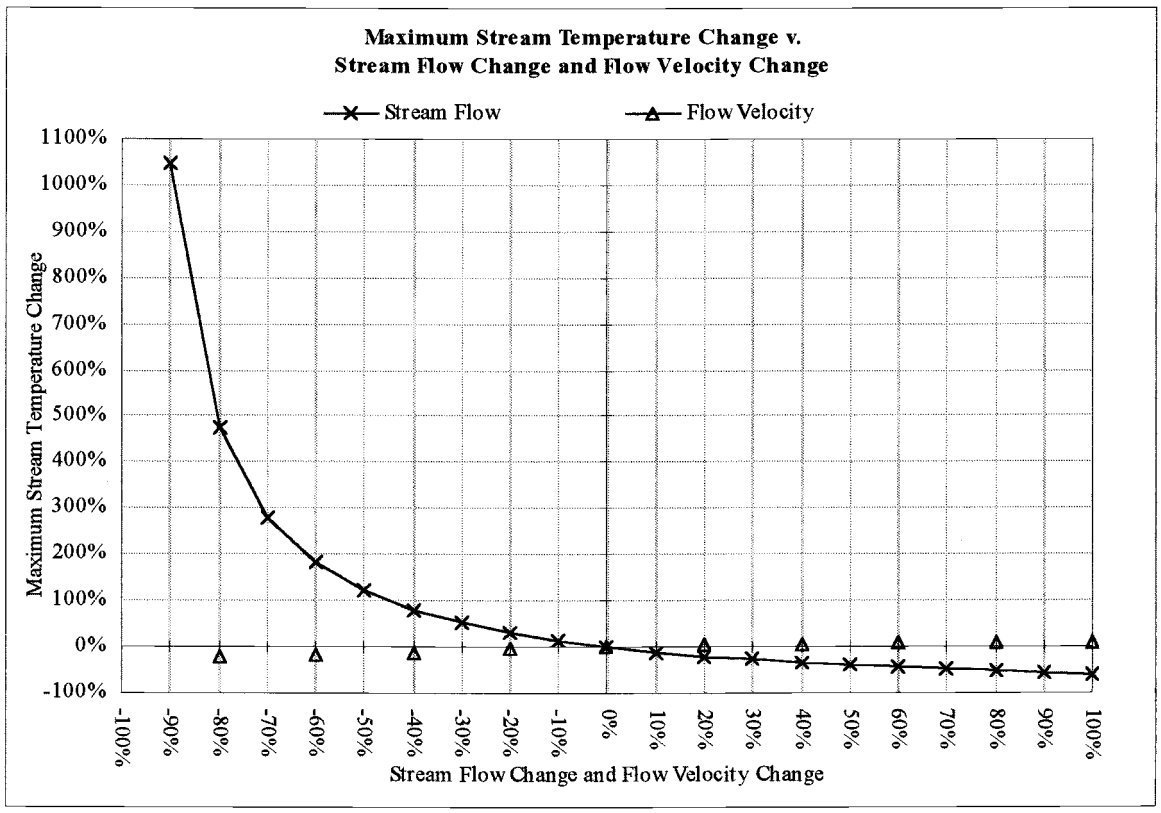

Figure 4.33. Maximum stream temperature sensitivity analysis for stream flow and flow velocity.

Stream Temperature change sensitivity to topographic shading was found to be low (Figure 4.34). This is not to say that topographic shading is insignificant. The topographic shade angles tested were 0° to 10°; the testing of sensitivity is limited to ±100% of the pre-existing input values. It is expected that increased values of the topographic shade angles, beyond those which were tested, would tend to increase the shading experienced by the stream and decrease stream temperature change.

Increasing in the vegetation shade angle significantly controlled stream temperature response. Solar altitude becomes important when considering the sensitivity of stream temperature change to the vegetation shade angle. Vegetation no longer protects the stream from incoming solar radiation once the angle of the sun is greater than the vegetation shade angle. When the sun's angle exceeds the vegetation shading angle, the stream becomes exposed to direct beam solar radiation. Therefore, the daily maximum stream temperature change is not significantly reduced unless the vegetation shading is equal to, or exceeding, the daily solar zenith.

The sensitivity to the canopy density coefficient for a vegetation shade angle equal to 45° is low because the stream is exposed to direct solar radiation for six hours, in which, the maximum change in stream temperature over the reach is only slightly reduced by the brief morning and late afternoon shading periods. When the stream is provided a full complement of shade, by increasing the shade angle to 90°, the maximum stream temperature sensitivity to the canopy density becomes extremely high.

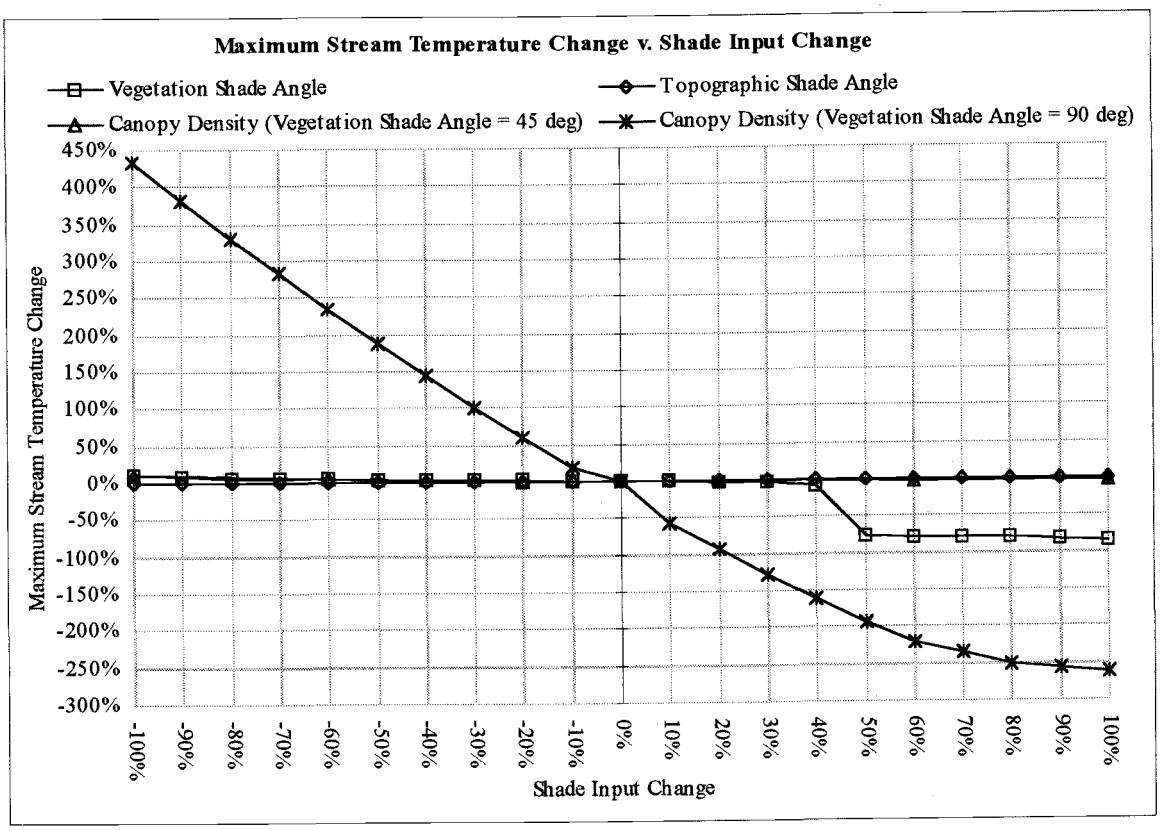

Figure 4.34. Maximum stream temperature change sensitivity analysis for shade input parameters.

Input parameter sensitivity is ranked as to magnitude of positive temperature change (water column heating) and the greatest negative temperature change (water column cooling). The ranking of all input parameters was performed at ±50% the initial value. The results of the sensitivity analysis and ranking allow for classifying stream parameters as high, medium and low sensitivity in inducing stream temperature change.

Ranking of Sensitivity Resulting in Positive Change in Stream Temperature (Sensitivity Reported at ± 50%)

Rank	Input Parameter	Input Change	Temperature Change
	High Sensitivity (> 67%)		
1	Canopy Density (Vegetation Shade Angle = 90°)	-50%	182%
2	Stream Flow	-50%	121%
3	Maximum Upstream Temperature	-50%	89%
	Moderate Sensitivity (33% to 67%)		
4	Channel Width	+50%	60%
	Low Sensitivity (< 33%)		
5	Wind Speed	-50%	14%
6	Percent Bedrock	-50%	10%
6	Relative Humidity	+50%	10%
6	Air Temperature	+50%	10%
7	Flow Velocity	-50%	7%
8	Canopy Density (Vegetation Shade Angle = 45°)	-50%	5%
9	Vegetation Shade Angle	-50%	4%
10	Elevation	+50%	3%
11	Topographic Shade Angle	+50%	0%

Table 4.11. Ranking of model input sensitivities that result in positive temperature change.

Ranking of Sensitivity Resulting in Negative Change in Stream Temperature (Sensitivity Reported at ± 50%)

Rank	Input Parameter	Input Change	Temperature Change
	High Sensitivity (> 67%)		
1	Canopy Density (Vegetation Shade Angle = 90°)	+50%	-190%
2	Maximum Upstream Temp.	+50%	-89%
3	Vegetation Shade Angle	+50%	-76%
	Moderate Sensitivity (33% to 67%)		
4	Channel Width	-50%	-59%
5	Stream Flow	+50%	-40%
	Low Sensitivity (< 33%)		
6	Minimum Air Temperature	-50%	-18%
7	Wind Speed	+50%	-14%
8	Flow Velocity	+50%	-14%
9	Relative Humidity	-50%	-10%
10	Percent Bedrock	+50%	-9%
11	Elevation	-50%	-3%
12	Canopy Density (Vegetation Shade Angle = 45°)	+50%	-2%
13	Topographic Shade Angle	-50%	0%

Table 4.12. Ranking of model input sensitivities that result in negative temperature change.

4.3 Model Application

Given that the model is validated and various input parameters have been ranked for sensitivity, *Heat Source* may then be used to demonstrate the magnitude of influence that specific stream parameters have upon water temperature. The usefulness of simulation becomes apparent when correlating a specific response of water temperature to individual stream parameters. Model application results correlate the magnitude of stream parameters to stream temperature for a hypothetical stream system, the same system used for the sensitivity analysis (Table 4.10).

4.3.1 Vegetation Shading

The timing and duration of stream surface shading is controlled by the vegetation shade angle. Vegetation shade angle magnitude was found to significantly affect stream temperature change (Figure 4.35), which is consistent with the model methodology and previous research. The interaction between the sun and stream side vegetation determines the timing of stream surface shading. Solar altitude becomes important when considering the magnitude and timing of stream temperature change. When the solar angle exceeds the vegetation shading angle, the stream no longer experience a shading level that reduces incoming short-wave radiation. Therefore, the daily maximum stream temperature change is not significantly reduced unless vegetation shading persists for the majority of sunlight hours.

The sun's zenith for July 20, 1996, was calculated as 65.6°, occurring at 1:00 PM. Simulation varied from no stream surface shading to a full compliment of shade

throughout the course of the day by increasing the shade angle beyond that of the local solar zenith. Increasing the shading angle considerably reduced stream temperature. Notice that in Figure 4.35, which displays several different simulations with varied shading angles, that the stream temperature change profiles do not experience a significant decrease until the shade angle is greater than the solar zenith (65.6°).

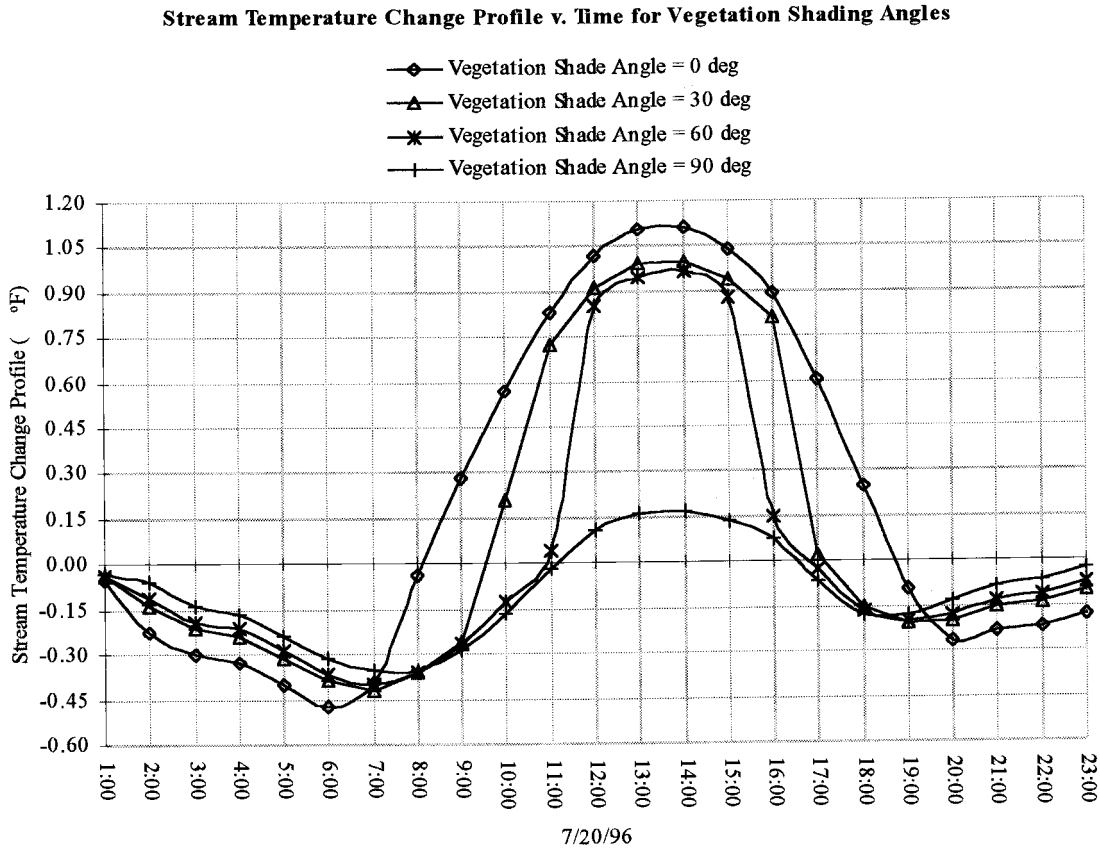

Figure 4.35. Stream temperature change profiles for various vegetation shading angles.

Vegetation density controls the quality of shade that the stream surface experiences. As would be expected, the quality of shade provided to the stream is reduced in less dense vegetation canopies. Figure 4.36 shows the stream temperature change that occurs for various canopy densities when the vegetation shade angle is 45°. At this

shading angle, significant temperature reduction does not occur, largely because the vegetation is not providing a full compliment of shade to the stream surface. The stream is only shaded until just before 10:00 AM when the sun's angle exceeds 45°. The predicted solar angle at 10:00 AM is 45.7°. Shade does not return until slightly after 4:00 PM when the solar angle is 45.9°. Direct exposure to solar radiation persists for six hours, in which, the maximum change in stream temperature is only slightly reduced by the brief morning and late afternoon shading periods. The results suggest that increased vegetation density does not buffer stream temperatures for streams that are provided limited shading duration.

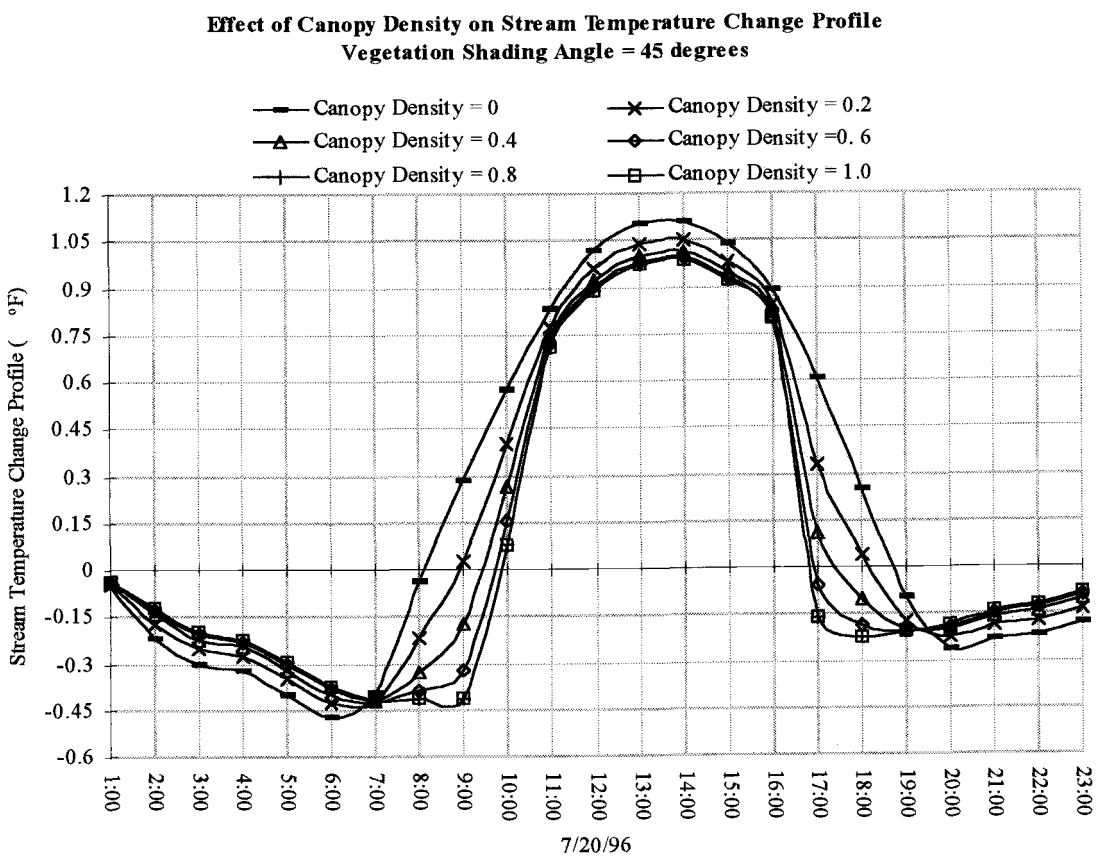

Figure 4.36. Stream temperature change profiles for various canopy densities (vegetation shade angle = 45°).

When the stream is provided a full complement of shade, by increasing the shade angle, increased vegetation density controls the quality of stream surface shading. Figure 4.37, the effect of vegetation density on stream temperature for a shade angle of 90°, not only shows the significance of providing the stream a shade duration that spans the length of the diurnal cycle, but demonstrates that the quality of the shade is just as important in controlling stream temperature. Even when the stream is fully shaded, less dense vegetation does not adequately prevent stream temperature increase. Incoming solar radiation is completely attenuated when the canopy coefficient is 1.0 for a vegetation shade angle of 90°, resulting in a stream temperature decreases over the reach.

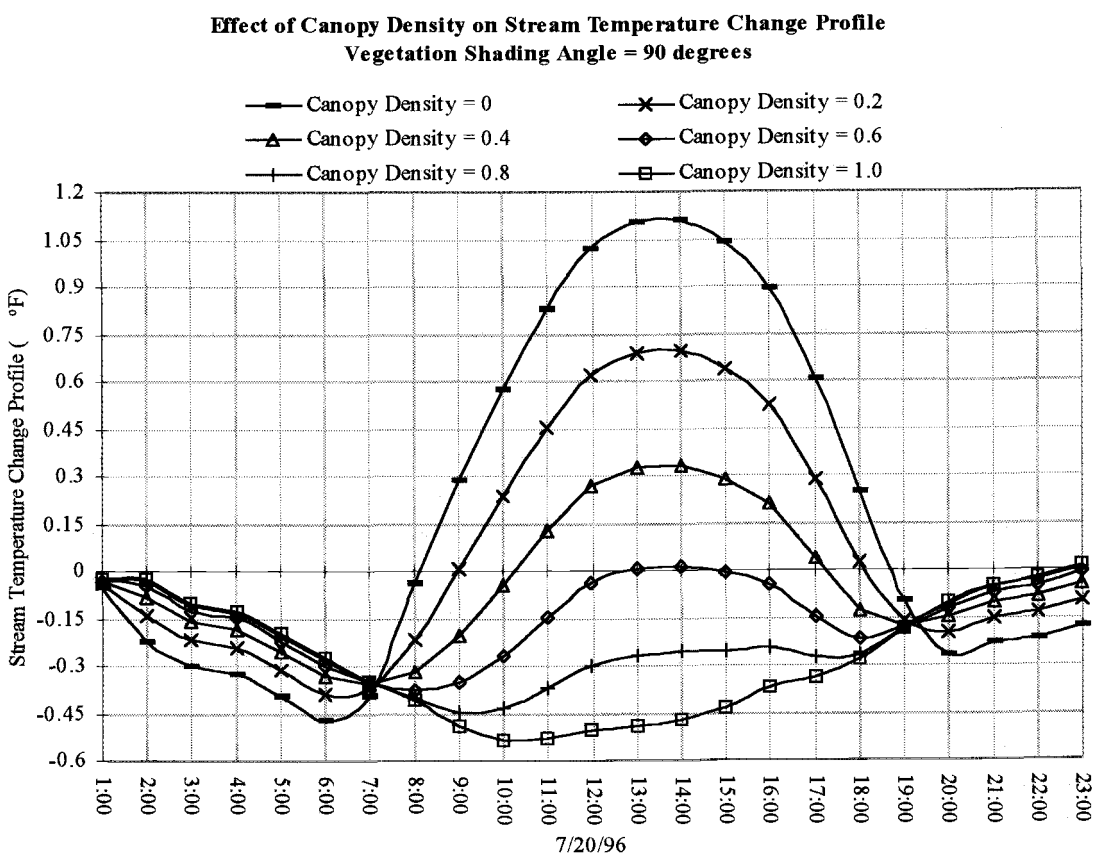

Figure 4.37. Stream temperature change profiles for various canopy densities (vegetation shading angle = 90°).

4.3.2 Wind Speed

Heat Source assumes that evaporation processes are a linearly dependent on wind speed. As wind speed increases, so does the evaporative flux that dissipates heat energy from the surface of the stream. As previously noted, evaporation is the primary heat energy component responsible for water column cooling. Due to differential heating of the earth's surface, late afternoon and evening portions of the diurnal cycle are typically the windiest portions of the day. The descending limb of the diurnal stream temperature spike is certainly most affected by wind induced cooling. As is evident in Figure 4.38, wind speed has the potential to significantly reduced stream temperature change.

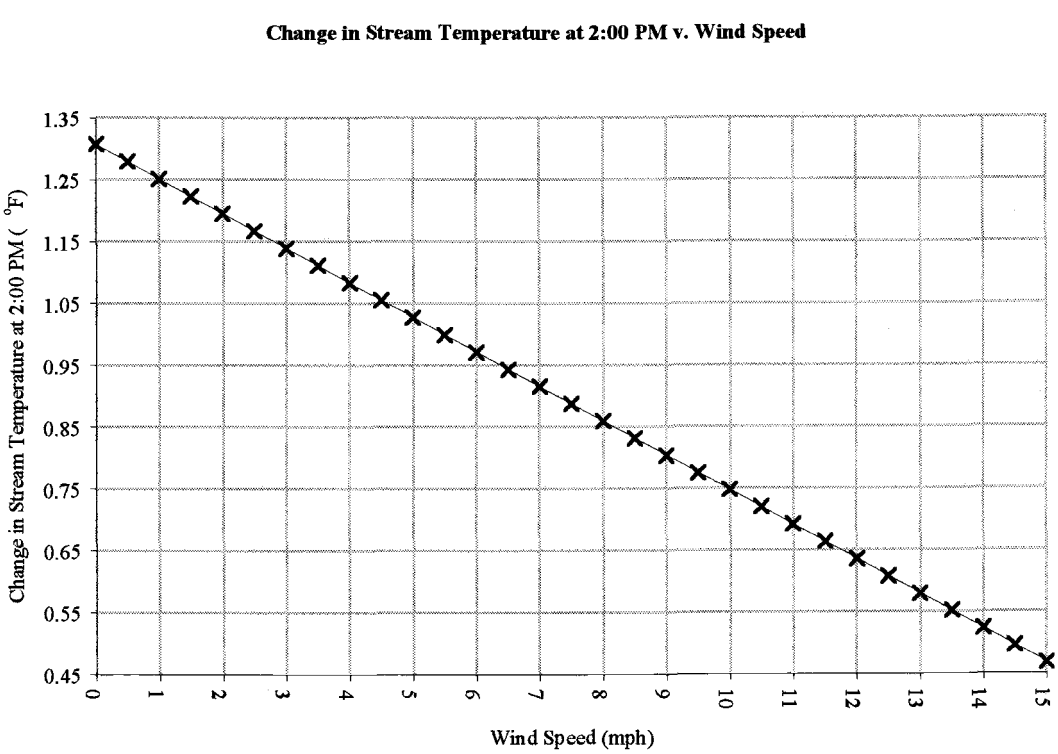

Figure 4.38. Change in stream temperature at 2:00 PM v. wind speed.

4.3.3 Stream Flow

Stream flow magnitude is potentially the most significant stream parameter leading to stream temperature change. Low flow streams are extremely sensitive to stream temperature change. The results of the simulation confirm that the majority of stream temperature increase comes from smaller, low ordered streams. Further, these results are consistent with the modeling methodology used by *Heat Source* and previous research. Figure 4.39 displays the results from stream flow simulation. Note the potential for large temperature change as the flow volume decreases.

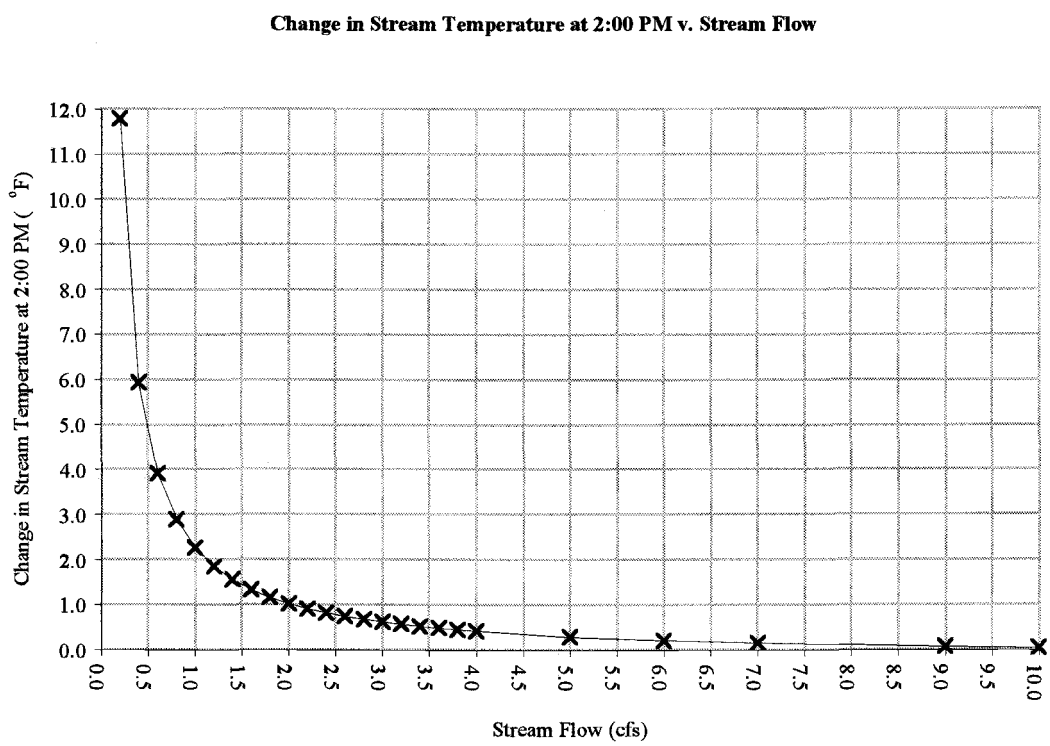

Figure 4.39. Change in stream temperature at 2:00 PM v. stream flow.

Brown's Equation (1969) predicts stream temperature change as inversely proportional to stream flow magnitude. As flow rate decreases, the volume of water that is involved in the energy balance is reduced. However, the energy processes inherent to the stream environment remain unchanged, resulting in more energy imparted to the stream per unit volume. Just as low flow streams tend to display temperature change sensitivity, high flow streams and rivers often are buffered against significant temperature change.

4.3.4 Stream Width

The width of a particular reach defines the surface area of the stream that is exposed to solar, long wave, evaporation and convection energy processes. Simple geometry also suggests that shade angle required to provide equivalent shade increases as stream width increases. Recall that decreased shade angles affect the timing and duration of vegetation shading. Due to increased surface area and decreased shade duration, wide streams experience greater heat energy loads from radiant energy when compared to streams that have a smaller width. The relationship between increased stream temperature to increased stream width is depicted in Figure 4.40.

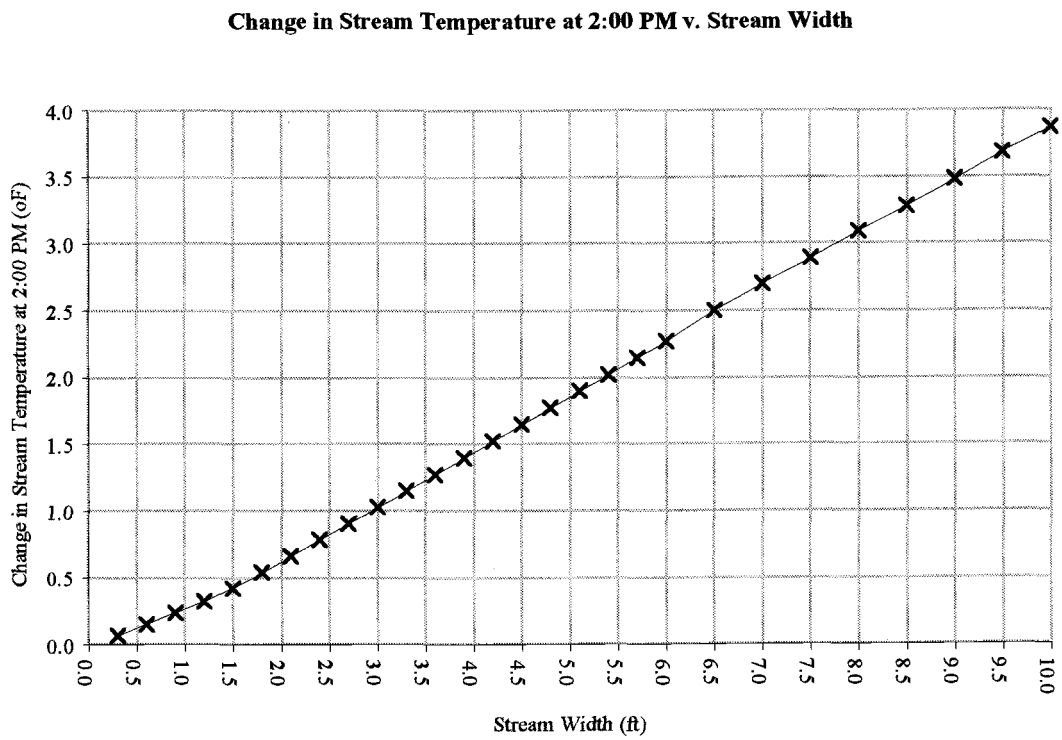

Figure 4.40. Change in stream temperature v. stream width.

4.3.5 Air Temperature

The temperature of the column of air directly above the stream surface is utilized for the simulation of convection energy processes. Air temperature also affects the ability of air to hold moisture, and thus, affects vapor pressure. Recall that the vapor pressure gradient between the stream surface and the air directly above the stream surface is utilized in the simulation of the evaporative flux.

Despite the involvement of air temperature in the model methodology, air temperature has little effect on stream temperature change when compared to other stream parameters. Figure 4.41 depicts the relationship between the maximum daily air temperature and stream temperature change at 2:00 PM. Note that the air temperature

values range from 30° F to 120° F, while stream temperature change ranges from 0.73° F to 1.14° F. To underscore the insensitivity of stream systems to air temperature, at a maximum daily air temperature of 70° F the stream temperature change was 0.99° F, and at a maximum daily air temperature of 90° F the stream temperature change was 1.06° F. The 20° F change in air temperature produced only a 0.07° F change in stream temperature. Such a small temperature difference can not be accurately measured and is considered negligible.

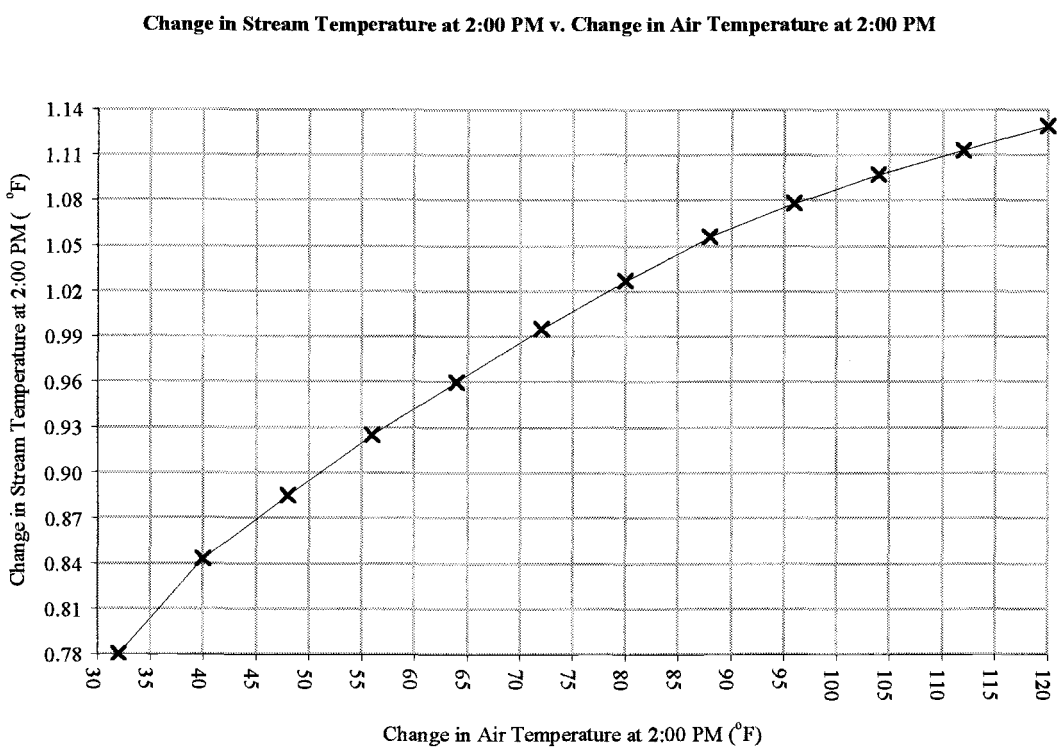

Figure 4.41. Change in stream temperature at 2:00 PM v. maximum air temperature.

4.3.6 Reach Length

The temperature response of a particular stream reach is dependent on the reach length, the stream parameters defined within the reach, and the water temperature entering the reach. Recall that at any instant of time, a defined stream reach is capable of sustaining a particular water column temperature. The temperature of a parcel of water that is traversing a defined reach enters with a given temperature that is either heated or cooled by the energy processes inherent to the defined reach. It takes time for the water parcel to traverse the longitudinal distance of the defined reach, during which the energy processes drive stream temperature change. Water that enters the upstream portion of the reach is never exactly the temperature that is supported by the defined reach. And, as the water is transferred downstream, heat energy and hydraulic process, that are variable with time and space, interact with the water parcel and induce water temperature change. It follows that the rate of temperature change slows as the temperature of the water parcel nears equilibrium with the energy processes. Due to the relatively high latent heat of water, temperature change occurs slowly, resulting in a relatively long travel distance through the stream system before achieving a water temperature that begins to stabilize.

Figure 4.42 shows the maximum stream temperature change at 2:00 PM as a function of reach length. Notice that after nearly six miles of travel, the temperature of the water parcel begins to stabilize. All systems that were studied in this research effort exhibited similar temperature response. The upper portions of the watershed were extremely sensitive to temperature change, while the lower and warmer portions of the watershed were less likely to provide large stream temperature change.

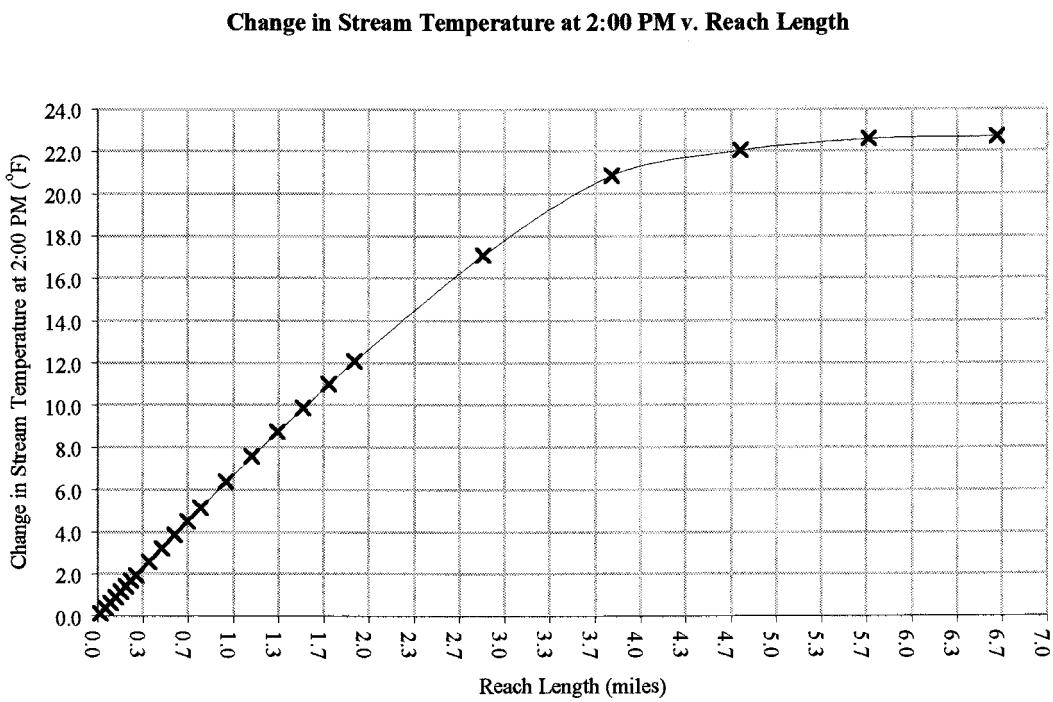

Figure 4.42. Change in stream temperature at 2:00 PM v. reach length

4.3.7 Annual Timing

Annual timing affects the position of the earth relative to the sun. Solar altitude, declination and azimuth are all functions of a defined Julian time. Solar intensity is primarily a consequence of the atmospheric path length that solar radiation must penetrate to reach the surface of the earth. As the earth tilts on its axis toward the sun, the length of atmosphere traversed by incoming solar radiation is reduced, resulting in decreased attenuation and scattering of radiant energy. Solar radiation experienced by the stream system is maximal in summer months, as demonstrated by Figure 4.43.

Simulation did not account for seasonal changes in flow rate, which has been shown to exhibit great influence on stream temperatures. The simulation results suggest

that heat energy delivered to the stream system is highest in June and July. Pacific Northwest stream flows are usually lowest, and therefore, stream temperatures are often greatest in late summer.

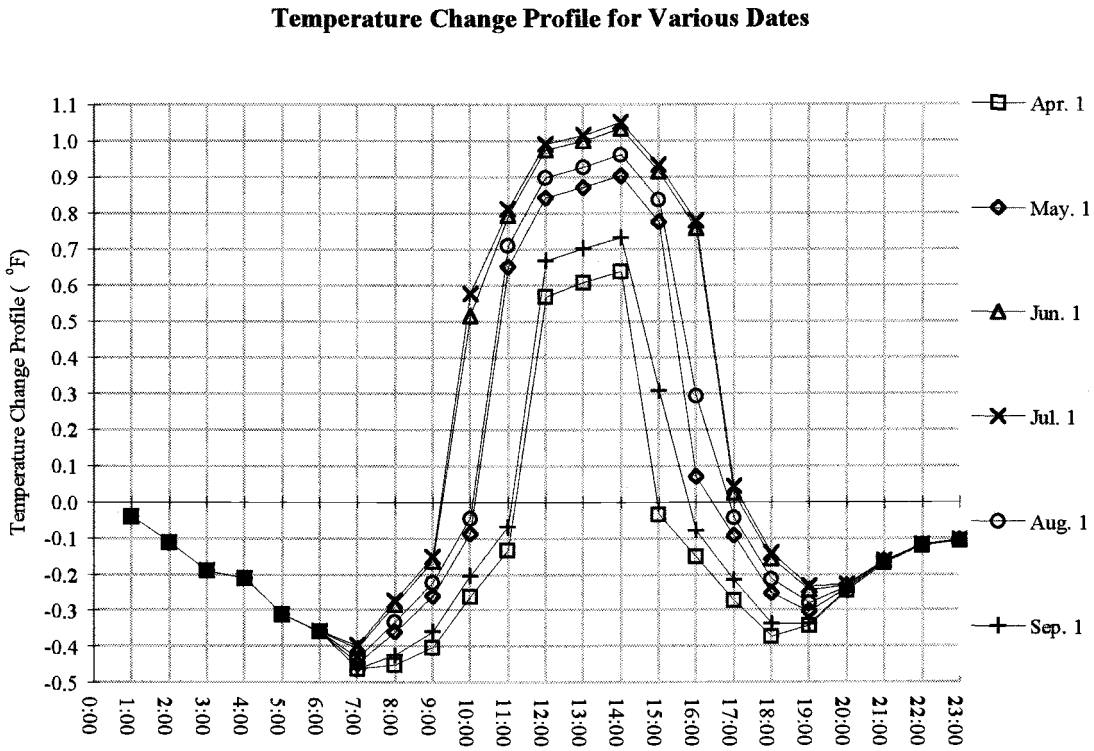

Figure 4.43. Temperature change profile for various dates.

5. CONCLUSION

5.1 Summary of Results

Statistical testing of the predicted temperature profile at the end of the defined reach compared to the actual temperature measurements resulted in a rounded average Pearson's product moment (R^2) of 1.00 and a standard error (S.E.) of 0.33° F (0.18° C). Statistical testing of the predicted temperature change profile occurring over the defined reach compared to the actual temperature change profile resulted in a rounded average Pearson's product moment (R^2) of 0.82 and a standard error (S.E.) of 0.35° F (0.19° C).

Testing of input parameter sensitivity revealed the significance of each model input parameter as to the magnitude of cooling or heating that results from incremental changes to the stream parameters. Input parameters were categorized, depending on whether a ±50% change produced a positive or negative change in the maximum stream temperature. The sensitivities were ranked and the sensitivity was classified as high, moderate or low.

Decreased canopy density produced the greatest increase in stream temperature, while increased canopy density produced the greatest decrease in stream temperature. Canopy density had very little effect in controlling maximum stream temperature change when the vegetation shade angle was less than 60°. Similarly, the vegetation shade angle had little effect in controlling maximum stream temperature change when it measured less than 60°. When the vegetation shade angle is less than 60°, little shade is experienced by the stream surface when the sun is at, or near, the daily solar zenith. Maximum daily

stream temperature change was greatly reduced when the vegetation shade angle was greater than 60° because the stream surface became shaded for majority of the diurnal cycle.

Positive stream temperature change was highly sensitive to decreased flow volume, however, negative stream temperature change exhibited little sensitivity to increased flow volume. Change in flow velocity produced little temperature sensitivity, however, flow velocity sensitivity is an artifact of the model methodology. Increased channel width produced moderate positive stream temperature sensitivity, while decreased channel width produced moderate negative stream temperature sensitivity.

The temperature of the stream entering the defined reach significantly affected the magnitude of stream temperature change that occurred in the reach. When upstream temperatures were decreased, the change in stream temperature that occurred in the defined reach increased. Similarly, when upstream temperatures were increased, the change in stream temperature that occurred in the defined reach decreased.

Stream temperature sensitivity to air temperature, wind speed, relative humidity, percent bedrock and site elevation was determined to be low.

5.2 Discussion

The development of standard methods for stream temperature data collection and analysis will promote uniformity among the many academic disciplines and institutions that have interest in stream/river temperature study. Future stream temperature measurements should be taken with external pig-tail thermistor units, instead of the internal encapsulated

thermistor units that are most commonly used. In addition to stream temperature data, site specific atmospheric, hydraulic and shade data, as detailed by this author, should be collected, or at least estimated, by the field researcher. Stream temperature has been demonstrated to be highly time and site dependent, so that without the additional site specific data, stream temperature data is of little use to the scientific community.

Heat Source relies on methodology that predicts the change in stream/river temperature that occurs over defined a stream/river reach throughout one full diurnal cycle. Such methodology has successfully been performed in previous research efforts (Jobson and Keefer 1979, Beschta and Weatherford 1984, Bashar and Stefan 1993). Upon validation, the methodology in which *Heat Source* is founded was determined to successfully predicted the change in stream/river temperatures over a defined reach.

Efforts to control stream/river temperatures must focus on the low flow tributaries and streams generally located in the upper portions of the watershed. It has been shown that low flow streams are particularly sensitive to temperature change. Further, this research effort demonstrates that the temperature change is most pronounced in low flow streams. In general, riparian vegetation should have a shade angle of 60°, or greater, to provide shading to the stream surface throughout the majority of the daily solar cycle. The vegetation/canopy density must be maintained to preserve the quality of the shade that is provided by the stream side vegetation.

Although stream temperature has become increasingly easy to accurately measure, proper analysis of temperature and stream parameter data is complex. Distinguishing sources of temperature change is difficult and unfortunately, has the potential to become speculative. The methods involved in reach defined analysis of stream temperature include

a relatively simple and short-term (one day) thermistor measurement of stream temperature and a description of the stream system. Simulation of stream thermodynamics with the computer model *Heat Source,* facilitated by actual stream data, provides a detailed energy balance and stream temperature response that occurs in the defined reach.

Reach defined analysis correlates the effects of individual stream system parameters to a simulated stream temperature response. The degree of influence that particular components of the stream's environment have on stream temperature is difficult to analyze by simply measuring stream temperature response. Stream system thermodynamics vary with respect to season, time and reach location. Analysis of stream temperature data yields little information about individual stream components unless the analysis includes the effects of date, time and defined stream parameters. Computer modeling allows for the simulation of stream temperature change induced by varying stream component magnitudes.

Stream reaches and segments that are prone to stream temperature increase are easily identified in a reach defined analysis offering a potential regulatory role for this methodology. Regulators may consider implementing a specific temperature change for a set reach length. Perhaps a 0.5° F change in water temperature that occurs over 1000 feet could be used to signal that a stream reach is experiencing an unhealthy temperature response. The result would be a concentrated effort on a direct source of temperature change. The only other option is basin or stream/river system regulation and land management. Forest practices adopted such basin wide management practices with the implementation of buffer strips. The systems that face increased regulation today are rangeland watersheds, largely used for agricultural production. The use of rangeland

watersheds is particularly intimate with the stream/river systems. Riparian and stream side vegetation is most often located on private lands. Resistance to basin wide regulation and management may be lessened if efforts are reach defined and concentrated on segments that contribute most to increased stream temperature. Further, reach defined analysis has the potential to educate land users about the relationship between land use, the stream environment and stream thermodynamics. Stream reach analysis is relatively easy to perform and involvement of private land owners will result in an informed public.

Regardless of the regulation scheme in which streams and rivers are evaluated, reach defined analysis provides suggestions for water temperature amelioration and management. Land managers should use the results of analysis to set goals for riparian health and stream morphology. Often the condition of one stream parameter is related to one or more other components of the stream system. The results from complete analysis and simulation provide a description of the relationship between stream parameters and water temperature from which a land user or manager may decide to implement a realistic management scheme to achieve desired stream parameters values.

Reach defined analysis and simulation can predict what management plans will accomplish. In order to prevent a specific temperature gain over the course of a stream reach, one or more of the stream parameters may require enhancement. Before actual management schemes are implemented, it would be helpful to predict what the stream thermodynamics are capable of, given different vegetation types and stream morphology. It is important to consider the natural ecosystem and the potential shading angles and canopy density that is inherent to particular vegetation types. Before embarking on an

enhancement project or land use activity, a defined reach analysis and simulation should be performed.

Increased stream and river temperatures have become, and will remain, an important water quality concern. Reach defined stream temperature analysis simplifies the complexity inherent to stream/river systems by correlating the effects of individual stream system parameters to a simulated stream temperature response. Stream reaches and segments that contribute to stream temperature increase can be easily identified. This offers a potential regulatory role for this methodology. Regardless of the regulation scheme in which unhealthy stream/river temperatures are identified, reach defined analysis provides a direct means for water temperature analysis and management.

Conceptually, the network of tributaries that contribute to the main stem flow volume, also contribute to the temperature of the main stem stream/river. Each tributary will exhibit unique temperature behavior, yet the instantaneous integration of the temperatures of the inflowing tributaries will yield the temperature of the main stem stream/river. As with most watershed studies, problems that exist in lower and mid portions of the watershed tend to originate from locations higher in the watershed. In the case of excessive stream/river temperatures, the source of the majority of stream/river temperature change occurs in the low flow tributaries. It is, therefore, in the low flow tributaries where the majority stream/river temperature research and land management should focus. Stream/river temperature problems are ultimately linked to degraded channel morphology, riparian vegetation, disconnectedness to the groundwater table and general stream/river health. The linkage of the temperatures of streams and rivers to channel width, bank stability, stream side vegetation quality and quantity, and flow

volume, serve to underscore that elevated stream/river temperatures are an indication of a degraded stream system.

5.3 Recommendations for Future Research

- Development and testing of evaporation rate models for open channel systems.
- Develop a data base of stream temperature data with the required hydraulic, atmospheric and shade data.
- Linkage of *Heat Source* to G.I.S. to improve stream side vegetation and channel morphology description.
- Correlation of potential shading angles and vegetation densities to specific vegetation types.
- Long-term study of best management practices in urban, rangeland agricultural watersheds.
- Feasibility study of defined reach water temperature analysis for regulation and remediation.

LITURATURE CITED

Anderson, R. 1954. Water loss investigations: Lake Hefner studies, Technical report, Professional Paper 269, U.S. Geological Survey. U.S. Government Printing Office, Washington D.C.

Anderson, J. R., R. L. Beschta, P. Boehne, R. Gill, S. Howes, B. McIntosh, M. Purser, J. Rhodes, J. Zakel. 1993. A comprehensive approach to restoring habitat conditions needed to protect threatened salmon species in a severely degraded river the upper Grande Ronde river anadromous fish habitat protection, restoration and monitoring plan. P. 175-179. *In:* Riparian Management: common threads and shared interests. U.S.D.A. Rocky Mt. For. And Ran. Exp. Sta. Gen. Tech. Rep. 226. Albuquerque, N.M.

Austin, R. W. and G. Halikas. 1976. The index of refraction of seawater. Scripps Instit. Oceanogr., San Diego, CA., Tech. Report SIO 76-1. 121 pp.

Bedient, P. B. and W. C. Huber. 1992. Hydrology and Floodplian Analysis. Addison-Wesley Publishing Company, New York, pp. 658-659.

Beschta, R.L and J. Weatherred. 1984. A computer model for predicting stream temperatures resulting from the management of streamside vegetation. *USDA Forest Service.* WSDG-AD-00009.

Beschta, R. L, R.E. Bilby, G. W. Brown, L. B. Holtby, and T. D. Hofstra. 1987. Stream temperature and aquatic habitat: fisheries and forest interactions. *In:* Streamside Management: Forestry and Fisheries Interactions. E. O. Salo and T. W. Cundy (Editors). Contribution No. 57, University of Washington, Institute of Forest Resources, 471 pp.

Bowie, G.L., Mills, W.B., Porcella, D.B., Campbell, C.L., Pagenkopf, J.R., Rupp, G.L., Johnson, K.M.,Chan, P.W., and Gherini, S.A. 1985. Rates, Constants and Kinetics Formulations in Surface Quality Modeling, 2nd Edition, EPA/600/3-85/040, U.S. Environmental Protection Agency, Athens, GA.

Bowen, I. S. 1926. The ratio of heat losses by convection and evaporation from any water surface. Physical Review. Series 2, Vol. 27: 779-787.

Brett, J. R. 1952. Temperature tolerance in young Pacific Salmon, genus oncorhynchus. *J. Fish. Res. Can.* **9(6)**: 256-323.

Brooks, F. A. 1959. An introduction to environmental biophysics. Springer-Verlag, Inc., New York. 159 pp.

Brown, G. W. 1969. Predicting temperatures of small streams. *Water Resour. Res.* **5(1)**: 68-75.

Brown, G. W. 1970. Predicting the effects of clearcutting on stream temperature. *Journal of Soil and Water Conseration.* **25**: 11-13.

Brown, G. W. and J.T. Krygier. 1970. Effects of clear cutting on stream temperatures. *Water Resour. Res.* **6(4)**: 1133-1140.

Brown, G. W., G. W. Swank and J. Rothacher. 1971. Water temperature in the Steamboat drainage. USDA For. Serv. Res. Pap. PNW-119. Pac. Northwest For. and Range Exp. Stn., Portland, Oregon, 17 pp.

Brown, G. W. 1971. An improved temperature prediction model for small streams. Research Report WRRI-16, Water Resource Research Institute, Oregon State University, Corvallis, Oregon, 20 pp.

Brown, G.W. 1983. Chapter III, Water Temperature. Forestry and Water Quality. Oregon State University Bookstore. pp. 47-57.

Brown, L. and Barnwell, T.O., Jr. 1987. The Enhanced Stream Water Quality Models QUAL2E and QUAL2E-UNCAS: Documentation and USER Manual, Report EPA/600/3-87/007, U.S. Environmental Protection Agency, Athens, GA.

Carnahan, B., H. A. Luther and J. O. Wilkes. 1969. Applied Numerical Methods. John Wiley and Sons. New York. 603 pp.

Claire, E. and R. Storch. 1977. Streamside management and livestock grazing: an objective look at the situation. Paper presented at symposium on livestock interactions with wildlife, fish, and their environments. Sparks, Nevada.

Constantz, J., Carole L. and G. Zellweger. 1993. Influence of diurnal variations in stream temperature on streamflow loss on streamflow loss and groundwater recharge. *Water Resource Research.* **30(12)**: 3253-3264.

Fisher, H. B. 1967. Dispersion predictions in natural streams. *J. Sanit. Eng. Div.*, American Society of Civil Engineers, **94(SA5)**, 927 pp.

Fisher, H. B. 1968. Methods for predicting dispersion coefficients in natural streams, with application to the lower reaches of the Green and Dunwamish Rivers. Washington, U.S. Geological Survey Professional Paper 582-

Fisher, H. B., E. J. List, R. C. Koh, J. Imberger, and N. H. Brooks. 1979. Mixing in Inland and Coastal Waters. Academic Press, New York, 1979.

Gibbons, D. R., and E. O. Salo. 1973. An annotated bibliography of the effects of logging on fish of the Western United States and Canada. U.S.D.A. For. Serv. Gen. Tech. Rep. PNW-10, 145 pp. Pac. Northwest For. And Range Exp. Stn.,Portland, Oregon.

Harbeck, G. E. and J. S. Meyers. 1970. Present day evaporation measurement techniques. *J. Hydraulic Division.,* A.S.C.E., Preceed. Paper 7388.

Hicks, B. J., R. L. Beschta and R. D. Harr. 1991. Long-term changes in streamfow following logging in western Oregon and associated fisheries implications. *Water Resour. Bull.* 27(2) p. 217-226.

Hostetler, S.W. 1991. Analysis and modeling of long-term stream temperatures on the Steamboat Creek basin, Oregon: implications for land use and habitat. *Water Resources Bulletin.* A.W.R.A. **27:4** 637-647.

Ibqal, M. 1983. An Introduction to Solar Radiation. Academic Press. New York. 213 pp.

Jobson, H. E. and T. N. Keefer. 1979. Modeling hihjly transient flow, mass and heat transfer in the Chattahoochee River near Atlanta, Georgia. Geological Survey Professional Paper 1136. United States Government Printing Office, Washington.

Kleinschmidt, E. 1935. Handbuch der meteorologischen instrumente. Speinger, Berlin. P. 201.

Kohler, M. A., T. T. Nordenson, and N. E. Fox. 1955. Evaporation from pans and lakes. U.S. Department of Commerce, Washington D.C. Research Paper No. 38.

Lee, R. 1978. Forest microclimatology. Columbia University Press, New York. 276 pp.

List, R.J. 1966. Smithsonian meteorological tables. Smithsonian Institute, Washington D.C. pp. 527.

McCutcheon, S.C. 1989. Water Quality Modeling: Vol. 1, Transport and Surface Exchange in Rivers. CRC Press, Boca Raton. pp. 183-209.

Marcuson, P. E. 1977. The effect of cattle grazing on brown trout in Rock Creek, Montana. Special Proj. Report F-20-R-21-11-a, 26 p. Mont. Dept. Fish and Game, Helena.

Oregon Department of Environmental Quality 1994. 1992-1994 Water quality standards review. Committee review draft. Water quality standards for temperature.

Parker, F.L. and Krenkal, P. A. 1969. Thermal Pollution: Status of the Art, Rep. 3, Vanderbilt University Dept. Environmental and Resources Engineering, Nashville, TN.

Platts, W. S. 1981. Influence of forest and rangeland management on anadromous fish habitat in western North America: effects of livestock grazing. Meehan, W. R. (editor). U.S.D.A. Forest Service General Technical Report, PNW - 124. Intermountan Forest and Range Experiment Station. Boise, Idaho.

Reifsynder, W.E. and H.W. Lull. 1965. Radiant energy in relation to forests. USDA Forest Service, Technical Bulletin No. 1344. 111 pp.

Rishel, G.B., Lynch, J.A., & Corbett, E.S. 1982. Seasonal Stream Temperature Changes Following Forest Harvesting. *J. Environ. Qual.* **11**: 112-116.

Robinson, N. 1966. Solar Radiation. Elsevier Publishing Company, New York. 347 pp.

Ryan, P.J. and D.F. Harleman. 1976. Transient cooling pond behavior. *Hydraul. Eng. and the Environ.*, Proc 21st Ann. Hydraul. Div. Specialty Conf., A.S.C.E., Boseman, Montana.

Scatterlund, D. R. and P. W. Adams. 1992. Wildland watershed management. 2nd edition. John Wiley and Sons, Inc.

Sellers, W. D. 1974. Physical Climatology. University of Chicago Press. Chicago, IL.

Sinokrot, B.A. and H.G. Stefan. 1993. Stream temperature dynamics: measurement and modeling. *Water Resour. Res.* 29(7): 2299-2312.

Thomas, L. H. 1949. Elliptic problems in lenear difference equations over a network. Watson Scientific Computing Laboratory. Columbia University, New York.

Trenberth, K. E. 1992. Climate System Modeling. Cambridge University Press. Cambridge. 788 pp.

U.S. Geological Survey. 1954. Water Loss Investigations: Lake Hefner Studies, Technical Report, Professional Paper 269, U.S. Government Printing Office, Washington D.C.

Wiget, R. and M. Reichert. (Unpublished). Aquatic survey of selected streams with critical habitats on NRL affected by livestock and recreation. U.S. Dep. Inter., Bur. Land Manage., Ohio State Office, Salt Lake City, 109 p.

Williams, J. 1970. Optical properties of the sea. U.S. Naval Instit., Annapolis, Maryland. 123 pp.

Wunderlich, . 1972. Heat and mass transfer between a water surface and the atmosphere. Tennessee Valley Authority. Water Reseaorces Research Laboratory Report No. 14. Norris, Tennessee. p. 4.20.

Zaykov, B. D. 1949. Evaporation from the water surface of ponds and small reservoirs of the U.S.S.R. *Trans. State Hydrol. Inst.* (Tr. Gos. Gidrol. Inst.).

Appendix: Heat Source Manual

The operation of *Heat Source* is relatively easy. It is hoped that most users will be able to use *Heat Source* after a brief initial consult with the user's manual. However, the basic sequence of the modeling process should be understood before the model is used. The input parameters required to run *Heat Source* must also be understood to ensure accurate input values. A step-by-step operation procedure and an explanation of the function of each menu is provided in this section.

Main Menu

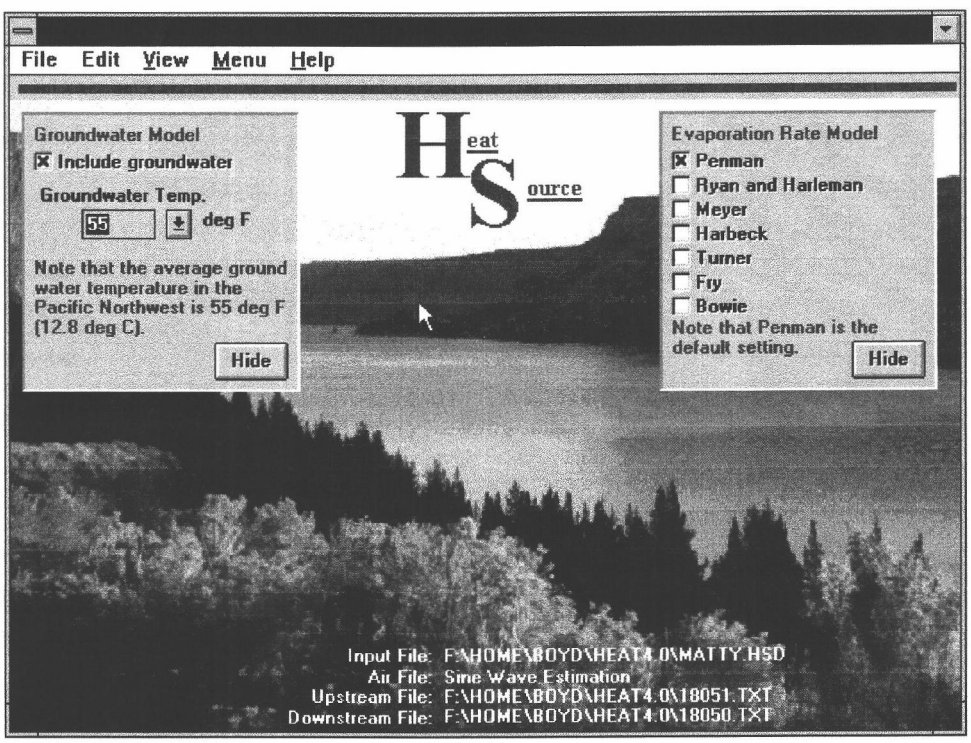

Figure A-1. Main Menu.

The main menu will be displayed once *Heat Source* is loaded. This menu will allow the user to:

- input new data
- open saved data
- input temperature data
- set the finite difference grid
- run the model
- save model input
- save model output
- display model output
- choose an evaporation rate model
- include effects of groundwater

From the main menu, the user can access all of the other *Heat Source* menus. In general, operation of *Heat Source* takes place in three stages: [1]stream parameter input, [2]temperature data input, and [3]temperature simulation. The model has been programmed so that the user will not be allowed to progress to the next step unless all of the required input data fields have been filled. For example, the temperature input selection is not available to the user until all of the stream data has been input.

Evaporation Rate Model

Seven different evaporation models are available to the user for predicting the evaporation rate over the reach length. For users who are unfamiliar with the various models, the default model is the *Penman Method.* To avoid confusion, the evaporation rate setting should not be changed unless the user is familiar with the methodology employed in each evaporation model. A summary of each evaporation model is listed below.

Penman: Developed with lake data using meteorological data collected on land. Employs vapor pressure gradient and wind speed to calculate evaporation rate

Ryan and Harleman: Employs a virtual temperature difference to estimate vapor and wind driven evaporation.

Meyer: Developed for small lakes and reservoirs using pan evaporation data.

Harbeck: Developed for Lake Mead, Nevada, and validated with pan coefficients.

Turner: Developed for Lake Michie, North Carolina, and validated with pan coefficients.

Fry: Developed for small lakes and reservoirs

Bowie: Developed for the San Diego aqueduct and cited by McCutcheon (1989) as suited for arid regions.

Groundwater Effects

Users can include groundwater effects by turning on the groundwater model and entering an average groundwater temperature. Groundwater effects will only be considered in gaining reaches. In most small reaches, groundwater effects are not noticeable. However, if the upstream and downstream boundary flow rates differ considerably, groundwater effects may be needed to preserve simulation accuracy.

General Site Inputs

General site inputs consist of name, date, geographic, meteorological and topographic data that apply to the entire sampling area, including both the upstream and downstream sites. The user must be sure to select the desired units . The units that are selected will be used throughout the entire simulation. In all cases where numerical data is displayed the appropriate units will be included.

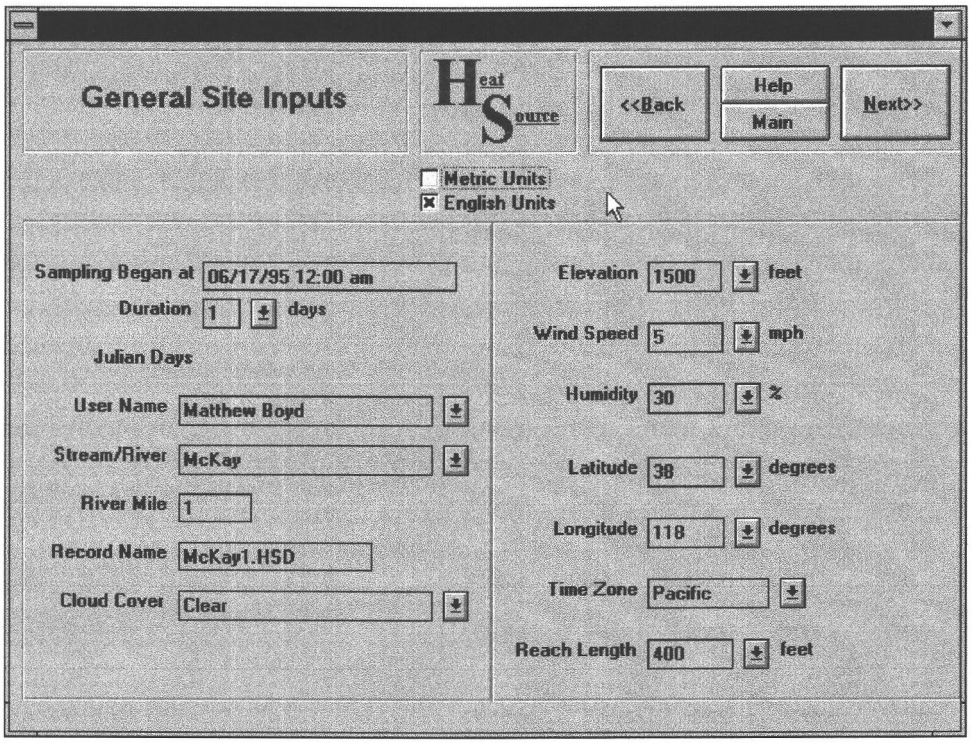

Figure A-2. General Site Input Menu.

Units: Select units that are to used for all model input and output data. It should be noted by the user that in the event that units have been changed, preexisting input values should be checked and updated as necessary.

Sampling Began At: Time at which *Heat Source* will begin temperature prediction formatted as 'Month/Day/Year Hour:Minute'. The user may also change this value when inputs and defining hourly temperature data on the **'Temperature Inputs'** Menu.

Duration: Length of time, in days, that *Heat Source* will predict stream temperatures. The user may also change this value when inputs and defining hourly temperature data on the **'Temperature Inputs'** Menu.

Julian Days: Automated calculation of Julian Day occurring in the specified year (accounts for leap year).

User Name: Name of user needed for general record keeping.

Stream/River: Stream/River name needed for general record keeping.

River Mile: River mile at which prediction is taking place.

Record Name: Suggested record name which *Heat Source* will save or open this general input file. Note that the record name is formatted as 'Stream/River Name + River Mile + .HSD'. *.HSD denotes that this file is '*Heat Source* Data' formatted.

Cloud Cover: Simply refers to the fraction of cloud coverage:

Clear : 0% cloud cover

Scattered: 33% cloud cover

Broken: 67% cloud cover

Overcast: 100% cloud cover

Elevation: Site elevation input according to specified units

Wind Speed: Wind speed directly above the stream surface. Estimates may be more accurate if local meteorological measuring site data is used (i.e. municipalities or airports).

Humidity: Percent relative humidity; mid-day is preferred.

Latitude: Latitude of sampling site; if possible include fraction of a degree. Do not use minutes or seconds. *Heat Source* is not able to simulate in South latitudes.

Longitude: Longitude of sampling site; if possible include fraction of a degree. Do not use minutes or seconds.

Time Zone: Time zone of sampling site.

Reach Length: Length of reach where prediction is taking place. Care should be taken in measurement, given that stream temperature change is very sensitive to reach length. Reaches should be chosen in relatively homogenous reaches up to the mid-point. At the mid-point of the reach *Heat Source* will assume the characteristics of the downstream site.

Upstream/Downstream Site Inputs

The second and third input menus are specific for the upstream and downstream sites. Both menus are identical for each site, with the exception of temperature data that is required for the upstream site. All input data required on these menus is defined below.

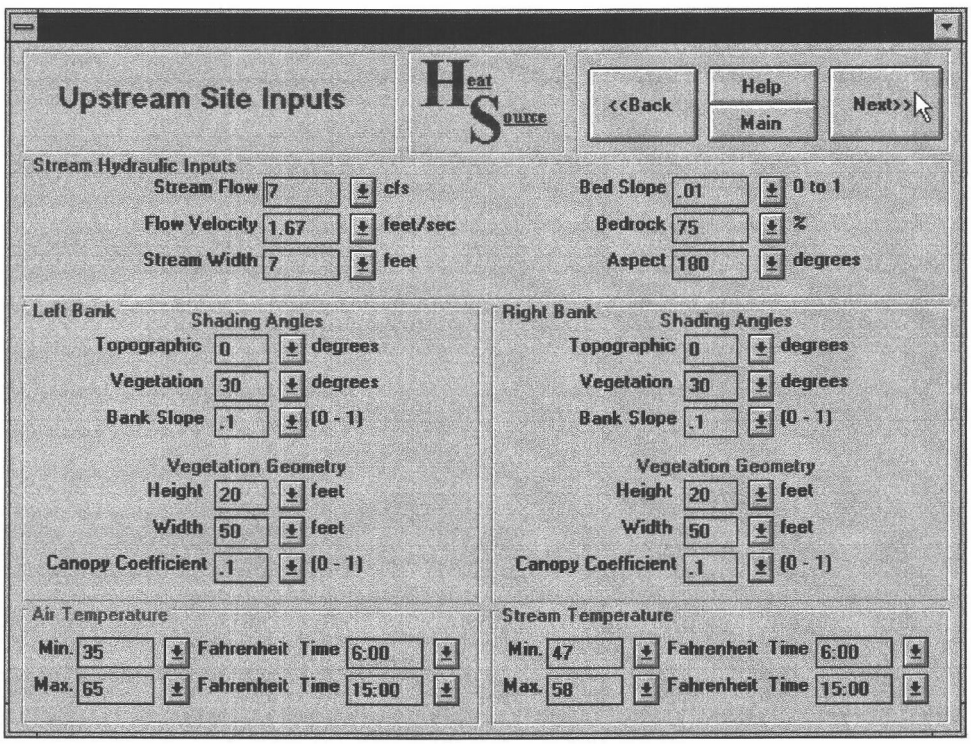

Figure A-3. Upstream Site Input Menu.

Stream Flow: Measured/Approximated stream flow. Note that flow units are either 'cfs' or 'cms'.

Flow Velocity: Measured/Approximated flow velocity. Note that velocity units are either 'ft/s' or 'm/s'

Stream Width: Measured stream width. Note that length units are either 'meters' or 'feet'.

Bed Slope: Measured/Approximated stream bed slope measured as a slope fraction (i.e. rise/run)

Bedrock: Percent of streambed material that has a diameter greater than or equal to 4 inches (10 cm). A good approximation method may be a quick survey of one square meter of streambed material.

Aspect: Stream aspect in degrees clockwise from the north.

i.e. North = 0°

West = 90°

South = 180°

East = 270°

Topographic Shading Angle: Maximum shading angle created by topographic features. Angle is measured from the center of stream facing the direction perpendicular to stream axis (stream flow) and is required for each stream bank. Values must be positive or zero and measurements are recorded in 'degrees'.

Vegetation Shading Angle: Maximum shading angle created by streamside vegetation. Angle is measured from the center of stream facing the direction perpendicular to stream axis (stream flow) and is required for each stream bank. Values must be positive or zero and measurements are recorded in 'degrees'.

Bank Slope: Bank slope for both banks measured as a slope fraction (i.e. rise/run)

Vegetation Height: Height of stream side vegetation found directly perpendicular to stream axis (stream flow).

Vegetation Width: Width of stream side vegetation found directly perpendicular to stream axis (stream flow).

Canopy Coefficient: Canopy density measured as a decimal fraction.

Air Temperature: Air temperature measured in shade. Minimum and maximum values are required, as well as, the times of occurrence.

Stream Temperature: Upstream site stream temperature preferably measured in

shade. Minimum and maximum values are required, as well as, the times of occurrence.

Temperature Inputs

Defining temperature inputs is an extremely important step in preparing *Heat Source* for stream temperature prediction. Upstream water temperatures and air temperatures are required, and downstream water temperatures are optional. However, if downstream temperatures are available to *Heat Source*, actual and predicted temperatures are easy to compare for simulation accuracy. Further, plots for temperature profiles and temperature changes occurring over the stream reach will include all actual and predicted temperature data.

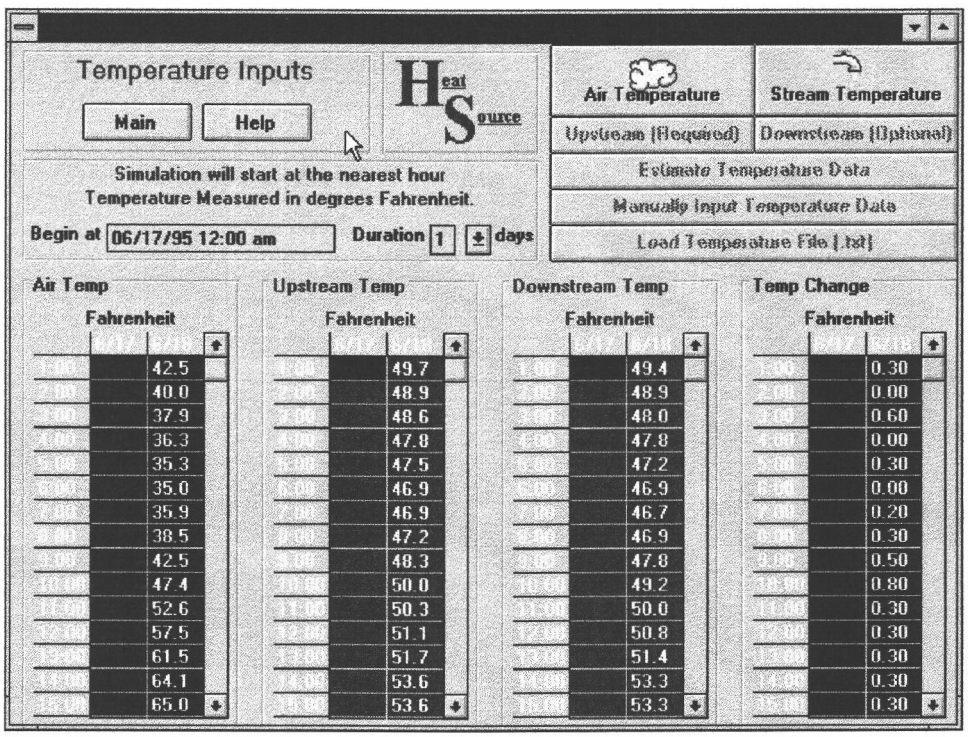

Figure A-4. Temperature Inputs Menu.

Begin At: Time at which *Heat Source* will begin temperature prediction formatted as 'Month/Day/Year Hour:Minute'.

Duration: Length of time, in days, that *Heat Source* will predict stream temperatures.

Air Temperature: Air Temperature may be estimated with a sine wave, input manually, or loaded from a data file. Air Temperatures are required.

Upstream Temperature: Upstream Temperature may be estimated with a sine wave, input manually, or loaded from a data file. Upstream Temperatures are required.

Downstream Temperature: Downstream Temperature may be input manually or loaded from a data file. Downstream Temperatures are optional.

Temperature Change: If both upstream Temperatures and downstream temperatures are input, *Heat Source* will automatically determine the instantaneous change in stream temperature.

Estimate Temperature Data: *Heat Source* uses the minimum and maximum temperatures, as well as the times of occurrence to calculate a sine wave that estimates the diurnal temperature fluctuation.

Manually Input Temperature Data: *Heat Source* allows the user to input hourly temperature data.

Load Temperature Data: *Heat Source* will read a temperature data file that is formatted as,

'time, °C, °F, AV'.

The time value should be in computer date formatted as a real number. Boxcar, the application used to download Hobo Thermistors will format data files appropriately.

Finite Difference Grid

Inherent to the numerical methods employed by *Heat Source* is the definition of a finite difference grid. Users that are not familiar with the appropriate value for dispersion, time step and distance step should resort to the default values.

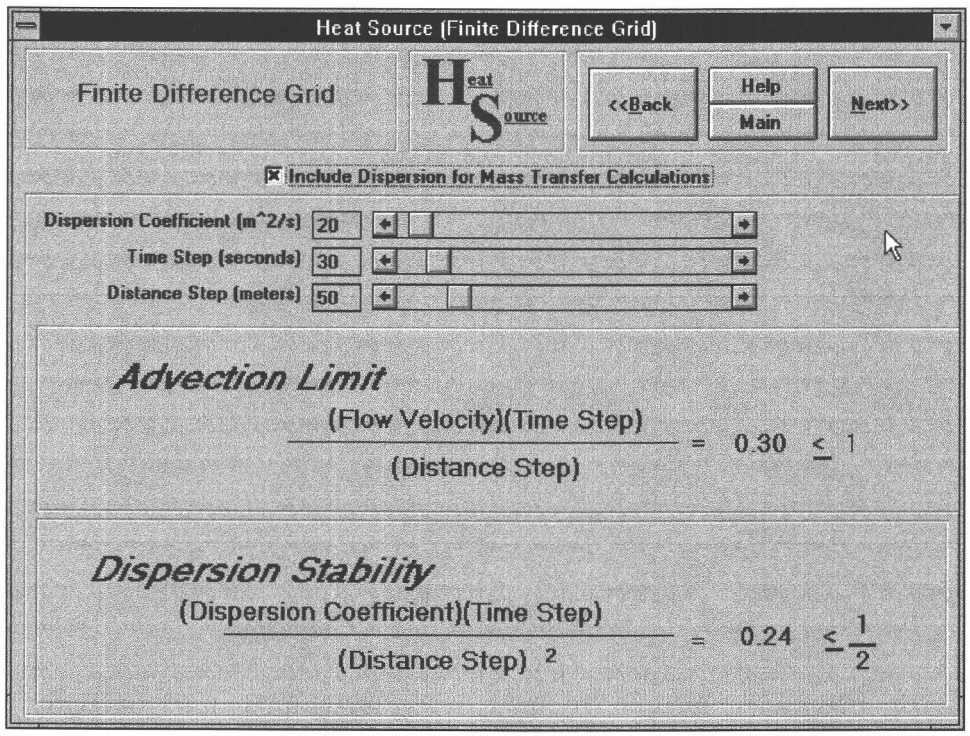

Figure A-5. Finite Difference grid Menu.

Dispersion Coefficient:	Set the dispersion coefficient finite difference solution
Time Step:	Set the time dimension of the finite difference grid
Distance Step:	Set the space dimension of the finite difference grid
Advection Limit:	User is notified when advection limit is violated
Dispersion Stability:	User is notified when dispersion stability is violated

Temperature Plots

The predicted temperature model output can either be displayed in a text grid or graphically. Both the predicted temperature profile and the predicted temperature change is plotted. If the user has input the actual downstream temperature data, it will also be included. It is often a good idea to input the actual downstream temperature data in order validate the performance of the model and/or to evaluate the accuracy of the input values.

Energy Balance Plot

The energy balance plot provides the magnitude of each energy process as a function of time. With a general knowledge of each energy process and the stream parameters that influence each energy component, the energy balance plot becomes an effective means to correlate the stream temperature response with the individual parameters. These values can also be viewed in text format by selecting 'Energy Balance Values'.

Model Operation and Procedures

The following flow chart shows the general model lay out and options.

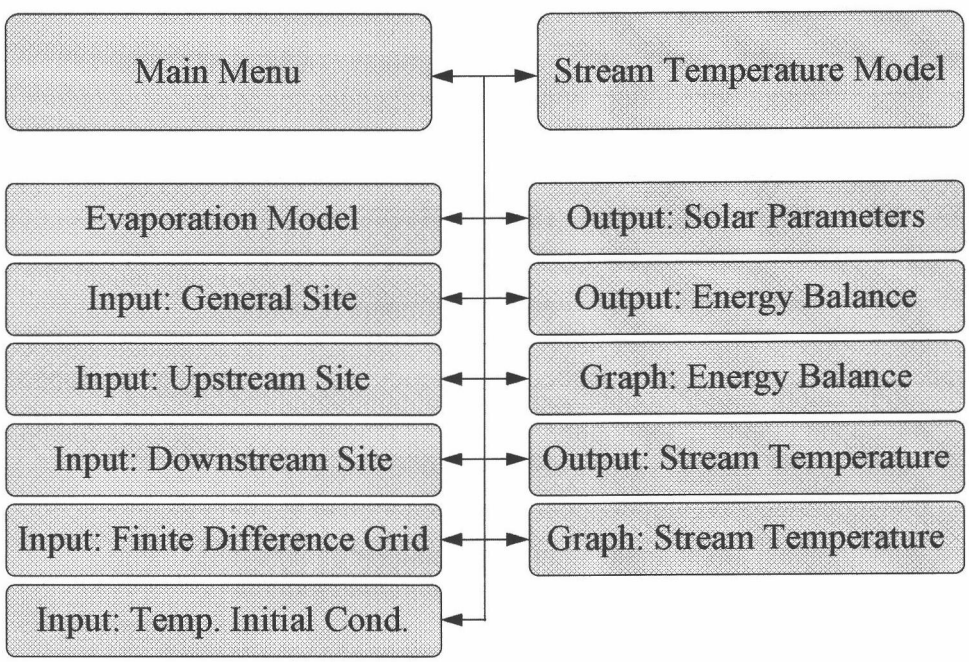

General model operation should take place in the listed sequence.

Step 1. Create/Load General Inputs (Required)

The first step in setting up *Heat Source* is the definition of input values which are required for stream temperature prediction. Input values may either be created or loaded from existing input data files denoted '*.hsd'. All input menus allow the user to go to the next input menu, back to the previous input menu, return to the main menu or access the *Heat Source* help file.

Either create new general inputs by selecting:

'File ⇒ New ⇒ General Inputs',

or load a previously created and saved general input file by selecting

'File ⇒ Open ⇒ General Inputs'.

All general inputs must be given values before *Heat Source* will allow the user to continue to the next menu. The general input menus are sequenced as follows:

General Site Inputs ⇔ Upstream Inputs ⇔ Downstream Inputs ⇔ Finite Difference Grid.

Step 2. Load Temperature Inputs (Required)

Temperature Inputs can be created or loaded by selecting:

'File ⇒ Temperature Inputs'.

Heat Source must be provided with *air temperatures* and *upstream site temperatures*, however, *downstream site temperatures* are optional. Temperature data can be generated with a sine wave estimation, manually input by the user or loaded directly from a data file.

Step 3. Evaporation Model (Optional)

Seven specific evaporation models are accessible when selecting:

'Edit ⇒ Evaporation Model'.

The various models serve to provide *Heat Source* with user defined evaporation rate methods. It should be noted that the *Penman Method* is the default setting.

Step 4. Groundwater Model (Optional)

To access the groundwater model the user needs to select:

'Edit ⇒ Groundwater Model',

where either groundwater effects can be ignored or included. Note that the default setting is to *ignore* groundwater effects.

Step 5. Predict Stream Temperature (Required)

Heat Source begins prediction when

'Menu ⇒ Predict Stream Temperature'

is selected. Simulation will span the entire specified duration.

Step 6. View Model Output

Output is categorized as solar and atmospheric parameters, energy balance and temperature predictions. All model output can be viewed in either text or graphical format.

'View ⇒ Solar and Atmospheric Parameters'

'View ⇒ Energy Balance Values'

'View ⇒ Energy Balance Plot'

'View ⇒ Temperature Values'

'View ⇒ Temperature Plots'

Specifications

Operating System: Windows 95® or Windows 3.1®

Memory: 8 MB

Monitor Resolution: 256 Colors, 640 x 480 or 800 x 600 pixels.